MECHANISM OF ARSENIC SORPTION ONTO LATERITE CONCRETIONS

Frederick Kenneh Partey

New Mexico Tech

Department of Earth and Environmental Science

MECHANISM OF ARSENIC SORPTION ONTO LATERITE IRON CONCRETIONS

By

Frederick Kenneh Partey

Submitted to the faculty of New Mexico Tech
in partial fulfillment of the requirements for the degree of

Doctor of Philosophy in Earth and Environmental Science with Dissertation in Geochemistry

New Mexico Institute of Mining and Technology
Department of Earth and Environmental Science

Socorro, New Mexico
January 2008

Advisory Committee

Advisor_____
Dr. Dave Norman

Member 1_____
Dr. Robert Bowman

Member 2_____
Dr. Jan Hendrickx

Member 3_____
Dr. Malcolm Siegel

Member 4_____
Dr. Virgil Lueth

Dedication

This Thesis is dedicated in loving memory of Mr. and Mrs. Henry Teye Partey and to my beloved wife Cynthia Partey not forgetting Deborah, Daisy, Dave and Diandra. Your support and encouragement has brought me this far.

Such is life

Men's evil deeds are written on brass the good ones on water when I am right no one remembers when I am wrong no one forgets.

ABSTRACT

The objective of this study is to understand the sorption mechanisms and to quantify sorption of arsenic on laterite concretions (LC). Laterite concretions are known to sorb arsenic. I investigated As (III) and As (V) sorption onto Prestea and Awaso laterite concretions (LC) to test its suitability for use in low-tech treatment of arsenic-bearing drinking water. The two Fe-Al oxide-hydroxide concretions were selected for the study because they represent compositional end members, Al-rich (Awaso) and Fe-rich (Prestea), of lateritic soil concretions. The ultimate goal of this project is to demonstrate how and why LC can be used as an effective and inexpensive means of water purification system for communities that cost less and is easy to maintain, and produced drinking water of high quality.

Attenuated Total Reflection Fourier transform infrared (ATR-FTIR) spectroscopic methods were combined with sorption experiments, electrophoretic mobility measurements, and surface complexation modeling to study the interaction of As (III) and As (V) with laterite concretion surfaces. Arsenic sorption on Prestea and Awaso laterite concretions was also investigated as a function of solution pH. The sorption capacity was determined for both concretions through batch experiments on crushed samples. Prestea LC was studied at different temperatures to evaluate the effect of temperature on the media. Competitive sorption experiments were also conducted in the presence of phosphate and sulfate, as this represents the case of greatest threat to arsenic remediation in most ground waters and sulfide mining waste waters from stock piles.

Experiments of Prestea LC show that sorption capacity for both arsenite and arsenate increases with temperature. The equilibrium sorption capacity for As (III) is larger than that for As (V) over temperatures ranging from 25° to 60°C. A Langmuir model satisfactorily fits the arsenite and arsenate sorption isotherm data for both Prestea and Awaso LC. Both As (III) and As (V) sorbed well for the pH range of natural waters with little change.

Arsenic (III) sorption on both Prestea and Awaso LC exhibits decreasing sorption with increasing ionic strength, indicating an outer-sphere sorption mechanism. Arsenic (V) sorption on both Prestea and Awaso LC shows slight ionic strength dependence with increasing solution pH, and an increase in sorption with increasing solution ionic strength. These behaviors are indicative of an inner-sphere sorption mechanism for As (V) on both studied types of LC.

The results of the electrophoretic measurements (EM) indicate that both As (III) and As (V) form inner-sphere complexes on Prestea LC. Arsenic (III) forms outer-sphere sorption mechanisms on Awaso LC because there is no shift in pHzpc even with an increase in As (III) concentration. Arsenic (V) however, forms inner sphere complexes on Awaso LC due to shifts in pHpzc and reversals of EM with increasing ion concentration.

The ATR-FTIR analysis shows an increase in peak intensities and band shift to lower wavelengths for both As (III) and As (V) on Prestea and Awaso LC. The presences of the peaks in the treated LC spectra that are not present in the untreated sample are an indication of chemical bonding between the arsenic species and the

surface of the Prestea LC. The peak shift and the change in peak intensity may be indicative of an inner-sphere sorption mechanism. The peak positions of the arsenic treated samples (sorbed samples for both Prestea and Awaso LC) are significantly different from those of the dissolved arsenic species and can be attributed to sorption of the arsenic species. In general, the spectra of both As (III) and As (V) sorbed onto the Prestea and Awaso LC are very different from those of arsenic aqueous solutions. This difference and the lack of pH dependence on the positions of the vibrational modes indicate that these modes are "protected" from changes in pH and indicate that these groups are involved in direct complexation to the surface. Another line of evidence for the mechanism of sorption that is converse to the ATR-FTIR spectra for dissolved arsenic species is that a shift in band position was not observed in As (V) and As (III) adsorbed spectra with changing pH. The lack of change in band position at various pH values suggests that arsenic formed the same inner-sphere surface complexes on both Prestea and Awaso LC.

Surface complexation models successfully constrained both macroscopic and microscopic measurements. The effect of changes in ionic strength on sorption of As (III) and As (V) on Prestea and Awaso was modeled using both diffuse and triple layer models. Arsenic (V) sorption, which is slightly affected by ionic strength, was modeled with both the diffuse layer and the triple layer model, although the triple layer model shows a better fit at higher pH's than the diffuse layer model. Arsenic (III) sorption, which is markedly reduced by increasing ionic strength, is best modeled using the triple layer model.

The presence of phosphate and sulfate reduces the amount (mg) of As (III) sorbed per gram of Prestea and Awaso LC. However, an aqueous solution of As (V) spiked with sulfate did not reduce As (V) sorption rather it increased the sorption. The increase was more prominent on Awaso than Prestea LC.

The negative "Gibbs free energy (ΔG^o)" values for arsenite and arsenate sorption on Prestea LC agree with spontaneous reaction between the species and the medium. Positive "entropy (ΔS^o)" values suggest the affinity of LC for the arsenic species in solution.

The sorption capacity value indicates that significant sorption sites are available for specific sorption of both arsenic species. The development of low-cost arsenic filters using LC is therefore practical. The Prestea and Awaso LC both treated approximately 5000 bed volumes of 42 µL As (V) Socorro water to the maximum contamination limit of 10 ppb. Analysis of the arsenic sorption data suggests that LC can be used for a low-tech natural-materials arsenic water treatment and has a number of advantages over commercial materials for this use including the ability to remove arsenic from waters with a wide range in pH, to sorb both common arsenic aqueous species equally well, and cost less. The positive sorption temperature dependence of LC will enhance sorption in tropical climates, and more especially in areas where groundwater sources are related to geothermal springs.

The media has potential in remediating other toxic trace elements to very low concentrations. A TCLP leaching test also reveals that the used adsorbent is not toxic and can be disposed of without the need for confinement. Investigations of arsenic sorption onto these two end members show that, all other laterites whose

mineralogical compositions fall within these two end members should filter arsenic from drinking water.

This dissertation is accepted on behalf of the faculty of the institute by the following committee.

Advisor

Date

I release this document to the New Mexico Institute of Mining and Technology.

Student's signature Date

ACKNOWLEDGEMENTS

I wish to express my deepest gratitude first to the almighty God who gave me the strength to undertake this project. I am very grateful to my committee members Dr. Dave Norman, Dr. Robert Bowman, Dr Jan Hendrickx, and Dr. Malcolm Siegel whose useful suggestions and encouragement led to the successful completion of this work. Further more I would like to thank Dr. Christa Hochensmith who helped me with all the ATR-FTIR work.

I am also grateful to Dr. Samuel Ndur and Matt Earthman for helping me with laboratory work. To all members of the faculty, staff, graduate students, and undergraduate students here in New Mexico Tech, I say thank you for your love and care. Lastly to all and sundry, I say thank you and God bless you.

This project was funded by the Sandia National Laboratories, the Geological Society of America, the Office of Advancement and Research at New Mexico Tech, and the Graduate Student Association at New Mexico Tech. I appreciate scholarships from these organizations: the American Federation of Mineralogical Societies, the Budding Geosciences Research Award, the Women's Auxiliary to the American Institute of Mining, and the Metallurgical and Petroleum Engineers for feeding myself and my family during the course of this work.

TABLE OF CONTENTS

List of figures

LIST OF TABLES

LIST OF SYMBOLS AND ABBREVIATIONS

As (III) arsenous acid, H_3AsO_3

As (V) arsenic acid, H_3AsO_4

ATR-FTIR Attenuated Transform Reflectance- Fourier Transform Infrared

BE Background Electrolyte

BET Brunauer-Emmett-Teller Surface Area

CA Component Additivity SC Method

$\Delta G°$ Gibbs Free Energy

$\Delta H°$ Standard Enthalpy

DLM Diffuse-Layer Model

$\Delta S °$ Standard Entropy Changes

EM Electrophoretic Mobility

EXAFS X-ray Absorption Fine Structure

F m^{-2} Faraday Per Square Meter

GC Generalized Composite SC Method

Kint Constant for Chemical-Specific Complexation with an Oxide Surface

LC Laterite Concretion

μg/g Micrograms per Gram

μg/L Micrograms per Liter

LC Laterite Concretion

nm Nano Meter

NMBGMR New Mexico Bureau of Geology and Mineral Resources

pH Negative Log of Hydrogen Iron Concentration

pKa Log Acid Disassociation Constant

ppb Part Per Billion

ppm Part Per Million

PZC Point of Zero Charge

SC Surface Complexation

T Temperature, Kelvin

TLM Triple-Layer Model

USEPA United States Environmental Protection Agency

WHO World Health Organization

XANES X-ray Absorption Near Edge Structure

XRD X-ray Diffraction

XRF X-ray Fluorescence

CHAPTER 1

INTRODUCTION

Drinking-water arsenic concentrations greater than 10 ppb pose a significant health problem throughout the world [1]. There are millions in Bangladesh and India suffering from cancer and keratosis as a consequence of chronic arsenic poisoning [2]. Waters with arsenic concentrations >10ppb are common in other less developed countries like Ghana, consequently there is a need in developing countries for low-cost materials and methods to remove arsenic from drinking water. The cost of arsenic removal in developed countries is also prohibitive. For example it costs the United States of America $195 million per year to remediate arsenic from drinking water [3]. Therefore there is an urgent need for arsenic removal technologies that are effective and inexpensive for communities with arsenic contaminated drinking water.

One method for filtering arsenic from drinking water is by using laterite concretions (LC), a natural substance, they are a combination of oxides of iron, manganese, aluminum, silica compounds, and clay minerals [4, 5]. This method has not been fully investigated due to limitation in our understanding in the mechanism of sorption. However, sorption mechanism(s) must be well understood for optimal LC application to filter arsenic**.**

Laterite concretions are formed by deep weathering in tropical and subtropical environments. The heavy rainfall in these regions leaches out all soluble weathering products in such soils, leaving behind clay minerals, rutile, and hydrated Al and Fe oxides that impart a red/yellow color to the concretions. Laterite iron concretions easily remove arsenic from drinking water sources, due to the presence of

metal oxy-hydroxides such as rutile and the hydrated Al and Fe oxides they contain. These metal oxides are known to remove arsenic from drinking water, but are usually synthesized in laboratories and are expensive. Hence the need for a natural substance such as LC that is readily available and costs little. Laterite iron concretions can be used to develop an effective and inexpensive means of water purification for a community that costs less and is easy to maintain, and the drinking water produced is of high quality.

The objective of this study is to delineate arsenic sorption mechanisms and to demonstrate laterite concretions as media that are low-cost and effective in removing arsenic from drinking water. This is done by:

(1) evaluating the effects of pH and ionic strength on arsenic sorption onto LC

(2) determining the LC point of zero charge (PZC)/electrophoritic mobility (EM) with and without bound arsenic

(3) using Fourier Transformed Infra-Red spectroscopy to investigate the form and structure of adsorbed ions on LC

(4) Using surface complexation models to describe arsenic sorption onto LC

A combination of these results will elucidate the mechanism(s) of arsenic sorption onto LC. The parameters obtained will be used to optimize LC applications and design appropriate and effective arsenic filtering devices.

Laterite concretions are a composite material whose sorption properties are unique and different from most natural media available. A specific example is that at a temperature of 25°C or higher LC removes As (III) better than As (V). Our data suggests that LC removes arsenic effectively over a wide pH range (4-9) and works

better for low-tech applications than other natural materials and has distinct advantages over engineered materials. The treatment process cost is estimated to be only US $0.003/1000L, hence the filter will be cost effective and user friendly since no pretreatment is required for its use. The study of arsenic sorption mechanisms using a complex composite material such as LC is new and most researchers shun away from it due to the difficulty in the detailed characterization of natural materials.

This research hopes to investigate the arsenic sorption techniques of Prestea and Awaso LC and show that they effectively filter arsenic from arsenic-bearing drinking water. The ultimate goal is to use laterite concretions from both Prestea and Awaso to develop an effective and inexpensive means of water purification system for communities that cost less and is easy to maintain, and produced drinking water of high quality. The parameters obtained will be used to optimize other applications and to design appropriate and effective arsenic filtering devices.

1.1 ARSENIC HEALTH EFFECTS

Arsenic is a unique human carcinogen in that it causes lung cancer by exposure through ingestion as well as through inhalation [6]. Over the past decade, there is accumulating evidence that arsenic at low levels in drinking water can seriously affect health [7]. Cancerous lesions are associated with waters containing 100's of ppb arsenic [8]. Increased rates of skin cancer, heart disease, infant mortality, and birth defects are related to arsenic levels less than 100 ppb [9]. These detrimental health effects of arsenic prompted the World Health Organization (WHO) and the United

States Environmental Protection Agency (EPA) to reduce the drinking water arsenic standard from 0.05 mg/L to 0.01 mg/L [10].

In Bangladesh there is an environmental disaster, with an estimated 1,000,000 people dying of arsenic-related cancer, and about 1,500,000 persons with some level of arsenic poisoning from ingestion of arsenic contaminated groundwater [11]. Data used to characterize the associations between ingested arsenic and cancer come from epidemiological studies in which exposure is assessed from individual drinking water sources used by the human subjects [12]. There may be other health affects not yet known. Recently, Duker et al. [13] show a spatial pattern of Buruli ulcer and arsenic concentration in drinking water in the Amansie West District of Ghana. Buruli ulcer or Bairnsdale ulcer occurs in 30 tropical and subtropical countries [14].

There is widespread concern about elevated concentrations of arsenic in the aquifers of Bangladesh. Of the 125 million people living in Bangladesh, the number adversely affected by arsenic-contaminated drinking water has been estimated to be between 40 and 70 million [11, 15]. Arsenic levels are lower in the USA; only a handful of municipalities report concentrations greater than 50 μg/L. However, individual US wells can contain extreme concentrations of arsenic of up to 12 mg/L in rare cases [16] and levels of 10-50 μg/L are not uncommon [17, 18]. Some researchers attribute elevated concentrations of arsenic to pyritic sedimentary rocks in contact with the aquifer [15], though there is no general consensus about what mechanisms are responsible for the increased concentration of arsenic in the groundwater. In addition, elevated concentrations of arsenic are found in agricultural drainage waters from some soils in arid regions [15].

1.2 ARSENIC GEOCHEMISTRY

In natural waters arsenic is found in the + (III) and + (V) oxidation states. Arsenic (III), is uncharged at the pH of natural water, while As (V), and is usually present as an anion with charge of minus one or two (Figure 1, Table 1). Arsenic (V) is thermodynamically favored under oxidizing conditions, while As (III), prevails in reduced settings such as groundwater.

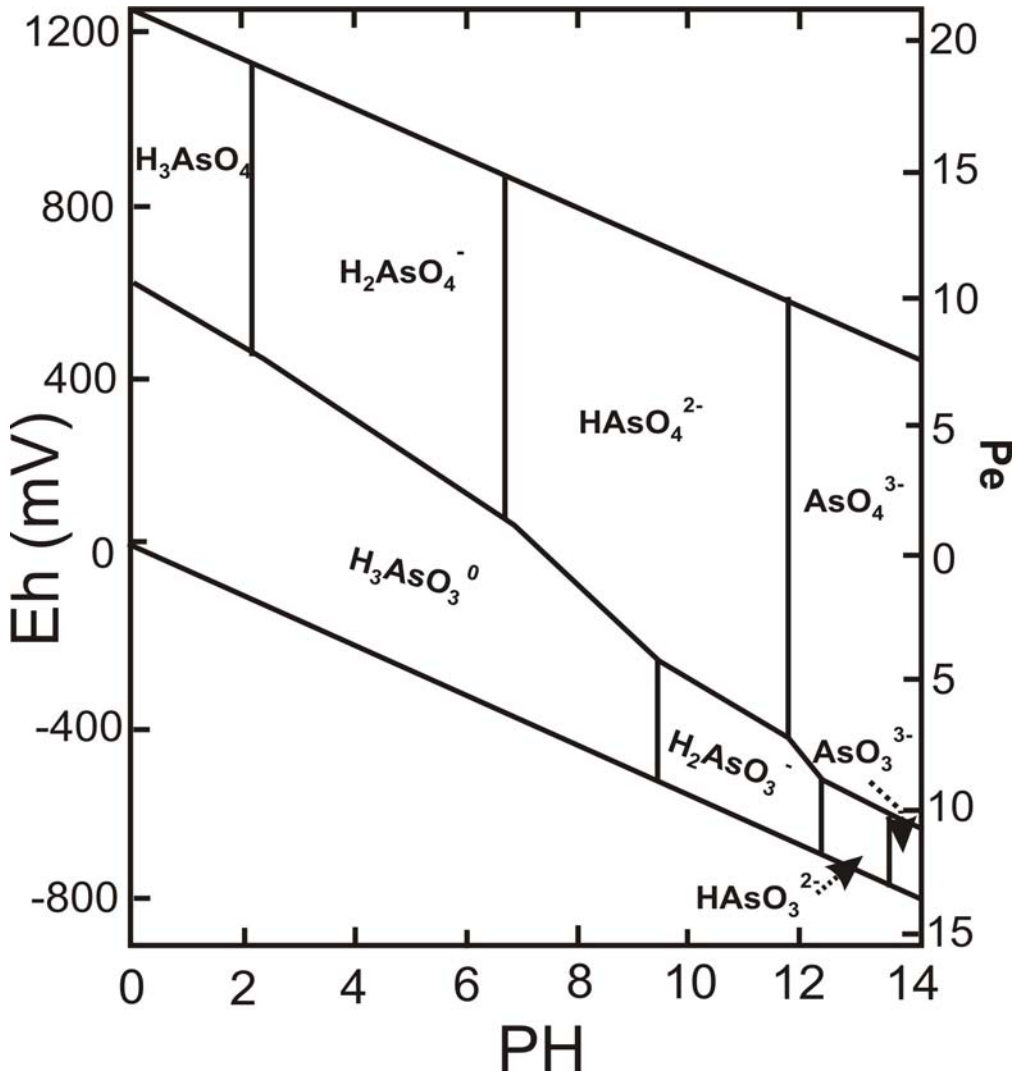

Figure 1. Eh-pH diagram for aqueous arsenic species in the system As–O_2–H_2O at 25 C and 1bar total pressure [11].

However, because the kinetics of arsenic redox transformations are relatively slow, both oxidation states are commonly found in soil and subsurface environments regardless of the redox condition [19]. Arsenic concentrations in groundwater vary widely because they are affected by rock type, mineralogy and geochemical conditions. Minerals such as iron oxides are thought to be important in controlling arsenic mobility [20].

Table 1 Acidity constants for As (V) and As (III) [21].

Reaction	Log K
As (V) (arsenic acid)	
$H_2AsO_4^- + H^+ = H_3AsO_4$	2.24
$HAsO_4^{-2} + H^+ = H_2AsO_4^-$	6.96
$AsO_4^{-3} + H^+ = HAsO_4^{-2}$	11.50
As (III) (arsenous acid)	
$H_2AsO_3^- + H^+ = H_3AsO_3$	9.22
$HAsO_3^{-2} + H^+ = H_2AsO_3^-$	12.11
$AsO_3^{-3} + H^+ = HAsO_3^{-2}$	13.41

Conflicting mechanisms are invoked including arguments based on microbial reduction of As V [22], reductive dissolution of iron oxy-hydroxides phases, and competition of solutes for sorption sites on iron oxides [11, 23-27].

Both As (III) and As (V) show high affinity for iron oxides in soil and subsurface environments. In fact, iron oxides are implicated as controlling the solid phase in Bangladeshi geologic materials [28]. Arsenic that is associated with pyritic

sandstones is thought to be associated with Fe oxides. Under reducing conditions the solubility of these arsenic-bearing solid phases is increased and is responsible, in part, for the elevated concentrations or arsenic in the water supply [28].

1.3.Arsenic Removal Technologies

Methods for arsenic removal are well studied. The principal arsenic-removal water treatment technologies currently in use include: metal-oxide sorption using packed beds of activated aluminum [29, 30] and ferric hydroxide [31-33]; coagulation using $FeCl_3$/filtration [34, 35]; and iron oxide coated sands [36-39]. Ion exchange methods include packed beds of chloride-forming anion exchange resins. Reverse osmosis, nano-filtration, and enhanced coagulation have also been used previously [40-43]. Interfering ions, such as F^-, PO_4^{3-}, and silicate are known to affect all these processes [1, 44, 45]. These methods are pH sensitive and are better in removing As (V) compared to As (III). Application of these technologies in removing arsenic require that As (III), if present in the water, is oxidized to As (V) prior to arsenic removal using free chlorine, hypochlorite, permanganate, hydrogen peroxide, oxygen or an alternative oxidant. Oxidation of reduced arsenic is reported through use of UV [46].

All oxidants have their advantages and disadvantages that should be taken into account when applying a particular method. For example, chlorine has the possibility of producing elevated concentrations of unwanted disinfection by-products with organic matter in addition to the release of taste and odor compounds from algal cells [47]. It should be noted that oxidation alone cannot serve as a sufficient technology

for arsenic removal, though it may well be employed as a pre-treatment step to increase the removal method efficiency. Other technologies are membrane units including coagulation/micro-filtration, reverse osmosis (e.g. nano-filtration and hyper-filtration), and electro-dialysis, which all use special filter media that physically retain the impurities present in water. Filtration methods require a power source that may be unavailable or unreliable (e.g. in the rural Ghana and Bangladesh delta areas). Other processes in addition to the widely used methods discussed above include microbial processes, *in-situ* immobilization, and point-of-use units. All the afore mentioned technologies are either expensive or not readily available to rural communities, commanding the need for cost-effective and widely available, naturally occurring mechanisms, namely adsorbant iron and aluminum oxy-hydroxides.

1.4. LATERITES AND LATERITIC SOILS

Laterites and lateritic soils composed of a wide variety of red, brown, and yellow fine-grained residual soils of light texture, as well as nodular gravels and cemented soils [4, 5, 48, 49]. They may vary from a loose material to a massive rock. They are characterized by the presence of iron and aluminum oxides or hydroxides, particularly those of iron, which give color to the soils [50]. For the purpose of this work, the term "laterite concretion" (LC) is confined to the coarse-grained vermicular concrete material, including massive laterite. The term "lateritic soils" refers to materials with lower concentrations of oxides. Lateritic soils behave more like fine-grained sands, gravels, and soft rocks. The laterite typically has a porous or vesicular appearance.

Some particles of laterite tend to crush easily under impact, disintegrating into a soil material that may behave plastically [50].

Lateritization is the removal of silicon through hydrolysis and oxidation that results in the formation of laterites and lateritic soils. The degree of lateritization is estimated by the silica-sesquioxide (S-S) ratio ($SiO_2/(Fe_2O_3 + Al_2O_3)$) calculated as the weight percent of the minerals. Soils are classified by the S-S ratios into the following categories:

- An S-S ratio of 1.33 or less = laterite.
- An S-S ratio of 1.33 to 2.00 = lateritic soil.
- An S-S ratio of 2.00 or greater = non-lateritic, tropical soil [51]

1.5. PRESTEA AND AWASO LATERITE CONCRETIONS

Laterite concretions, a natural substance, contain intergrowths of iron, manganese, titanium and aluminum, as oxides and hydroxides, with admixed quartz grains and clay minerals [4, 5, 48, 49]. They are a product of intensive chemical weathering in tropical and subtropical environments under strong oxidizing conditions. Heavy rainfall leaches out soluble weathering products in lateritic soils, leaving behind clay minerals (koalinite), rutile (TiO_2), gibbsite ($Al_2O_3.3H_2O$), goethite ($HFeO_2$), lepidocrosite (FeOOH), and hematite (Fe_2O_3) [4, 5, 48, 49]. Iron is mobile in the weathering zone (C-horizon), most likely as Fe^{2+}, and migrates to the B-Horizon. Well-developed lateritic soils have a lower iron-free, buff-colored horizon, called the paled zone or B2 horizon and an upper brick red, iron-rich B1 horizon. Commonly iron mineral concretions form that incorporate other soil constituents [50, 52]. In

extreme cases fericrete (called *canga* in South America) forms that may be up to 5m thick. Most commonly, lateritic soils have iron concretions that vary from pebble-size to cobble-size [53].

Lateritic soils are abundantly available in Ghana and other tropical regions. Notable areas in Ghana where these lateritic soils abound are Prestea and Awaso (Fig. 2). These two areas were selected because they represent the end members of most lateritic soils. Prestea is located in southwest Ghana approximately 200 kilometers west of the capital, Accra, and is accessible by sealed road. Prestea lies within the Eburnean Tectonic Province (1,800-2,166 Ma) in the West African Precambrian Shield. The bed rock there –consists of Proterozoic Birimian greenstones that contain metamorphosed basaltic and andesitic lavas (hornblende-actinolite-schist, calcareous-chlorite-schist and amphibolites/greenstones) of the West African craton [54, 55]. The original soil mantle of Prestea contained feldspathic materials, other silicates, and minor amounts of stable materials. Intense chemical weathering subsequently transformed the feldspathic material into clay, then leaching and re-deposition occurred in which iron and aluminum oxides remained after the removal of bases and combined silica [52]. Next in the forming process is a dramatic change in environment: physical, such as evaporation of the remaining water: chemical, such as the reduction of groundwater temperature; ion exchange; or pH change [52]. This results in the deposition of iron compounds and concretions. These concretions usually form as nodules with a hard outer shell of ferrous material surrounding an inner core of softer or un-cemented materials [52]. A crust thus develops which, in French-speaking Africa, is known as fericrete (iron breast plate) [52].

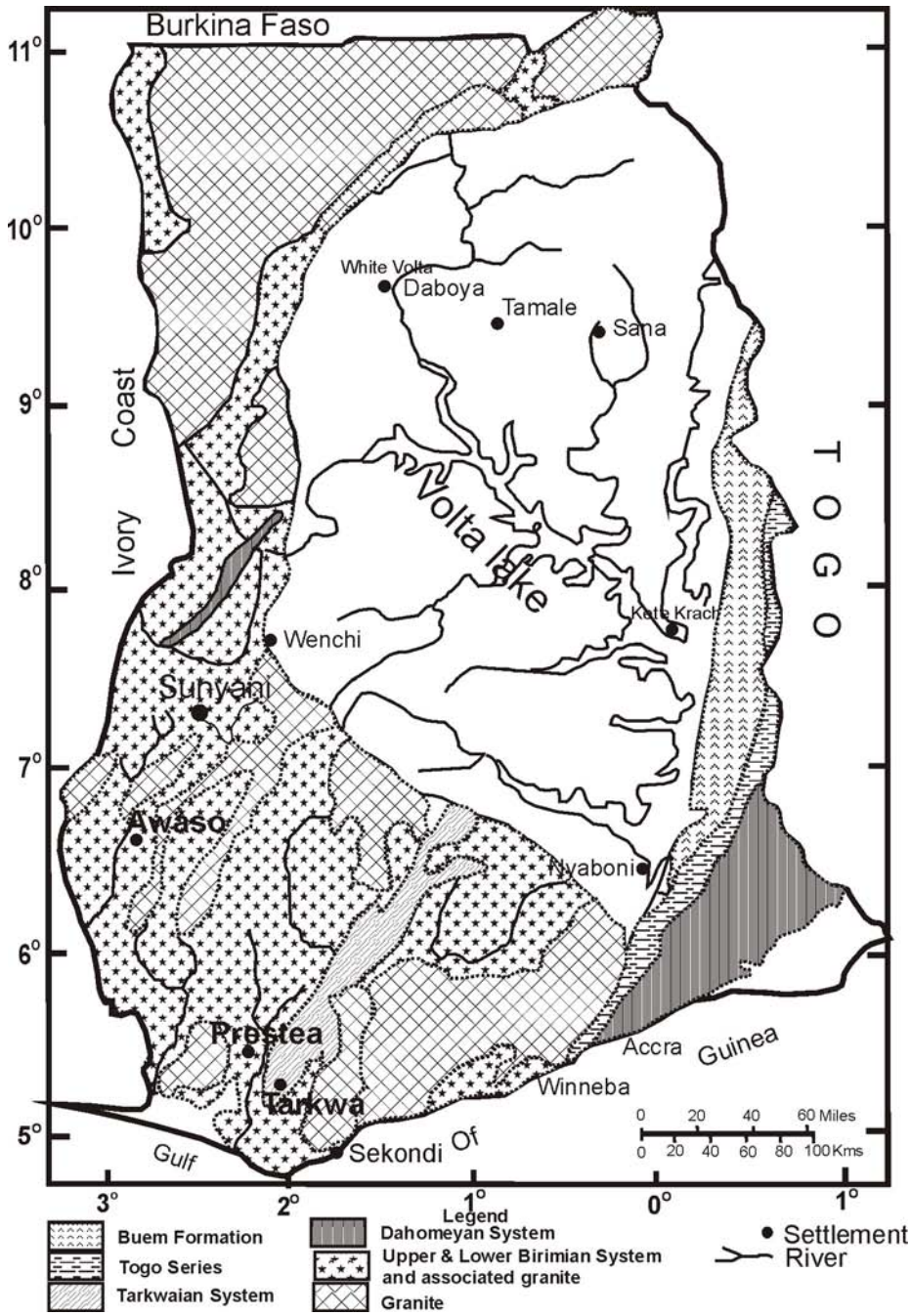

Figure 2. Map of Ghana showing geologic units.

Awaso is located in the north-eastern part of the Western Region of Ghana approximately 220 kilometers north of Prestea. The bed rock of Awaso contains

aluminum rich facies that have given rise to the secondary residual accumulation of bauxite [54, 55]. The formation of Awaso Laterite concretion is different from that of the Prestea laterite concretions. Intense chemical weathering of the impermeable feldspathic materials (clays and silts) from weathered igneous rocks present a horizon that further weathers to kaolinite. The process of lateritization proceeds, which is essentially a de-silication process, laterite being formed by the decomposition of hydrated silicates of alumina, accompanied by the freeing of the silica into solution. The residual alumina takes up water from groundwater percolating downward and leaches the soluble minerals leading to the accumulation of tri-hydrate of aluminum (gibbsite $Al_2O.3H_2O$) and iron compounds. In areas where the process continues to completion, oxides of titanium are formed together with gibbsite. This process forms canga or hardpan, which is developed over the bauxite [52].

Laterite can be used to develop an effective and inexpensive water purification system for communities that costs little, is easy to maintain, and produces high quality drinking water [56-59]. Bhattacharyya et al. 2002 [56] establish the role of laterite (ferralite) enriched with natural HFO as an arsenic scavenger through batch studies and demonstrated the better competency of the material over the natural/commonly used chemical coagulants generally used for water treatment. They conclude that materials with a wide pH range sorb both As (III) and As (V) from well-buffered groundwater and the presence of Fe (II) in the system enhances the arsenic removal process.

Ndur and Norman, 2003 [58] developed an arsenic filter that uses laterite concretions to remove arsenic. Their goal was to make an arsenic-iron removal

system for less developed countries that costs little to operate and could be fabricated with locally obtained supplies. They showed that the sorption capacity for 2 mm grains is about 300 bed volumes of 1 ppm arsenic water. Contact times of 10 to 15 minutes reduce arsenic concentrations by about a factor of 100 to 1000, which allow the fabrication of fast-flow filters [58].

1.6. RELATED RESEARCH ON MECHANISM OF ARSENIC SORPTION

Studies regarding mechanisms responsible for arsenic sorption onto metal oxides have greatly enhanced the understanding of sorption processes, and an extension of this approach to natural systems is now beginning. There is little reported on mechanisms of arsenic sorption onto natural materials due to problems with detailed characterization of the solid phases and their surface composition [60]. Various researchers [15, 61-70] have combined microscopic and macroscopic techniques to delineate sorption mechanisms of arsenic onto single hydrous metal-oxides but not onto natural materials that are combinations of many oxides and of unknown crystalinity. One tool widely used to delineate sorption mechanisms is ionic strength. Hayes et al. [70], Goldberg and Johnson, [15], and Pena et al. [71] postulated anion sorption, which is either markedly reduced or increased by increasing ionic strength, can be used to describe sorption mechanisms. Others [15, 71, 72] use electrophoretic mobility (EM) measurements, including point of zero charge (PZC), and potentiometric titration data to distinguish between inner- and outer-sphere complexes.

X-ray Absorption Spectroscopic evidence indicates that arsenic forms either inner-sphere or outer-sphere complexes on iron and aluminum oxide surfaces [61, 63, 65, 66, 73]. Extended X-ray absorption fine structure (EXAFS) spectroscopy shows evidence of an inner-sphere bidentate binuclear surface complex [61, 63, 65, 66, 73, 74], wide angle X-ray scattering (WAXS) [75], and Fourier transform infrared (FTIR) spectroscopy [63]. Several different surface species can form a mono-dentate complex at low surface coverage and bidentate complexes at moderate to high surface loadings [68]. O'Reilly et al. [66] found further EXAFS evidence of a bidentate binuclear structure at the As (V)-goethite surface and showed that sorption was rapid with 93% of sorption occurring within the first 24 hours. Arsenic (V) desorption in a phosphate solution was initially rapid, but reached a plateau after ~35% of the arsenic was desorbed. Extended X-ray absorption fine structure [64] and FTIR [63, 76] studies of As (III) at the goethite surface suggest an inner-sphere bidentate binuclear bridging complex similar to that of As (V). Fourier transform infrared studies [15] of As (III) sorption at the amorphous aluminum oxide surface suggest an outer-sphere complex unlike the inner-sphere complex for As (V). Information on the structure of arsenic surface complexes gleaned from spectroscopic studies may also be used to determine the mechanism of arsenic sorption onto metal oxides.

1.7 SORPTION CHEMISTRY AND APPROACHES TO SORPTION MECHANISMS WITH COMPOSITE MATERIAL

Understanding sorption mechanism is crucial to optimal use of composite materials in remediating arsenic from drinking water. Several approaches has been used, here I present four of these approaches. The first approach to sorption using

composite/natural materials in detailed solid phases characterization is to know the surface composition of the material. Physical and chemical properties of the composite materials mineral assemblage are needed to design sorption experiments. X-ray diffraction and X-ray fluorescence can be used to determine the predominant mineral phases. These analyses help identify dominant adsorptive phases to design sorption experiments and for surface complexation modeling purposes. In surface complexation theory, surface functional groups are the reactants with ions that determine surface speciation. A thorough understanding of the concentration (surface density) and types of functional groups are needed to calculate the effects of sorption equilibra on aqueous composition [60].

The second approach is to determine the material's specific surface area by a surface area analyzer.

The third approach is quantification of proton-binding sites of the composite material. This can be carried out by a conventional potentiometric titration method. Quantities of the composite material suspension should be well equilibrated for 24 hours at the desired ionic strength. Prior to the equilibration and throughout the titration the sample can be purged with pure N_2 (99.996%) to minimize CO_2 contamination. Three titration experiments should be performed on the basis of different electrolyte concentrations (0.1, 0.01, and 0.001 M NaCl). The surface charge (σ H) can be calculated using equation (1) below.

$$\sigma \mathrm{H} = \frac{\left(C_A - C_B + \left[OH^-\right] - \left[H^+\right]\right)}{a} \frac{F}{S} \qquad (1)$$

Where σ H is the surface charge (C/m2), C_A is added acid concentration, C_B is added base concentration, [OH^-] is the hydroxyl ion concentration, [H^+] is the proton concentration, a is solid used (g/L), F is the Faraday constant (96,500 C), and S represents the specific surface area (m^2/g). Variation of surface charge as a function of pH in background electrolyte (0.1, 0.01, and 0.001 M NaCl) can be estimated experimentally for proton-binding sites of the material.

The fourth is a surface complexation modeling approach. Two approaches exist in literature: (1) Component additivity approach and (2) the generalized composite modeling approach. Both of these approaches have their pros and cons. The component additivity approach assumes that (A) the relative abundance of surface functional groups is proportional to the bulk mineralogical composition as determined by X-ray analysis, or (B) the adsorptive reactivity of the mineral assemblage is dominated by one or two specific mineral phases, such as iron and aluminum oxides [77]. This approach requires mass action equations and associated stability constants for every mineral phase, which makes the approach complex. However, the advantage of this approach is that the stability constants can be valid for other mineral assemblages. The generalized composite modeling approach requires less information and can be viewed as more practical for application within solute transport models. However, the generalized composite approach's mass action equations and associated stability constants are valid only for the specific mineral assemblage studied and are not transferable to other mineral assemblages. In addition this approach does not utilize conclusions about actual surface speciation that may be determined from spectroscopic methods [60, 77].

The fifth approach is to delineate mechanisms of ion attachment on composite material surfaces using spectroscopic techniques. For applicability to natural systems, spectroscopic methods must be capable of evaluating surface-adsorbed ions in the presence of water. Fourier transform infrared (FTIR) and extended X-ray absorption fine structure (EXAFS) are both capable of investigating the position of As-O stretching bands for arsenic in aqueous conditions.

CHAPTER 2

MATERIALS AND EXPERIMENTAL PROCEDURE

2.1. Characterization of Prestea and Awaso LC

The LC used for this study was obtained from Prestea, Ghana (5^{o} $28^{'}$ 15.06" N and 2^{o} 11 27.17" W) and Awaso, Ghana (6^{o} $27^{'}$ 31.68" N and 2^{o} 19 39.72" W). X-ray diffraction (XRD) and X-ray fluorescence (XRF) were used to determine the predominant mineral phases. The X-ray diffraction pattern for the Prestea laterite concretions was determined on a Rigaku DMAX/2 in the Chemistry Department at New Mexico Tech using a purpose-designed in-process powder X-ray diffraction system recently enhanced through the incorporation of a Bede Micro source high-brightness X-ray generator. Samples were crushed to fine powder (< 63 μm), then 4-5 g of powder was compressed into an *in situ* X-ray cell. Profiles were measured from 2–70^{o} in step sizes of 0.02^{o}/s requiring 56 min. Major and minor minerals in concentrations > than about 5% were identified using the MDI Jade7 software [78].

X-ray fluorescence experiments were done by Thermo-ARL automated X-ray fluorescence spectrometer (XRF) at Washington State University. Samples were crushed into fine powder, weighed with dilithium tetraborate flux (2:1 flux: rock), fused at 1000°C in a muffle furnace, and then cooled; the bead was then reground, refused and polished on diamond laps to provide a smooth flat surface. Advantages of the low-dilution fusion method include reduction of matrix effects, robustness, economy of sample preparation time, and cleanliness of the instrument. The same suite of elements was analyzed for all samples, which includes the 10 major rock-forming elements, plus 18 trace elements.

Specific surface areas of ground Prestea and Awaso LC used for sorption experiments were determined with a single-point BET N_2 sorption isotherm using a Quantasorb Jr. Surface area analyzer. Samples of LC were degassed at 70°C before determining the surface area.

2.2 Sorption Isotherm

Arsenic (III) and As (V) stock solutions were prepared by dissolving sodium arsenite, $AsNaO_2$ (J.T. Baker, reagent grade) and sodium biarsenate ($Na_2HAsO_4.7H_2O$ (BDH, reagent grade)) in water purified by reverse osmosis (RO). Prestea and Awaso laterite concretions were crushed to <63 μm and the fines removed by washing. To determine the sorption isotherms, 50cc aliquots of 20°C As (III) and As (V) solutions with concentrations ranging from 0.1 to 2.0 mg/L arsenic were reacted with 0.25 g or 0.75 g of either Prestea or Awaso ground laterite concretions. Samples and solutions were placed in 100 mL polypropylene centrifuge tubes with covers.

The As (III) mixtures were shaken with a tumbler revolving at 20 revolutions per minute for 2 hours and the As (V) mixtures for 1 hour at 20°C. Previous work showed that these times were sufficient to reach near equilibrium [79]. Equilibrium pH was measured using a Mettler Toledo MP 125 (THOMAS SCIENTIFIC). The samples were centrifuged at a relative centrifugal force of 7800 *g* for 20 min. The supernatants were analyzed for pH and filtered through a 0.2μm Whatman filter. The supernatant liquid was analyzed for arsenic concentration using a Varian 600 Atomic Adsorption Spectrometer with Graphite Furnace.

Isotherm experiments were conducted following batch experiment procedures described above at 25°C, 35°C, 45°C and 60°C in a temperature controlled bath to investigate the effect of temperature on arsenic sorption. Fifty cc aliquots of As (III) and As (V) solutions with concentrations ranging from 0.1 to 2.0mg/L arsenic were reacted with 0.25g of ground Prestea laterite concretion. Blank tests with no laterite demonstrated no arsenic was adsorbed on the wall of the flask during the reaction period. Duplicate experiments demonstrated that results obtained from this sorption procedure are repeatable and with a maximum experimental error of 3%.

2.3. Sorption Envelopes

Arsenic (III) and As (V) stock solutions were prepared with reverse osmosis (RO) water using sodium arsenite, (AsNaO2, J.T. Baker, reagent grade) and sodium biarsenate ($Na_2HAsO_4.7H_2O$, BDH, reagent grade), respectively. Sorption envelopes were determined for an arsenic concentration of 1.0 mg/L by varing the pH from 4 to 10 and at ionic strengths of 0.001, 0.01, and 0.1 M NaCl. Then these solutions were placed into 50 cc polypropylene centrifuge tubes containing either 0.25 g or 0.75 g of ground laterite concretions. The tubes were put in a tumbler rotating at 20 revolutions per minute for 2 hours and 1 hour for As (III) and As (V), respectively, at 20^oC. Kinetic results [80] show that 2 hour and 1 hour contact times were sufficient to reach sorption equilibrium for As (III) and As (V), respectively. Ionic strengths were adjusted to 0.001, 0.01, and 0.1 M NaCl. To obtain the required pH the suspension was adjusted with 1.0 M HCl or NaOH, which caused a less than 0.00001 M change in the final concentration of the ionic strengths tested. The equilibrium pH was

measured using a Mettler Toledo MP 125 (THOMAS SCIENTIFIC). The samples were centrifuged at a relative centrifugal force of 7800*g* for 20 min. The decantates were analyzed for pH and filtered through a 0.2μm Whatman filter. The supernatant was analyzed for arsenic concentration using a 600 Varian Graphite Atomic Absorption Spectrometer. The quantity of adsorbed arsenic was calculated by the difference between the initial and residual amounts of arsenic in the solution divided by the weight of the adsorbent. Blank tests under the same conditions demonstrated no arsenic adsorbed on the wall of the flask during the reaction period. Duplicate experiments demonstrated that results obtained from this sorption procedure were repeatable with a precision of 97%.

2.4 Competitive sorption

The interference of phosphate and sulfate on arsenic sorption was investigated in batch experiments. The methods used are similar to the batch experiments described above. The difference is arsenic concentration of 1.0 mg/L was added to the 10.0 mg/L of phosphate solution, and in a separate experiment 1.0 mg/L of arsenic solution was added to a 500.0 mg/L sulfate solution.

2.5 Surface titration

The quantification of proton-binding sites was carried out by a conventional potentiometric titration method. A quantity of 20 g/L of the <63μm fraction of the NRE suspension was equilibrated well at the desired ionic strength for 24 hours. Prior to the equilibration and throughout the titration the sample was purged with pure N2

(99.996%) to minimize CO_2 contamination. Three titration experiments were performed on the basis of different electrolytic concentrations (0.1, 0.01, and 0.001 M NaCl). The initial pH of the LC suspension was ≈6.0 and it was raised to ≈10 with 0.1 M NaOH before commencement of titrations. In order to minimize the solid dissolution the solution pH was kept above 4.0. The surface charge (σ H) was calculated using equation (1) above. The surface charge is needed as an input parameter in the computer program FITEQL [81] to determine surface acidity and arsenic binding constants. The variation of the surface charge of LC suspensions as a function of pH in 0.1, 0.01, and 0.001 M NaCl shows that the σ H is mainly controlled by the H^+ and OH^- ions.

2. 6. Electrophoritic Mobility

The electrophoretic mobility (EM) for the LC was determined by micro-electrophoresis using a Zeta-Meter 3.0 system. The EMs of < 5μm LC suspensions containing 0.2g of solid L^{-1} in 0.01M NaCl were determined at various pH values. Electrophoretic mobility measurements were also determined in the presence and absence of 0.035mM and 3.5mM of arsenic and with a final volume of 50mL after adjusting to the desired pH (4-10) with 0.1M HCl or NaOH. The suspension was shaken for 2 hours and 1 hour respectively for As (III) and As (V) at 22°C. In general, an average EM value was obtained after 20 particles were counted. The point of zero charge was obtained by interpolating the data to zero EM.

2.7. ATR-FTIR Spectroscopy

Samples for spectroscopic analysis were prepared by reacting 2.0g of LC with 20ml of a 0.1M NaCl solution containing 0.1M of either As (III) at pH 5 and 10.5 or As (V) at pH 5 and 9. Samples were used wet or rinsed with 20ml of doubly de-ionized water and air-dried. Reference samples were reacted with a solution containing only 0.1M NaCl. Fourier Transformed Infra Red spectra were obtained with an Avatar 370 Model spectrometer and a horizontal attenuated total reflectance (ATR) attachment (see appendix 1.0 for detailed theory). Spectra were obtained at a resolution of $4cm^{-1}$ with each spectrum corresponding to the co-addition of 64 scans using a medium-band liquid N_2 cooled DTGS detector. Infrared spectra of As (V) and As (III) sorbed on LC were obtained as dry samples in KBr pellets prepared by adding 3mg of ground LC in approximately 250mg of spectral grade KBr. Attenuated total reflectance of 1ml of 0.1M NaCl and 0.1M arsenic, a reference solution, was recorded.

2.8. Surface Complexation Models

I modeled the surface complexation of laterite concretions using the generalized composite approach (GC). This approach assumes that all mineral phases contribute to sorption and the sorption sites are represented by one type of surface group. Several caveats exist with the GC approach. Derived constants for surface complexation are valid only for the system under study and cannot be transferred to other systems; in addition, it has fewer equations hence the degrees of freedom are likely to be very small. The computer program FITEQL [81] was used to determine

the surface acidity and arsenic binding constants. The stoichiometries of the surface complexes used to fit sorption data are listed in Tables 2 and 3. The specific surface area of the LC was determined with a single-point BET N_2 adsorption isotherm using a Quantasorb, Jr. Surface area analyzer. The surface site densities were set at a value of 2.31 sites/nm^{-2} as set by Davis and Kent [60] for natural materials. Surface complexation constants were optimized, model predictions with fixed site densities and complexation constants were performed using MINTEQA2 [82]. The activity coefficients of aqueous species were calculated using the Davies equation for both model fitting and predictions. The concepts behind several models and an excellent review of the current state of SC modeling theory are presented by Goldberg et al. [15] (Also see Appendix 2.0).

In the diffuse double layer model, surface complexation reactions for the surface functional group SOH (where SOH represents a reactive surface hydroxyl bound to a metal ion in the oxide mineral) are defined in Tables 2 and 3. The diffuse double layer model assumes that the surface complexes are all inner-sphere. The intrinsic equilibrium constants for the inner-sphere surface complexation reactions of the surface functional group are given in Table 2.

The triple-layer model (TLM) is more intricate than the DLM which allow ion sorption as either inner-sphere or outer-sphere complexes. As the name indicates, three electrostatic boundaries are used. In the TLM, the electrostatic layer closest to the solid surface uses a linear decay function for charge. The innermost layer is used for inner-sphere surface complexation. The second layer, which uses a linear decay function of smaller magnitude than the inner layer, is used for sorption of outer-

sphere complexes. The outermost layer from the surface uses the exponential decay function found in the diffuse layer model.

The triple-layer model considers outer-sphere surface complexation reactions for the background electrolyte in addition to the inner-sphere surface complexation reactions. Triple-layer model inner-sphere surface complexation reactions and intrinsic equilibrium constant expressions for As (V) and As (III) are given in Table 3. The outer-sphere surface complexation reactions and the intrinsic equilibrium constants for As (V) and As (III) are also given in Table 3.

Table 2. Equations and Reactions Used in the Diffuse double layer Models.

Diffuse double layer model	
Surface complexation reactions	
$SOH_{(s)} + H^{+}_{(aq)} \Leftrightarrow SOH_2^{+}{}_{(s)}$	(2)
$SOH_{(s)} \Leftrightarrow SO^{-}_{(s)} + H^{+}_{(aq)}$	(3)
$SOH_{(s)} + H_3AsO_{4\,(aq)} \Leftrightarrow SH_2AsO_{4(s)} + H_2O$	(4)
$SOH_{(s)} + H_3AsO_{4\,(aq)} \Leftrightarrow SHAsO_4^{-}{}_{(s)} + H^{+}_{(aq)} + H_2O$	(5)
$SOH_{(s)} + H_3AsO_{4(aq)} \Leftrightarrow SAsO_4^{2-}{}_{(s)} + 2H^{+}_{(aq)} + H_2O$	(6)
$SOH_{(s)} + H_3AsO_{3\,(aq)} \Leftrightarrow SH_2AsO_{3\,(s)} + H_2O$	(7)
$SOH_{(s)} + H_3AsO_{3\,(aq)} \Leftrightarrow SHAsO_3^{-}{}_{(s)} + H_2O$	(8)
Surface complexation constants	
$K_{+\,(int)} = \dfrac{[SOH_2^{+}]}{[SOH][H^{+}]} \exp(F\Psi_o / RT)$	(9)
$K_{-\,(int)} = \dfrac{[SO^{-}][H^{+}]}{[SOH]} \exp(-F\Psi_o / RT)$	(10)
$K^{lis}_{As(V)}(\text{int}) = \dfrac{[SH_2AsO_4]}{[SOH][H_3AsO_4]}$	(11)

$$K^{2is}_{As(V)}(\text{int}) = \frac{[SHAsO_4^-][H^+]}{[SOH][H_3AsO_4]}\exp(-F\Psi_o / RT) \quad (12)$$

$$K^{3is}_{As(V)}(\text{int}) = \frac{[SHAsO_4^{2-}][H^+]^2}{[SOH][H_3AsO_4]}\exp(-2F\Psi_o / RT) \quad (13)$$

$$K^{1is}_{As(III)}(\text{int}) = \frac{[SH_2AsO_3]}{[SOH][H_3AsO_3]} \quad (14)$$

$$K^{2is}_{As(III)}(\text{int}) = \frac{[SHAsO_3^-][H^+]}{[SOH][H_3AsO_3]}\exp(-F\Psi_o / RT) \quad (15)$$

Mass balance

$$[SOH]_T = [SOH]+[SOH_2^+]+[SO^-]+[SH_2AsO_4]+[SHAsO4_4^-]+[SAsO_4^{2-}] \quad (16)$$

$$[SOH]_T = [SOH]+[SOH_2^+]+[SO^-]+[SH_2AsO_3]+[SHAsO4_3^-] \quad (17)$$

Charge balances

$$\sigma_o=[SOH_2^-]-[SO^-]-[SHAsO_4^-]-2[SAsO_4^{2-}] \quad (18)$$

$$\sigma_o=[SOH_2^-]-[SO^-]-[SHAsO_3^-] \quad (19)$$

Surface charge/ surface potential relationships

$$\sigma_o=\frac{S_A C_P}{F}\Psi_o \quad (20)$$

Table 3. Equations and Reactions Used in the Triple-Layer Models.

Triple layer model (includes Eqs. [11] – [24] from the diffuse double layer model	
$SOH_{(s)} + Na^+_{(aq)} \Leftrightarrow SO^- - Na^+_{(s)} + H^+_{(aq)}$	(21)
$SOH_{(s)} + H^+ + Cl^-_{(aq)} \Leftrightarrow SOH_2^+ - Cl^-_{(s)}$	(22)
$SOH_{(s)} + H_3AsO_4\ _{(aq)} \Leftrightarrow SOH_2^+ - H_2AsO_4^-\ _{(s)}$	(23)
$SOH_{(s)} + H_3AsO_4\ _{(aq)} \Leftrightarrow SOH_2^+ - HAsO_4^{2-}\ _{(s)} + H^+_{(aq)}$	(24)

$$SOH_{(s)} + H_3AsO_{4\ (aq)} \Leftrightarrow SOH_2^+ - AsO_{4\ (s)}^{3-} + 2H^+_{(aq)} \quad (25)$$

$$SOH_{(s)} + H_3AsO_{3\ (aq)} \Leftrightarrow SOH_2^+ - H_2AsO_{3\ (s)}^- \quad (26)$$

$$SOH_{(s)} + H_3AsO_{3\ (aq)} \Leftrightarrow SOH_2^+ - HAsO_{3\ (s)}^{2-} + H^+_{(aq)} \quad (27)$$

$$SOH_{(s)} + H_3AsO_{3\ (aq)} \Leftrightarrow (SOH_2^+)_2 - HAsO_{3\ (s)}^{2-} \quad (28)$$

$$SOH_{(s)} + H_3AsO_{3\ (aq)} \Leftrightarrow (SOH_2^+)_2 - AsO_{3\ (s)}^{3-} + H^+_{(aq)} \quad (29)$$

Surface complexation constants

$$K_{Na+}(\text{int}) = \frac{[SO^- - Na^+][H^+]}{[SOH][Na^+]} \exp[F(\Psi_\beta - \Psi_o)/RT] \quad (30)$$

$$K_{Cl-}(\text{int}) = \frac{[SOH_2^+ - Cl^-]}{[SOH][H^+][Cl^-]} \exp[F(\Psi_o - \Psi_\beta)/RT] \quad (31)$$

$$K^{1os}_{As(V)}(\text{int}) = \frac{[SOH_2^+ - H_2AsO_4^-]}{[SOH][H_3AsO_4]} \exp[F(\Psi_o - \Psi_\beta)/RT] \quad (32)$$

$$K^{2os}_{As(V)}(\text{int}) = \frac{[SOH_2^+ - HAsO_4^{2-}][H^+]}{[SOH][H_2AsO_4]} \exp[F(\Psi_o - 2\Psi_\beta)/RT] \quad (33)$$

$$K^{3os}_{As(V)}(\text{int}) = \frac{[SOH_2^+ - AsO_4^{3-}][H^+]^2}{[SOH][H_2AsO_4]} \exp[F(\Psi_o - 3\Psi_\beta)/RT] \quad (34)$$

$$K^{1os}_{As(III)}(\text{int}) = \frac{[SOH_2^+ - H_2AsO_3^-]}{[SOH][H_3AsO_3]} \exp[F(\Psi_o - \Psi_\beta)/RT] \quad (35)$$

$$K^{2os}_{As(III)}(\text{int}) = \frac{[SOH_2^+ - HAsO_3^{2-}][H^+]}{[SOH][H_3AsO_3]} \exp[F(\Psi_o - 2\Psi_\beta)/RT] \quad (36)$$

$$K^{1os}_{As(III)}(\text{int}) = \frac{[SOH_2^+ - HAsO_3^{2-}]}{[SOH]^2[H_3AsO_3]} \exp[F(2\Psi_o - 2\Psi_\beta)/RT] \quad (37)$$

$$K^{2os}_{As(III)}(\text{int}) = \frac{[SOH_2^+ - AsO_3^{3-}][H^+]}{[SOH]^2[H_3AsO_3]} \exp[F(2\Psi_o - 3\Psi_\beta)/RT] \quad (38)$$

Mass Balance

$$[SOH]_T = [SOH]+[SOH_2^+]+[SO^-]+[SH_2AsO_4]+[SHAsO_4^-]+[SAsO_4^{2-}]+[SOH_2^+ - H2AsO_4^-]+[SOH_2^+ - HAsO_4^{2-}]+[SOH_2^+ - AsO_4^{3-}]+[SO^-Na^+]+[SOH_2^+ - Cl^-] \quad (39)$$

$$[SOH]_T = [SOH]+[SOH_2^+]+[SO^-]+[SH_2AsO_3]+[SAsO_3^-]+[SOH_2^+ - H_2AsO_3^-]+[SOH_2^+ - HAsO_3^{2-}]+[SO^-Na^+]+[SOH_2^+ - Cl^-] \quad (40)$$

Charge balances

$$\sigma_o + \sigma_\beta + \sigma_d = 0 \quad (41)$$

$$\sigma_o = [SOH_2^+]+[SOH_2^+ - H2AsO_4^-]+[SOH_2^+ - HAsO_4^{2-}]+[SOH_2^+ - AsO_4^{3-}$$

$$+ [SOH_2^+ - Cl^-]-[SO^-]- [SHAsO_4^-] - 2[SAsO_4^{2-}] -[SO^- - Na^+] \quad (42)$$

$$\sigma_\beta = [SO^- - Na^+] -[SOH_2^+ - H2AsO_4^-] - [SOH_2^+ - HAsO_4^{2-}] - 3[SOH_2^+ - AsO_4^{3-}]$$

$$- [SOH_2^+ - Cl^-] \quad (43)$$

$$\sigma_o = [SOH_2^+]+[SOH_2^+ - H2AsO_3^-]+[SOH_2^+ - HAsO_3^{2-}]+[SOH_2^+ - Cl^-]+ [SO^-] -$$

$$[SHAsO_3^-] - [SO^- - Na^+] \quad (44)$$

$$\sigma_\beta = [SO^- - Na^+] -[SOH_2^+ - H2AsO_3^-] - 2[SOH_2^+ - HAsO_3^{2-}] - [SOH_2^+ - Cl^-] \quad (45)$$

Surface charge/ surface potential relationships

$$\sigma_o = \frac{C_1 S_A C_P}{F}(\Psi_o - \Psi_\beta) \quad (46)$$

$$\sigma_d = \frac{C_2 S_A C_P}{F}(\Psi_d - \Psi_\beta) \quad (47)$$

$$\sigma_d = \frac{S_A C_P}{F}\left(8\varepsilon_o DRTI\right)^{1/2} \sinh\left(F\Psi_d / 2RT\right) \quad (48)$$

Note. F is the Faraday constant (C mol_c^{-1}); Ψo is the surface potential (V); *o* refers to the surface plane of sorption; R is the molar gas constant (J mol^{-1} K^{-1});T is the absolute temperature (K); square brackets represent concentrations (mol L^{-1}); is refers to inner-sphere surface complexation; $[SOH]T$ is related to the surface site density; Ns, by $[SOH]_T = (S_A C p 10^{18})/NA * Ns$, where SA is the surface area (m^2 g^{-1}); Cp is the solid suspension density (g L^{-1}); NA is Avogadro's number; Ns has units of sites nm^{-2}; σ_o represents the surface charge (mol_c L^{-1}); C is the capacitance (F m^{-2}); β refers to the plane of outer-sphere sorption; *os* refers to outer-sphere surface complexation; $C1$ and $C2$ are capacitances; *d* refers to the plane of the diffuse ion swarm; ε_o is the permittivity of vacuum; D is the dielectric constant of water; and I is the ionic strength

CHAPTER 3

RESULTS

3.1 XRD, XRF and BET

Figure 3 and 4 show x-ray powder diffraction patterns for major and minor minerals greater than 5% in laterite concretions from Prestea and Awaso. The main minerals in Prestea laterite concretion are hematite/goethite, gibbsite, and silica. The predominant mineral phases in the Awaso laterite concretions are gibbsite, hematite and silica. Other minerals such as rutile and pyrolusite were less than 3% hence were not included in the figure. X-ray fluorescence analyses for Prestea and Awaso laterite concretions are shown in Table 4. The major oxides for both types of laterite concretion are Fe_2O_3, Al_2O_3 and SiO_2 while the minor oxides are TiO_2, Mn_2O_3, P_2O_5, CaO, and K_2O.

The specific surface area of ground Prestea and Awaso LC was performed on three samples each and the average value reported. The single-point BET N_2 sorption isotherms indicate surface areas respectively of $32m^2/g$ and $18m^2/g$.

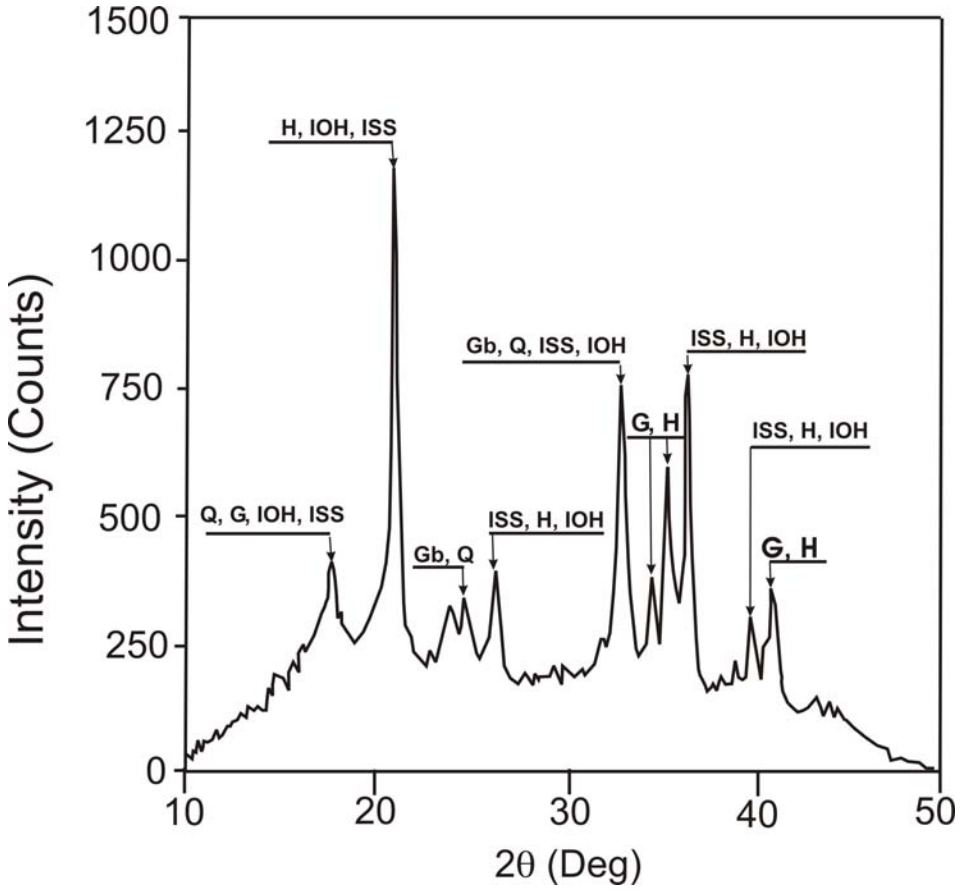

Figure 3. XRD diffractogram studies of Prestea LC with minerals greater than 5% in laterite concretions. Wavelength to compute d-spacing = 1.54A^{o} (Cu/K-alpha 1). Predominant mineral phases are Q = Quartz, G = Goethite, IOH = Iron Oxide Hydroxide, ISS = Iron Silicon Sulfide, H = Hematite, Gb = Gibbsite. The poor diffraction pattern (bump shape) shows Prestea LC is amorphous.

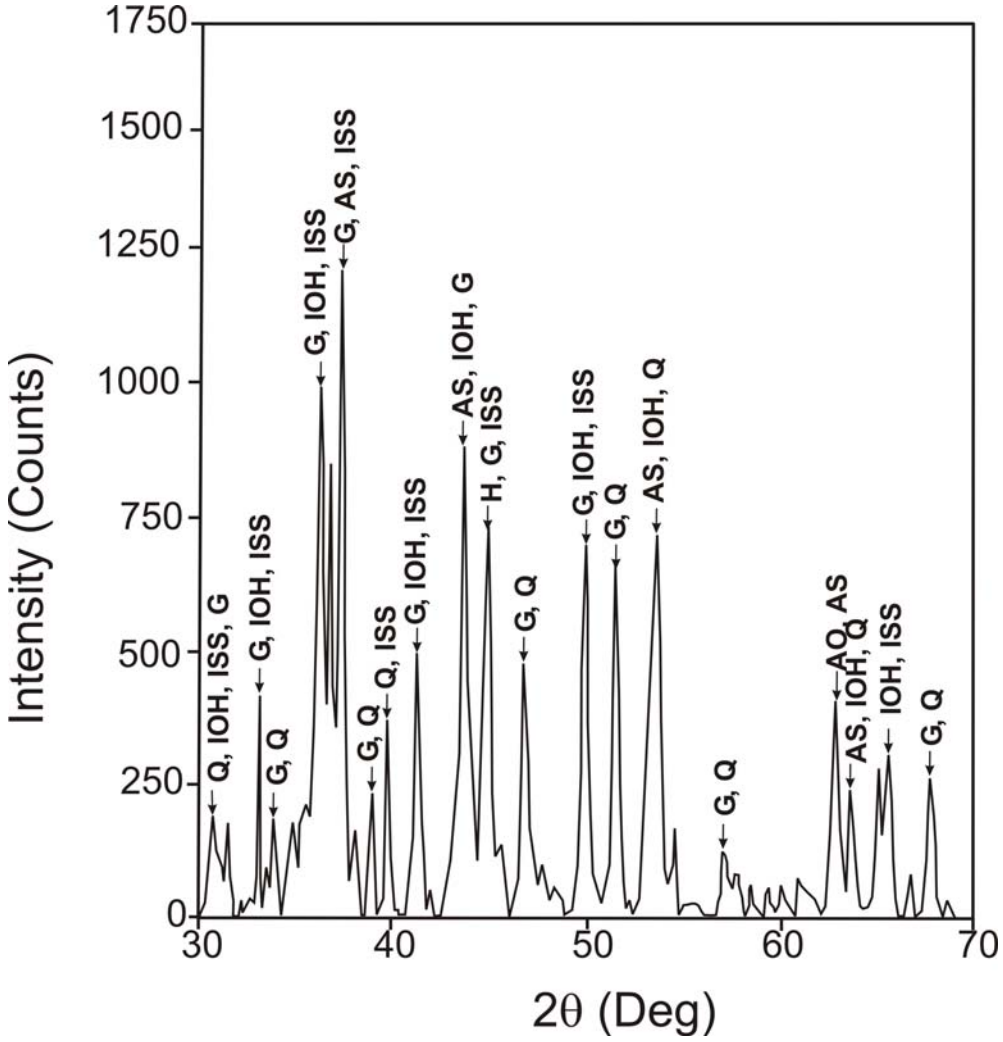

Figure 4. XRD diffractogram studies of Awaso LC with minerals greater than 5% in laterite concretions. Wavelength to compute d-spacing = 1.54A^{o} (Cu/K-alpha 1). Predominant mineral phases are Q = Quartz, G = Goethite, IOH = Iron Oxide Hydroxide, ISS = Iron Silicon Sulfide, H = Hematite, G = Gibbsite, AS = Aluminum Silicate. The excellent diffraction pattern shows Prestea LC is crystalline.

Table 4. Chemical composition of Prestea and Awaso laterite concretions

Constituents	Prestea (W) %	Awaso (W) %
SiO_2	12.47	4.80
TiO_2	0.94	3.450
Al_2O_3	13.72	78.95
Fe_2O_3	64.65	8.19
Mn_2O_3	0.02	0.003
MgO	0.00	0.00
CaO	0.06	0.04
Na_2O	0.03	0.06
K_2O	0.03	0.06
P_2O_5	0.37	4.453
LOI*	8.96	11.36

*loss on ignition

3.2 Degree of Lateritization

The calculated degree of lateritization for Prestea and Awaso laterite concretions estimated from the silica-sesquioxide (S-S) ratio ($SiO_2/(Fe_2O_3 + Al_2O_3)$) is 0.147 and 0.055 respectively.

3.3 Sorption Isotherms Results

Figures 5 and 6 show arsenic sorbed as a function of equilibrium concentration at 25°C. At all the concentrations, As (III) sorbs better than As (V) on Prestea LC (Fig. 5). However, the opposite was observed for the Awaso LC (Fig.6).

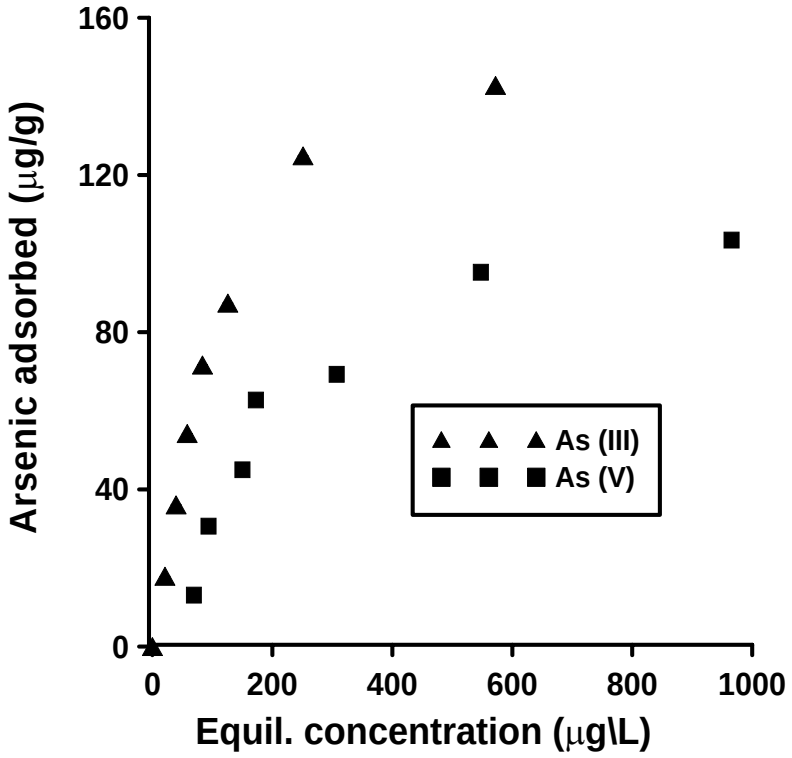

Figure 5. As (III) and As (V) sorption onto Prestea LC at 25°C. Solid suspension density = 15g/L. The pH is 7.0 ± 0.1. The 2 σ error on arsenic analysis is 3% based on the variance of measurements of 50 replicate samples. (*50 replicates are based on analysis done through out the entire arsenic analysis)

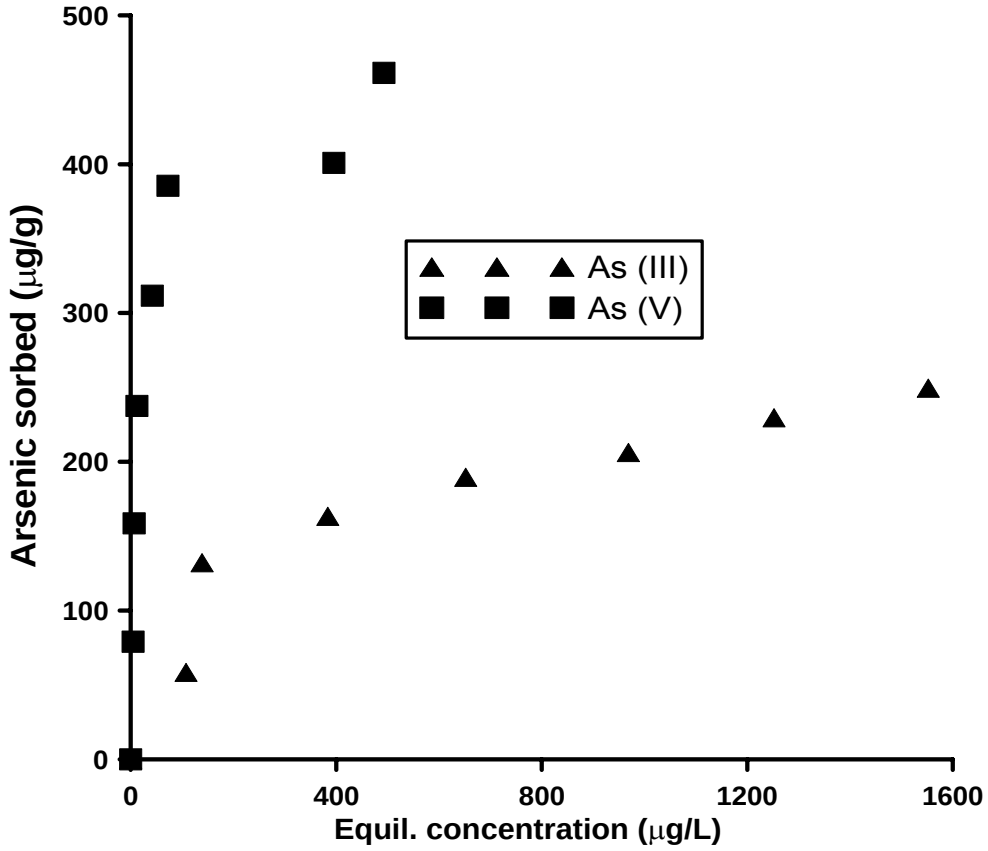

Figure 6. As (III) and As (V) sorption onto Awaso LC at 20°C. Solid suspension density = 5g/L. The pH is 7.0 ± 0.1. The 2σ error on arsenic analysis is 3% based on the variance of measurements of 50 replicate samples.

The Langmuir (equation 49) and Freundlich (equation 50) isotherms are used to fit the experimental data:

Langmuir equation: $$Q = bq_mC/(1 + bC) \quad [49]$$

Freundlich equation: $$Q = KC^{1/n} \quad [50]$$

Where Q is the amount of sorbed arsenic at equilibrium in μg/g, C is the arsenic equilibrium concentration in solution in μg/L and q_m is the maximum sorption capacity. The parameters b, K, and n are isotherm constants determined by linearization of equations 49 and 50 to:

$$1/Q = 1/q_mbC + 1/b \quad [51]$$

$$\text{Log } Q = 1/n \log C + \log K \qquad [52]$$

The estimated model parameters with their coefficient of determination (R^2) for the linearized forms are presented in Tables 5 and 6.

Table 5. Estimated Parameters for arsenic sorption (Prestea).

	Arsenite Sorption				Arsenate Sorption			
Langmuir Isotherm	25°C	35°C	45°C	60°C	25°C	35°C	45°C	60°C
$Q=q_mbC/(1+bC)$								
b (L/mmol)	1.000	1.079	0.712	0.416	0.019	0.025	0.022	0.024
q_m(µg/g)	909	1111	1428	1666	714	1000	1098	1538
R^2	0.985	0.982	0.987	0.932	0.842	0.913	0.999	0.957
Freundlich Isotherm								
$Q = KC^{1/n}$								
K	1.000	1.078	0.712	0.416	0.601	0.916	0.862	0.681
1/n	0.7496	0.7181	0.8108	0.9982	0.689	0.661	0.751	0.871
R^2	0.866	0.922	0.918	0.844	0.816	0.888	0.897	0.819

Table 6.. Estimated Parameters for arsenic sorption (Awaso).

	Arsenite Sorption	Arsenate Sorption
Langmuir Isotherm	25°C	25°C
$Q=q_mbC/(1+bC)$		
b (L/mmol)	0.11	14.87
q_m(µg/g)	434	555
R^2	0.975	0.971
Freundlich Isotherm		
$Q = KC^{1/n}$		
K	5.433	10
1/n	0.851	0.85
R^2	0.958	0.955

3.4 Effect of Temperature and Thermodynamic Parameters

The effect of temperature on arsenic sorption was considered only for Prestea LC. Results of As (III) and As (V) equilibrium sorption at 25°C, 35°C, 45°C, and 60°C are shown in Fig. 7 and 8 respectively. The sorption capacity for both As (III) and As (V) increases with increasing temperature (Table 5); however, the increase for As (V) is significantly greater than for As (III). The "Gibbs free energy ($\Delta G°$)", "standard enthalpy ($\Delta H°$)", and "standard entropy changes ($\Delta S°$)" are calculated in J $mol^{-1}K^{-1}$ for the sorption process using Eqs 53, 54, and 55 following the method of Altundogan et al. [83] and Gupta [84]:

$$\Delta G^o = -RT \ln b \text{ ----------[53]}$$

$$\ln\left(\frac{b_1}{b_2}\right) = -\frac{\Delta H}{R}\left[\frac{1}{T_1} - \frac{1}{T_2}\right] \text{ ----------[54]}$$

$$\Delta G^o = \Delta H^o - T\Delta S^o \text{ ---------- [55]}$$

Where b is a Langmuir isotherm constant (L/mol) at temperature T (K) and R is an ideal gas constant (8.314 J/mol.K). The data and calculated thermodynamic parameters are given in Table 7. The Langmuir isotherm constant was used in place of the "real" thermodynamic constant in order to calculate the thermodynamic parameters. Also the Langmuir constant is equivalent to equilibrium constant in adsorption solutions and, arbitrarily, it is used in place of equilibrium constant [84].

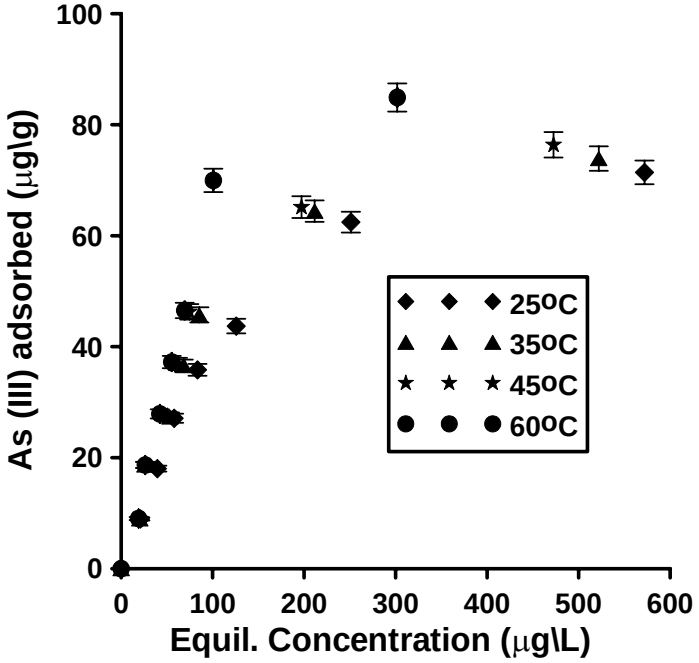

Figure 7. As (III) at 25 °C, 35°C, 45 °C, and 60 °C. Solid suspension density = 15 g/L. The pH is 7.0 ± 0.1. The 2σ error on arsenic analysis is 3% based on the variance of measurements of 50 replicate samples.

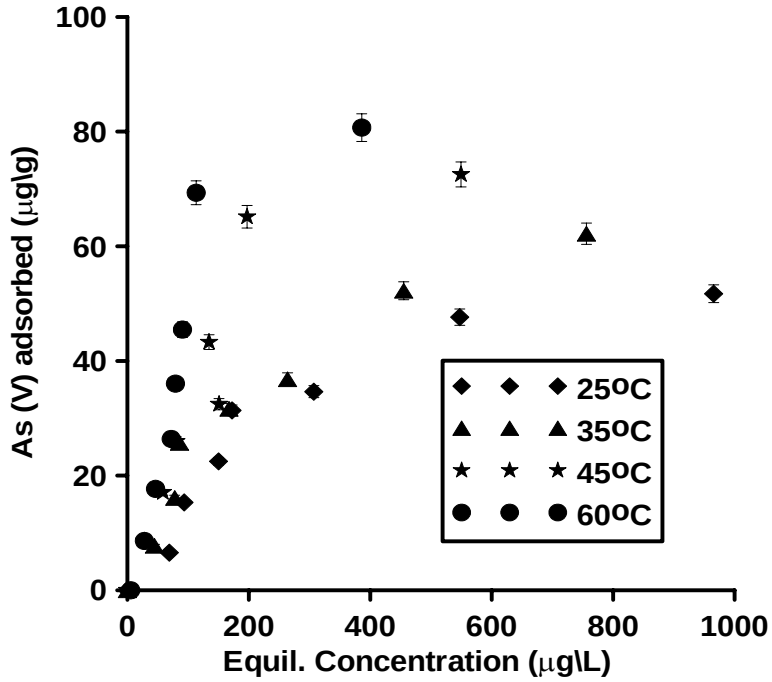

Figure 8. As (V) at 25 °C, 35°C, 45 °C, and 60 °C. Solid suspension density = 15 g/L. The pH is 7.0 ± 0.1. The 2σ error on arsenic analysis is 3% based on the variance of measurements of 50 replicate samples.

Table 7. Calculated Langmuir constants and thermodynamic parameters at pH 7.0

As species	T°C	b (L/mmol)	q_m (µg/g)	ΔG^o (kJ/mol)	ΔG^o [99]	ΔH^o (kJ/mol)	ΔH^o[99]	ΔS^o (kJ/mol)	ΔS^o [99]
arsenite	25	0.0639	909	-27.42	-26.53	9.33	15.54	0.123	0.1435
arsenite	35	0.0565	1111	-28.03	-28.69				
arsenite	45	0.0455	1428	-28.36					
arsenite	60	0.0386	1667	-29.25					
arsenate	25	0.0198	714	-24.51	-35.47	17.83	-31.57	0.032	0.0133
arsenate	35	0.0249	1000	-25.93	-35.67				
arsenate	45	0.0223	1098	-26.47					
arsenate	60	0.0243	1538	-27.96					

3.5 Effect of pH

The effect of pH on As (III) sorption is shown in Figures 9 and 11 for Prestea and Awaso, respectively. Arsenic (III) sorption for both media has little effect at pH 6-8. However effects exist at pH 4-5 and 9-10 for 1.0 mg/L arsenic concentrations (Fig. 9 and 11). Arsenic (V) sorption for both Prestea and Awaso LC, on the other hand, shows little change by varying from pH 4 to 8, however above pH 8 sorption decreases (Fig. 10 and 12).

3.6 Effect of ionic strength

Arsenic (III) sorption decreases with increasing ionic strength for both Prestea and Awaso LC (Fig. 9 and 11), whereas As (V) shows no dependence or slightly increases (Fig. 10 and 12) with increasing solution ionic strength. The effects are opposite for the two arsenic compounds, though the ionic strength effect is more significant in As (III) as compared to that of As (V).

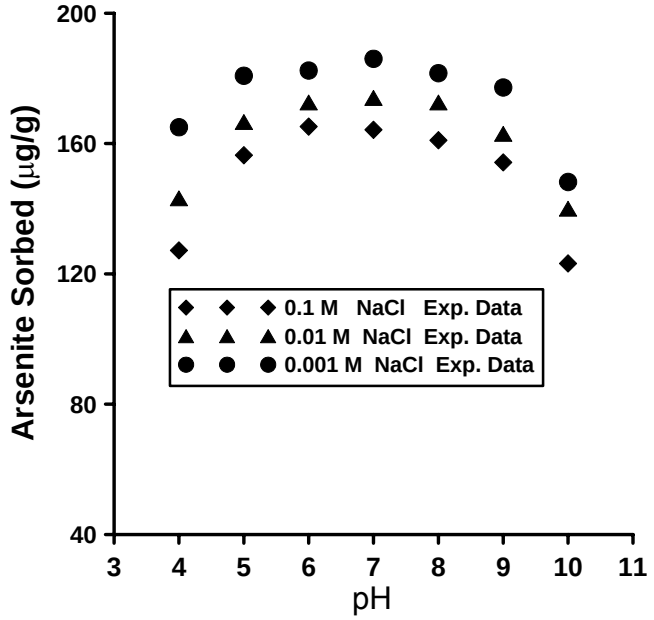

Figure 9. Arsenic (III) sorption on Prestea LC as a function of pH and ionic strength. Solid suspension density = 5g/L, solution arsenic concentration = 1.0mg/L, T=20°C. The 2σ error on arsenic analysis is 3%, based on the variance of measurements of 50 replicate samples.

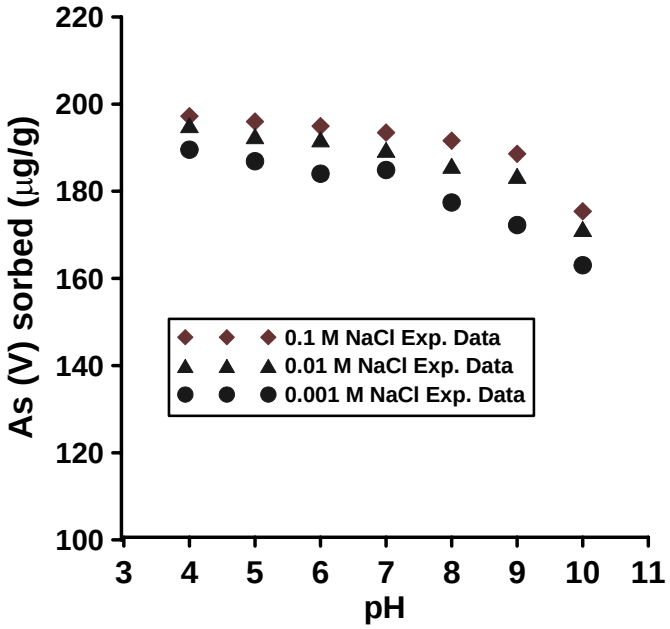

Figure 10. Arsenic (V) sorption on Prestea LC as a function of pH and ionic strength. Solid suspension density = 5g/L, solution arsenic concentrations = 1.0mg/L, T=20°C. The 2σ error on arsenic analysis is 3%, based on the variance of measurements of 50 replicate samples.

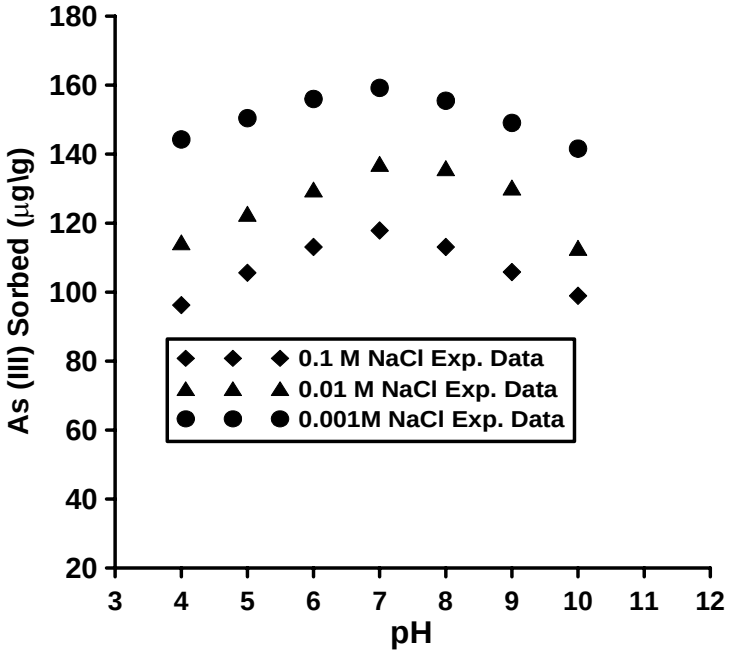

Figure 11. Arsenic (III) sorption on Awaso LC as a function of pH and ionic strength. Solid suspension density = 5g/L, solution arsenic concentration = 1.0mg/L, T=20^{o}C. The 2σ error on arsenic analysis is 3%, based on the variance of measurements of 50 replicate samples.

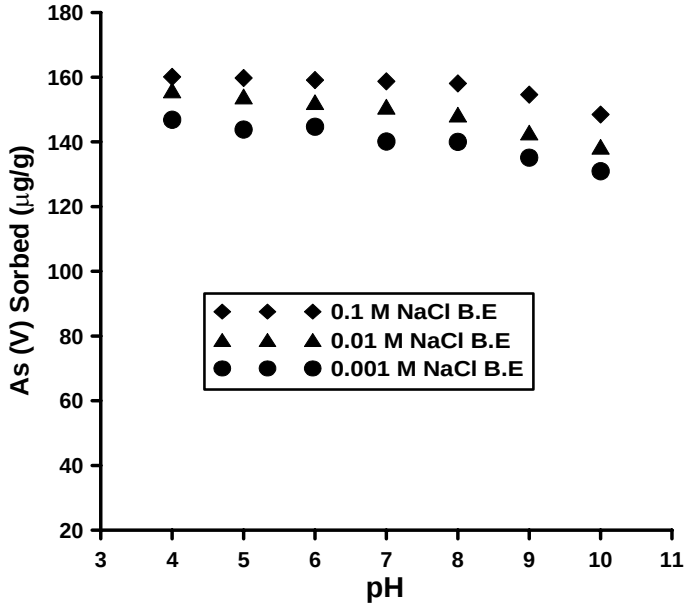

Figure 12. Arsenic (V) sorption on Awaso LC as a function of pH and ionic strength. Solid suspension density = 5g/L, solution arsenic concentration = 1.0mg/L, T=20^{o}C. The 2σ error on arsenic analysis is 3%, based on the variance of measurements of 50 replicate samples.

3.7 Competitive sorption on Prestea and Awaso LC

Arsenic (III) and As (V) sorption on Prestea LC in a phosphate-bearing solution is shown in Figures 13 and 14, respectively. Comparing As (III) sorption in phosphate-free water and a solution with 10mg/L phosphate indicates sorption is reduced by 5-16%, depending on solution pH (Fig. 13). Arsenic (V) sorption is reduced by 5-14% depending on pH (Fig. 14). At near neutral pH, sorption of As (III) is affected by phosphate to greater degree than As (V) sorption.

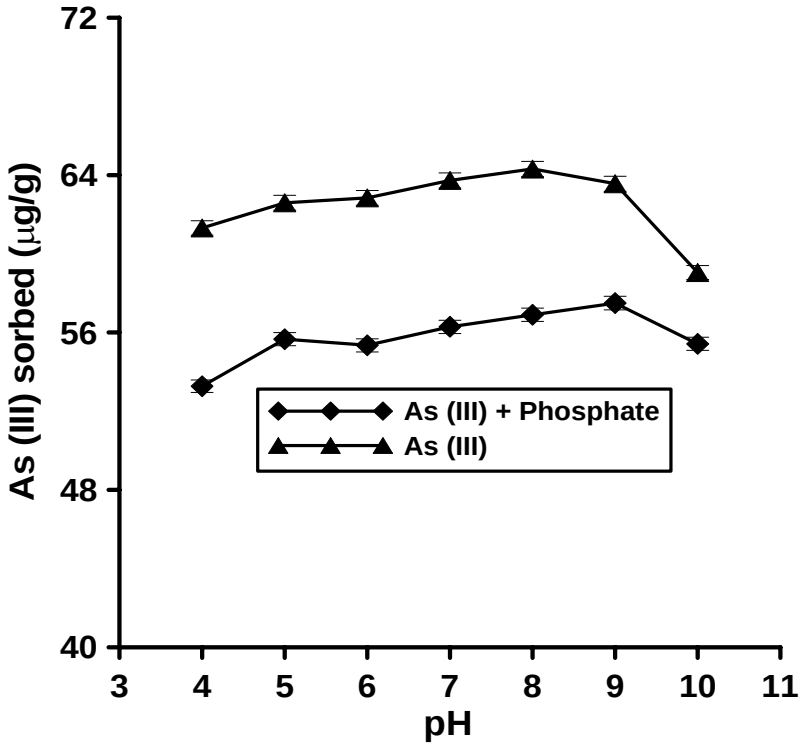

Figure13. Comparing sorption of As (III) on Prestea LC in phosphate-free and phosphate-bearing solutions as a function of pH and ionic strength. As (III) = 1.0mg/L, phosphate = 10mg/L, and suspension concentration, is15g/L.

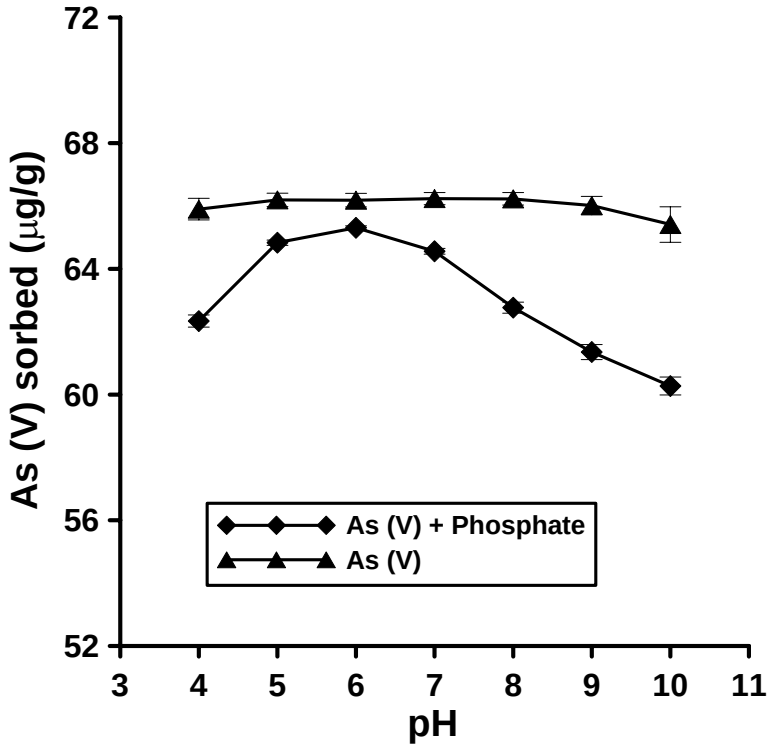

Figure 14. Comparing sorption of As (V) on Prestea LC in phosphate-free and phosphate-bearing solutions as a function of pH and ionic strength. As (III) = 1.0mg/L, phosphate = 10mg/L, and suspension concentration, is15g/L.

Figures 15 and 16 respectively show the results of sulfate effect on As (III) and As (V) sorption on Prestea LC. Arsenic (III) sorption is reduced 25-30%, depending on solution pH, by adding 500mg/L sulfate in solution (Fig. 15); As (V) sorption shows a slight increase of 0.2-1.2% in a similar solution (Fig. 16).

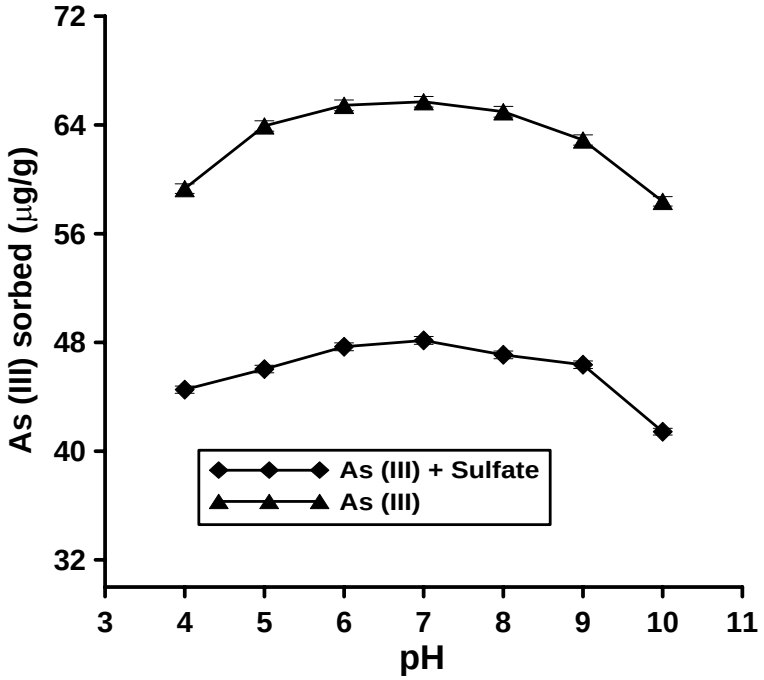

Figure 15. Comparing sorption of As (III) on Prestea LC in sulfate-free and sulfate-bearing solutions as a function of pH and ionic strength. As (III) = 1.0mg/L, phosphate = 10mg/L, and suspension concentration, is15g/L.

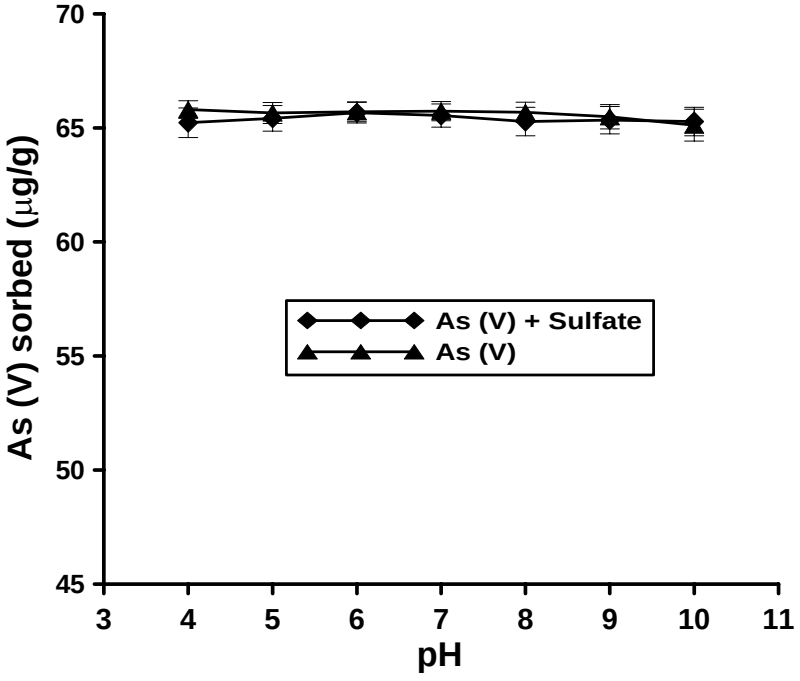

Figure 16. Comparing sorption of As (V) on Prestea LC in sulfate-free and sulfate-bearing solutions as a function of pH and ionic strength. As (III) = 1.0mg/L, phosphate = 10mg/L, and suspension concentration, is15g/L.

Arsenic (III) and arsenic (V) sorption on Awaso LC in a phosphate-bearing solution is shown in Figures 17 and 18, respectively. Sorption of As (III) is reduced by 0.2-4 % (Fig. 17) while that of As (V) is reduced by 0.5-11% depending on the given pH (Fig. 18) when 10mg/L of phosphate was spiked to the arsenic solution (either As (III) or As (V)).

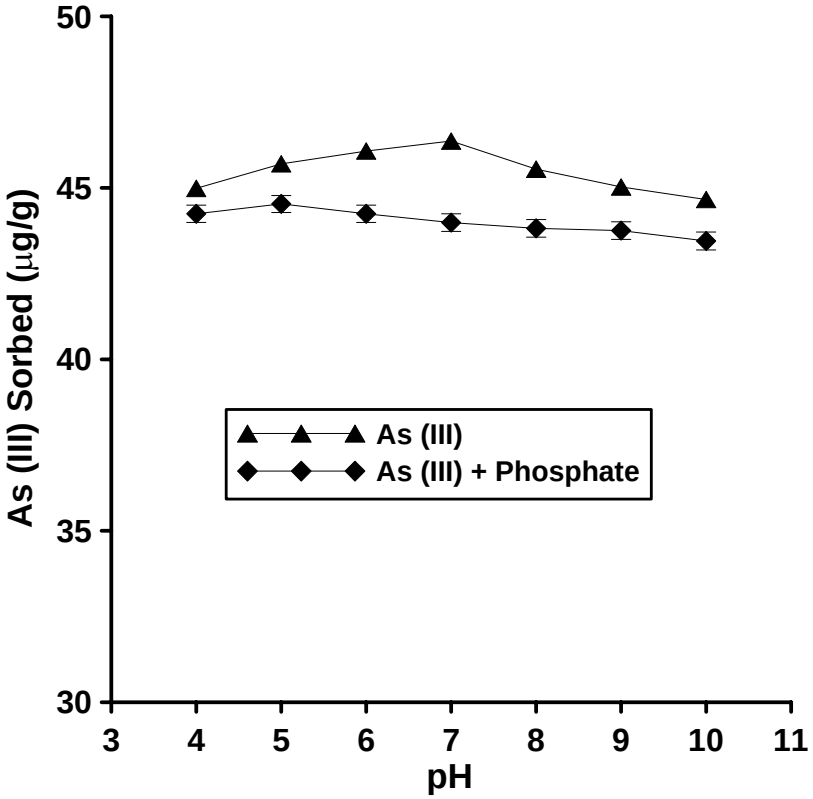

Figure 17. Comparing sorption of As (III) on Awaso LC in phosphate-free and phosphate-bearing solutions as a function of pH and ionic strength. As (III) = 1.0mg/L, phosphate = 10mg/L, and suspension concentration, is15g/L.

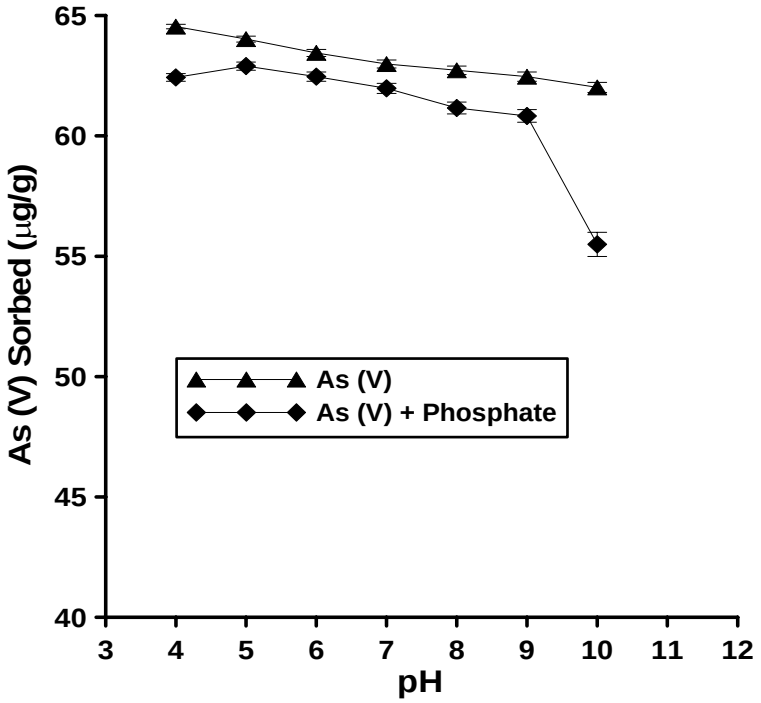

Figure 18. Comparing sorption of As (V) on Awaso LC in phosphate-free and phosphate-bearing solutions as a function of pH and ionic strength. As (III) = 1.0mg/L, phosphate = 10mg/L, and suspension concentration, is15g/L.

Figures 19 and 20 respectively show the results of sulfate interference with As (III) and As (V) sorption on Awaso LC. The decrease in sorption of As (III) is 16-26% (Fig. 19) when 500mg/L sulfate solution was added to the arsenic solution. However the addition of 500mg/L sulfate to the As (V) solution rather increased the sorption capacity of the Awaso LC by 2-6% (Fig. 20).

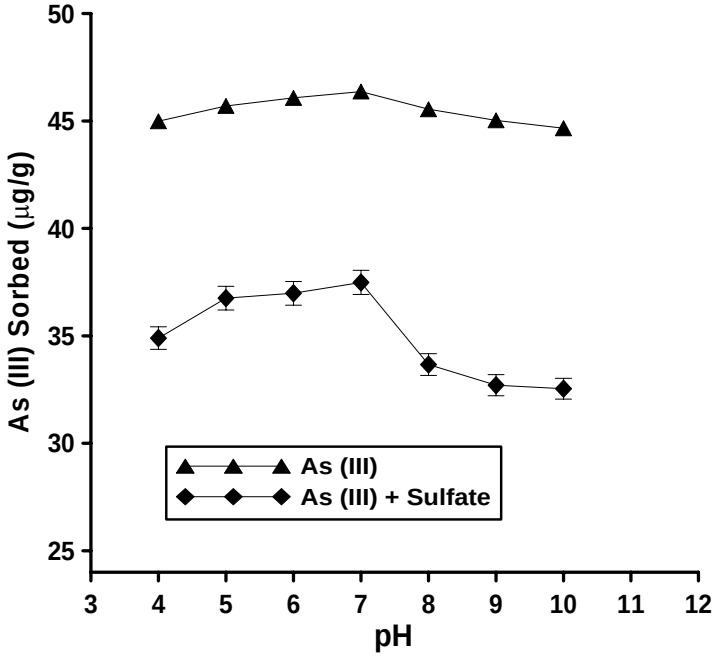

Figure 19. Comparing sorption of As (III) on Awaso LC in sulfate-free and sulfate-bearing solutions as a function of pH and ionic strength. As (III) = 1.0mg/L, phosphate = 10mg/L, and suspension concentration is15g/L.

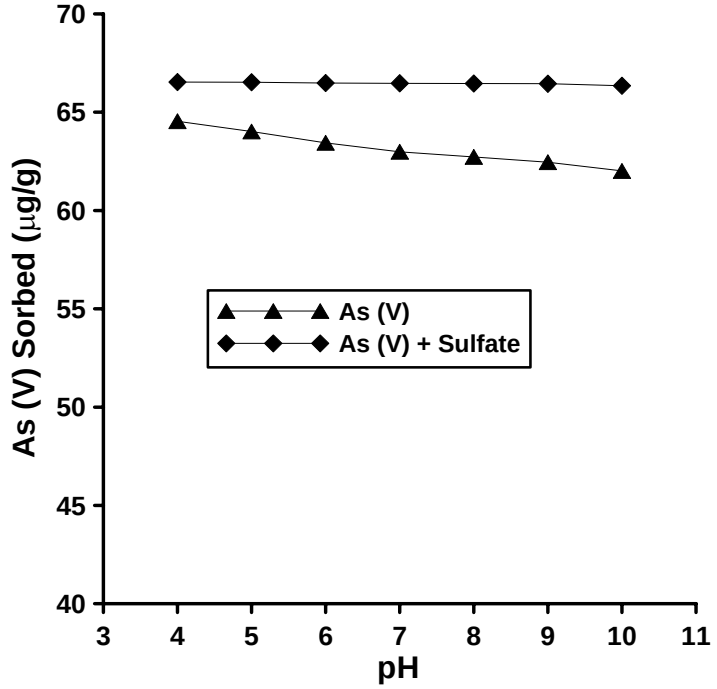

Figure 20. Comparing sorption of As (V) on Awaso LC in sulfate-free and sulfate-bearing solutions as a function of pH and ionic strength. As (III) = 1.0mg/L, phosphate = 10mg/L, and suspension concentration is15 g/L.

3.8 Electrophoretic mobility

Electrophoretic mobilities of Prestea and Awaso LC suspensions with and without 0.035mM or 3.5mM As (III) or As (V) are shown as a function of pH in Figs. 21, 22, 23, and 24. The pHzpc of metal oxides is determined by protonation and deprotonation of surface hydroxyl groups and was derived by linear interpolation of measurements. The point of zero charge (pHzpc) is 8.3 for Prestea LC (Fig.21 and 22) and 8.5 for Awaso LC (Fig.23 and 24). The pHzpc decreases with the addition of arsenic solutions, with Prestea LC showing a significantly greater change. In 0.035mM As (III) or As (V) solutions the pHzpc is approximately 5.7 and 6.3 respectively for the Prestea LC (Fig. 21 and 22), and 6.3 and 6.1 respectively for Awaso LC (Fig. 23 and 24). Increasing the concentration of As (III) or As (V) to 3.5mM changes the pHzpc to 4.3 and 4.5 respectively for the Prestea LC (Fig. 21 and 22), in the case of Awaso LC the pHzpc shifted to 5.3 when the As (V) concentration was increased from 0.035mM to 3.5mM (Fig. 24) but there was no change in pHzpc when the concentration of As (III) was increased (Fig. 23).

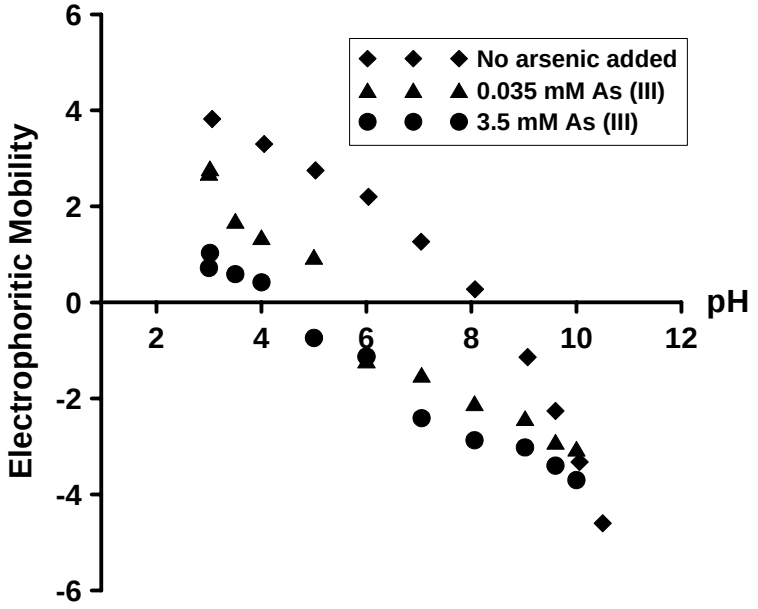

Figure 21. Electrophoretic mobility of Prestea laterite concretion as a function of pH and total As (III) concentration in 0.01M NaCl solution. Zero point of charge for the three solutions inferred by extrapolating the data points to an electrophoretic mobility of zero are: 8.3 (untreated LC), 5.7 (0.035mM As (III) treated LC), and 4.3 (3.5mM As (III) treated LC).

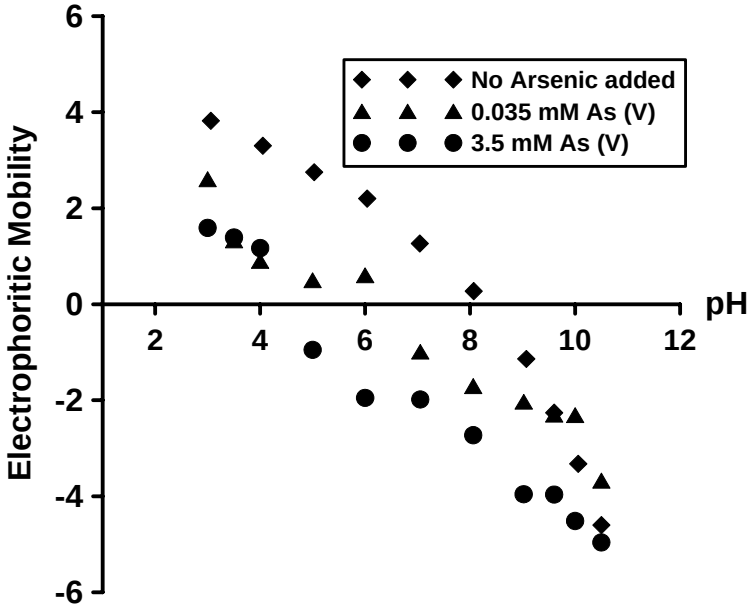

Figure 22. Electrophoretic mobility of Prestea laterite concretion as a function of pH and total As (V) concentration in 0.01M NaCl solution. Zero point of charge for the three solutions inferred by extrapolating the data points to an electrophoretic mobility of zero are: 8.1 (untreated LC), 6.3 (0.035mM As (III) treated LC), and 4.4 (3.5mM As (III) treated LC)

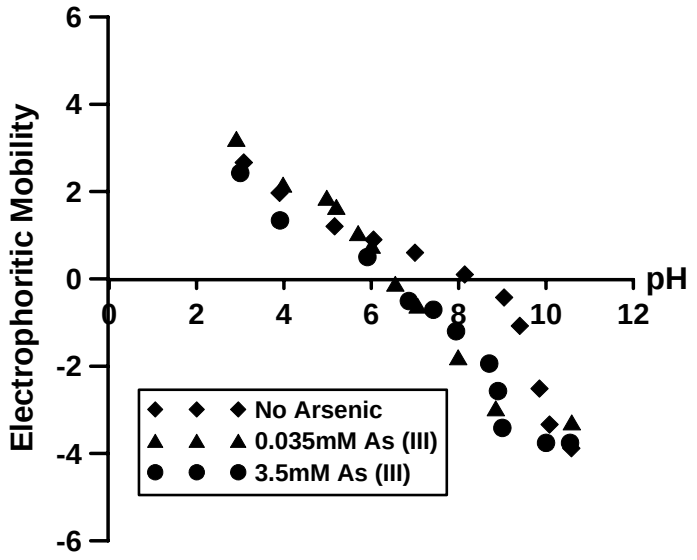

Figure 23. Electrophoretic mobility of Awaso laterite concretion as a function of pH and total As (III) concentration in 0.01M NaCl solution. Zero point of charge for the three solutions inferred by extrapolating the data points to an electrophoretic mobility of zero are: 8.5 (untreated LC), 6.3 (0.035mM As (III) treated LC), and 6.1 (3.5mM As (III) treated LC).

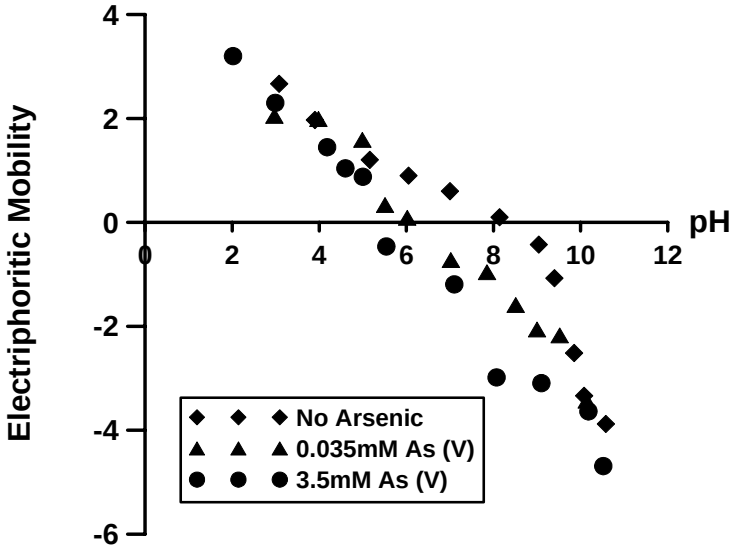

Figure 24. Electrophoretic mobility of Awaso laterite concretion as a function of pH and total As (V) concentration in 0.01M NaCl solution. Zero point of charge for the three solutions inferred by extrapolating the data points to an electrophoretic mobility of zero are: 8.5 (untreated LC), 6.0 (0.035mM As (III) treated LC), and 5.7 (3.5mM As (III) treated LC).

3.9 ATR-FTIR Spectroscopy

Figure 25 presents ATR-FTIR spectra for dissolved As (III) and As (V) species. The peaks and the relative intensities for As (III)- and As (V)-treated Prestea LC are the same at both pH 5 and pH 10. 5 with the exception of one peak that is measured at 792 cm^{-1} for As (III) (Fig. 26) and 794 cm^{-1} for As (V) (Fig 27). Peaks and relative intensities for As (III)- and As (V)-treated Awaso LC, however, are different with the exception of peak values 794 cm^{-1}, 738 cm^{-1}, and 672 cm^{-1} which are the same for both species (Fig. 28 and 29). The untreated Prestea LC shows peaks at 1088, 1027, and 1006 cm^{-1} (Fig. 26 and 27); the untreated Awaso LC shows spectra at 1021 cm^{-1}, 971 cm^{-1}, and 909 cm^{-1} (Fig.28 and 29).

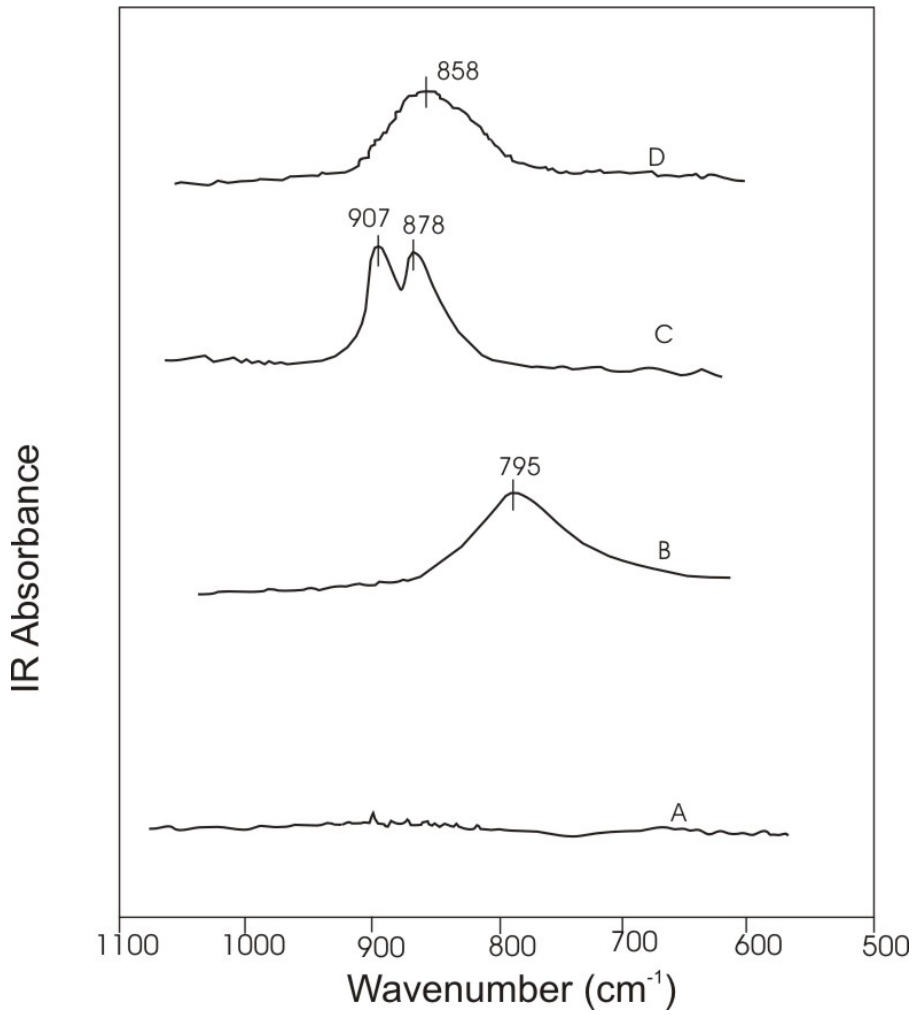

Figure 25. ATR-FTIR spectra of 0.1M As (III) and As (V) solutions: (A) spectra for As (III) solution, pH = 5; (B) spectra for As (III) solution, pH = 10.5; (C) spectra for As (V) solution, pH = 5; and (D) spectra for As (V) solution, pH = 9.

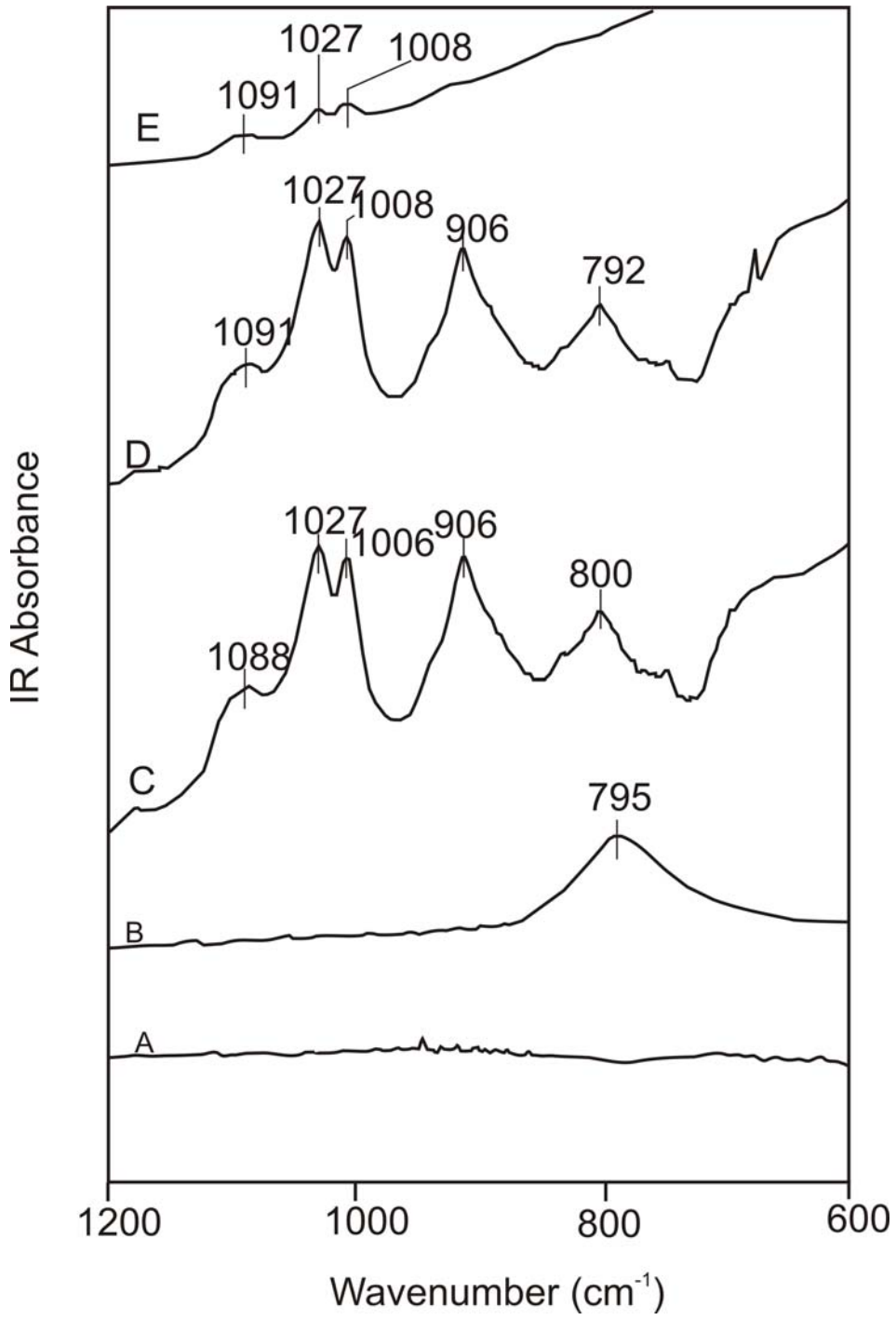

Figure 26. ATR-FTIR spectra of aqueous suspension of Prestea LC, 0.1M As (III)-treated LC and 0.1M As (III) solution for the region 1400-600cm^{-1} (A) As (III) solution , pH 5; (B) As (III) solution, pH 10.5; (C) As (III)-treated LC solution, pH 5; (D) As (III)-treated LC solution, pH 10.5; (E) aqueous suspension of untreated LC. Suspension concentration is 5g/L; ionic strength = 0.01M NaCl

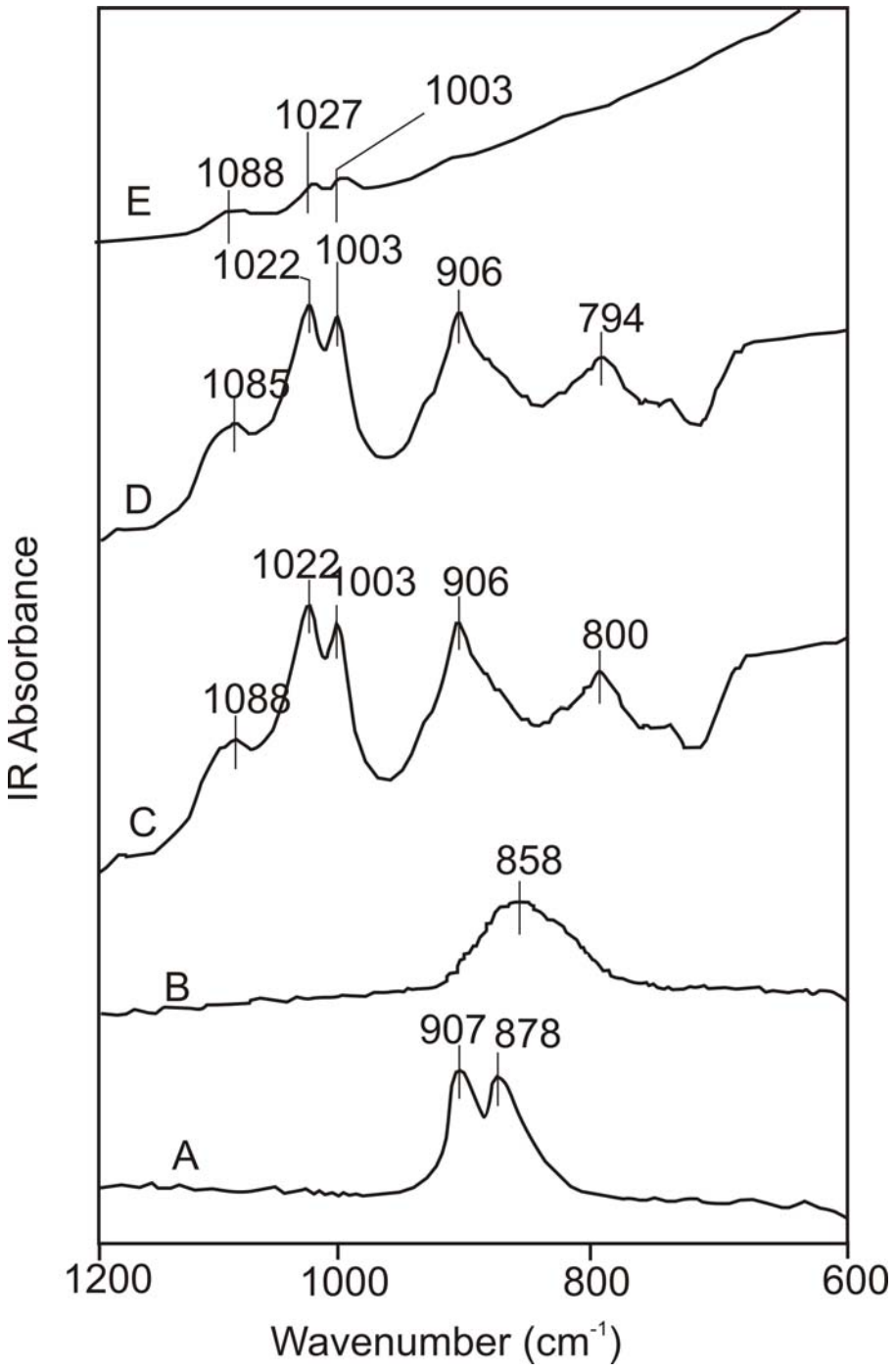

Figure 27. ATR-FTIR spectra of aqueous suspension of Prestea LC, 0.1M As (V)-treated LC and 0.1M As (V) solution for the region 1400-600cm^{-1} (A) As (V) solution, pH 5; (B) As (V) solution, pH 9; (C) As (V)-treated LC solution, pH 5; (D) As (V)-treated LC solution, pH 9; (E) aqueous suspension of untreated LC. Suspension concentration is 5g/L; ionic strength = 0.01M NaCl.

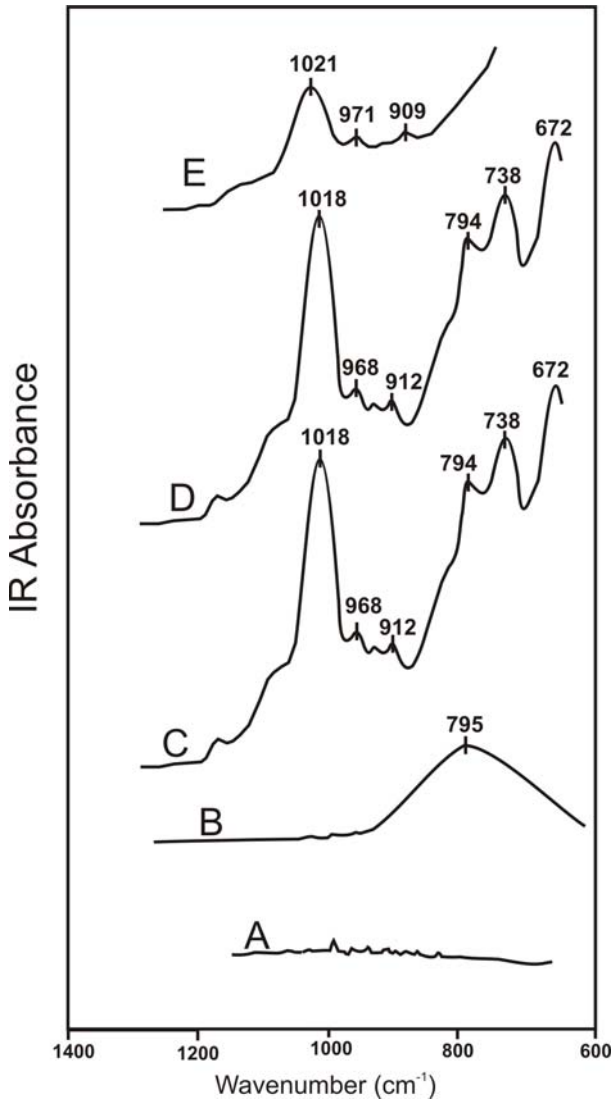

Figure 28. ATR-FTIR spectra of aqueous suspension of Awaso LC, 0.1M As (III)-treated LC and 0.1M As (III) solution for the region 1400-600cm^{-1} (A) As (III) solution, pH 5; (B) As (III) solution, pH 10.5; (C) As (III)-treated LC solution, pH 5; (D) As (III)-treated LC solution, pH 10.5; (E) aqueous suspension of untreated LC. Suspension concentration is 5g/L; ionic strength = 0.01M NaCl.

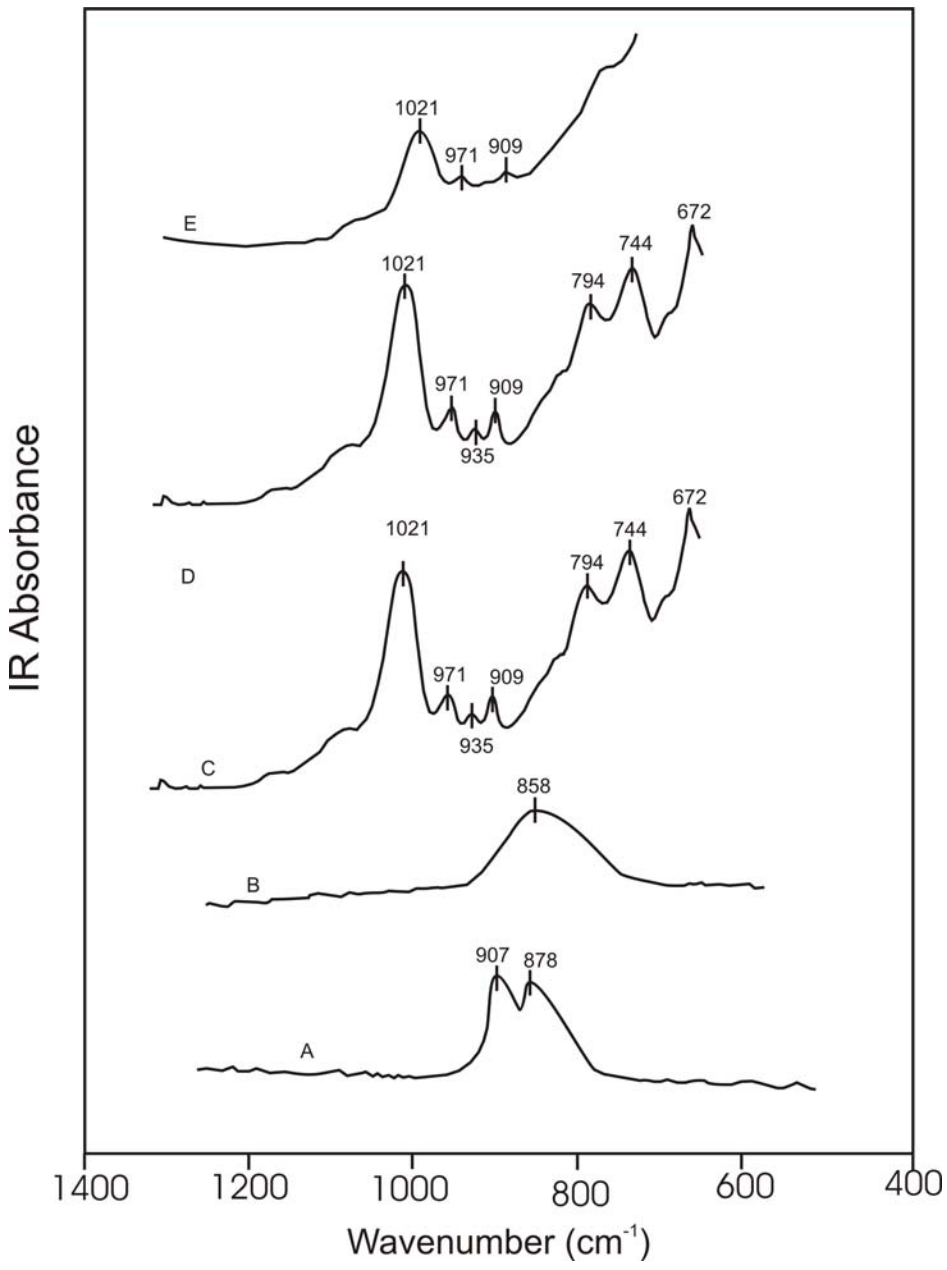

Figure 29. ATR-FTIR spectra of aqueous suspension of Awaso LC, 0.1M As (V)-treated LC and 0.1M As (V) solution for the region 1400-600cm^{-1} (A) As (V) solution, pH 5; (B) As (V) solution, pH 9; (C) As (V)-treated LC solution, pH 5;

(D) As (V)-treated LC solution, pH 9; (E) aqueous suspension of untreated LC. Suspension concentration is 5g/L; ionic strength = 0.01M NaCl

3.10 Surface Complexation Models

The modeling of both As (III) and As (V) sorption onto Prestea and Awaso LC was carried out with the diffuse-layer model and the triple-layer model. The computer program FITEQL [81] was used to determine surface acidity and arsenic binding constants. The stoichiometries of the surface complexes used to fit sorption data are listed in Tables 8, 9, 10, and 11). The general approach was to determine the best fit to the sorption data at median ionic strength (eg. 0.01M). Then using the best fit value, model computations were made for the other two ionic strength values (0.1M and 0.001M). The model predictions with fixed site densities and complexation constants were performed using MINTEQA2 [82]. The activity coefficients of aqueous species were calculated using the Davies equation for both model fitting and predictions.

Table 8. Reactions Used in the Diffuse Double Layer Modeling and Equilibrium Constants for Prestea LC.

	0.1 M	0.01 M	0.001 M
Site Concentration (mol/L)	**1.063E-06**	**1.063E-06**	**1.063E-06**
Surface hydrolysis reactions			
Log K_+			
$\equiv SOH + H^+ \Leftrightarrow SOH_2^+$	7.30(4.26)	7.30(5.30)	7.30(4.60)
Log K_-			
$\equiv SOH \Leftrightarrow SO^- + H^+$	-9.10(-9.86)	-9.10(-8.16)	-9.10(-8.87)

As (III) sorption reactions

Log K_{int}			
$\equiv SOH + H_3AsO_3 \Leftrightarrow SH_2AsO_3 + H_2O$	3.65	3.65	3.65
$\equiv SOH + H_3AsO_3 \Leftrightarrow SHAsO_3^- + H^+ + H_2O$	-4.80	-4.80	-4.80

As (V) sorption reactions

Log K_{int}			
$\equiv SOH + H_3AsO_4 \Leftrightarrow SH_2AsO_4 + H_2O$	12.35	12.35	12.35
$\equiv SOH + H_3AsO_4 \Leftrightarrow SHAsO_4^- + H^+ + H_2O$	5.62	5.62	5.62
$\equiv SOH + H_3AsO_4 \Leftrightarrow SAsO_4^{2-} + 2H^+ + H_2O$	-1.40	-1.40	-1.40

TABLE 9. Reactions Used in the Diffuse Double Layer Modeling and Equilibrium Constants for Awaso LC

	0.1 M	0.01 M	0.001 M
Site Concentration (mol/L)	**5.652E-05**	**5.652E-05**	**5.652E-05**
Surface hydrolysis reactions			
Log K_+			
$\equiv SOH + H^+ \Leftrightarrow SOH_2^+$	7.01(7.23)	7.01(6.97)	7.01(7.58)
Log K_-			
$\equiv SOH \Leftrightarrow SO^- + H^+$	-8.79(-10.1)	-8.79(-8.61)	-8.79(-9.56)

As (III) sorption reactions

Log K_{int}			
$\equiv SOH + H_3AsO_3 \Leftrightarrow SH_2AsO_3 + H_2O$	3.62	3.62	3.62
$\equiv SOH + H_3AsO_3 \Leftrightarrow SHAsO_3^- + H^+ + H_2O$	-4.15	-4.15	-4.15

As (V) sorption reactions

Log K_{int}			
$\equiv SOH + H_3AsO_4 \Leftrightarrow SH_2AsO_4 + H_2O$	12.15	12.15	12.15
$\equiv SOH + H_3AsO_4 \Leftrightarrow SHAsO_4^- + H^+ + H_2O$	6.16	6.16	6.16
$\equiv SOH + H_3AsO_4 \Leftrightarrow SAsO_4^{2-} + 2H^+ + H_2O$	-0.91	-0.91	0.91

Note: Values in brackets are from Vithanage et al., 2006 [85]

TABLE 10. Reactions Used in the Triple Layer Modeling and Equilibrium Constants for Prestea LC

	0.1 M	0.01 M	0.001 M
Site Concentration (mol/L)	6.963E-06	6.963E-06	6.963E-06
Capacitance (F m^{-2})	C1=1.2 C2=0.2		

Surface hydrolysis reactions

Log K_+			
$\equiv SOH + H^+ \Leftrightarrow SOH_2^+$	4.30(4.30)	4.30(4.30)	4.30(4.30)
Log K_-			
$\equiv SOH \Leftrightarrow SO^- + H^+$	-9.03(-9.80)	-9.03(-9.80)	-9.03(-9.80)

Surface complexation reactions

Log K_{Na}^+ (int)			
$\equiv SOH_{(s)} + Na^+_{(aq)} \Leftrightarrow SO^- - Na^+_{(s)} + H^+_{(aq)}$	-5.21	-5.21	-5.21
Log K_{Cl}^- (int)			
$\equiv SOH_{(s)} + H^+ + Cl^-_{(aq)} \Leftrightarrow SOH_2^+ - Cl^-_{(s)}$	7.93	7.93	7.93

As (III) sorption reactions

Log K_{int}

$\equiv SOH + H_3AsO_3 \Leftrightarrow SH_2AsO_3 + H_2O$	8.16	8.16	8.16
$\equiv SOH + H_3AsO_3 \Leftrightarrow SHAsO_3^- + H^+ + H_2O$	-0.10	-0.10	-0.10
$\equiv SOH_{(s)} + H_3AsO_{3\ (aq)} \Leftrightarrow SOH_2^+ - H_2AsO_{3\ (s)}^-$	4.48	4.48	4.48
$\equiv SOH_{(s)} + H_3AsO_{3\ (aq)} \Leftrightarrow SOH_2^+ - HAsO_{3\ (s)}^{2-} + H^+_{(aq)}$	-3.24	-3.24	-3.24

As (V) sorption reactions

Log K_{int}

$\equiv SOH + H_3AsO_4 \Leftrightarrow SH_2AsO_4 + H_2O$	14.99	14.99	14.99
$\equiv SOH + H_3AsO_4 \Leftrightarrow SHAsO_4^- + H^+ + H_2O$	8.26	8.26	8.26
$\equiv SOH + H_3AsO_4 \Leftrightarrow SAsO_4^{2-} + 2H^+ + H_2O$	-1.01	-1.01	-1.01
$\equiv SOH_{(s)} + H_3AsO_{4\ (aq)} \Leftrightarrow SOH_2^+ - H_2AsO_{4\ (s)}^-$	9.82	9.82	9.82
$\equiv SOH_{(s)} + H_3AsO_{4\ (aq)} \Leftrightarrow SOH_2^+ - HAsO_{4\ (s)}^{2-} + H^+_{(aq)}$	7.15	7.15	7.15
$\equiv SOH_{(s)} + H_3AsO_{4\ (aq)} \Leftrightarrow SOH_2^+ - AsO_{4\ (s)}^{3-} + 2H^+_{(aq)}$	-0.55	-0.55	-0.55

Table 11. Reactions Used in the Triple Layer Modeling and Equilibrium Constants for Awaso LC

	0.1 M	0.01 M	0.001 M
Site Concentration (mol/L)	5.453E-06	5.453E-06	5.453E-06
Capacitance (F m^{-2})	C1=1.2 C2=0.2		

Surface hydrolysis reactions

Log K_+

$\equiv SOH + H^+ \Leftrightarrow SOH_2^+$	3.22(5.0)	3.22(5.0)	3.22(5.0)

Log K_-

$\equiv SOH \Leftrightarrow SO^- + H^+$	-11.20(-11.2)	-11.20(-11.2)	-11.20(-11.2)

Surface complexation reactions

Log K_{Na}^+ (int)

$\equiv SOH_{(s)} + Na^+_{(aq)} \Leftrightarrow SO^- - Na^+_{(s)} + H^+_{(aq)}$	-5.21	-4.51	-4.68

Log K_{Cl}^- (int)

$\equiv SOH_{(s)} + H^+ + Cl^-_{(aq)} \Leftrightarrow SOH_2^+ - Cl^-_{(s)}$	6.93	7.56	8.09

As (III) sorption reactions

Log K_{int}

$\equiv SOH + H_3AsO_3 \Leftrightarrow SH_2AsO_3 + H_2O$	6.62	6.62	6.62
$\equiv SOH + H_3AsO_3 \Leftrightarrow SHAsO_3^- + H^+ + H_2O$	1.20	1.20	1.20
$\equiv SOH_{(s)} + H_3AsO_{3\ (aq)} \Leftrightarrow SOH_2^+ - H_2AsO_{3\ (s)}^-$	7.68	7.68	7.68
$\equiv SOH_{(s)} + H_3AsO_{3\ (aq)} \Leftrightarrow SOH_2^+ - HAsO_{3\ (s)}^{2-} + H^+_{(aq)}$	-1.24	-1.24	-1.24

As (V) sorption reactions

Log K_{int}

$\equiv SOH + H_3AsO_4 \Leftrightarrow SH_2AsO_4 + H_2O$	13.88	13.88	13.88
$\equiv SOH + H_3AsO_4 \Leftrightarrow SHAsO_4^- + H^+ + H_2O$	5.99	5.99	5.99
$\equiv SOH + H_3AsO_4 \Leftrightarrow SAsO_4^{2-} + 2H^+ + H_2O$	-1.21	-1.21	-1.21
$\equiv SOH_{(s)} + H_3AsO_{4\ (aq)} \Leftrightarrow SOH_2^+ - H_2AsO_{4\ (s)}^-$	9.72	9.72	9.72
$\equiv SOH_{(s)} + H_3AsO_{4\ (aq)} \Leftrightarrow SOH_2^+ - HAsO_{4\ (s)}^{2-} + H^+_{(aq)}$	7.80	7.80	7.80
$\equiv SOH_{(s)} + H_3AsO_{4\ (aq)} \Leftrightarrow SOH_2^+ - AsO_{4\ (s)}^{3-} + 2H^+_{(aq)}$	-0.44	-0.44	-0.44

Note: Values in parentheses are from Goldberg et al. [15]

The ability of the diffuse layer model to describe As (III) and As (V) sorption on Prestea LC is shown in Figures 30 and 31. Arsenic (III) sorption shows both ionic strength and pH dependence as compared to As (V) (Figs. 30 and 31). The diffuse-layer model shows a poor fit to As (III) experimental data over the pH measured (Figs. 30). The model is able to describe As (V) experimental data quite well between pH 4-7; however after pH 7 the model shows a poor description of the experimental data (Fig. 31).

Figures 32 and 33 also show diffuse-layer model fit to As (III) and As (V) respectively for Awaso LC. The model predictions of both As (III) and As (V) experimental data for Awaso LC are similar to the Prestea LC (Fig. 32and 33). The model shows a poor fit to As (III) experimental data over the pH and ionic strength measured (Figs. 32). Arsenic (V) however, shows a good model fit between pH 4-7, after which the model is unable to describe the experimental data (Fig. 33).

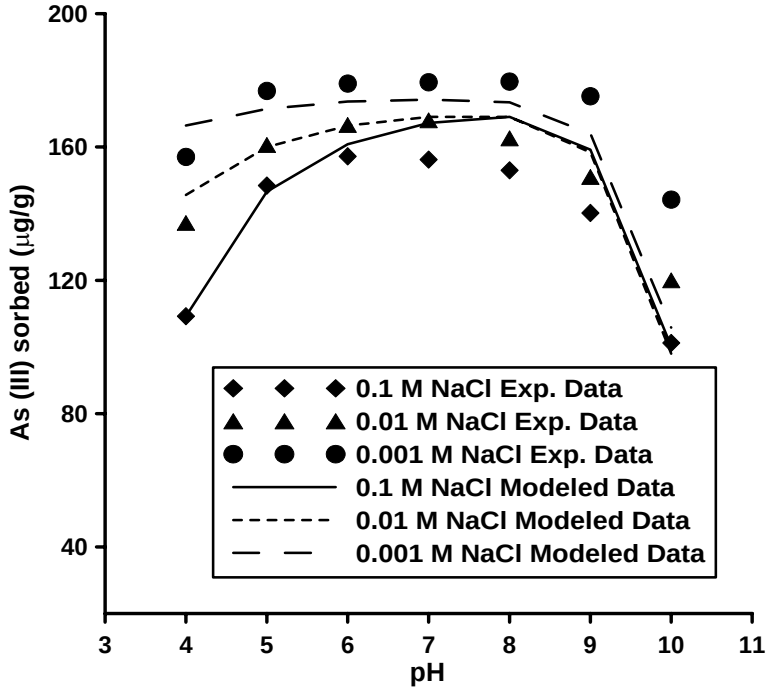

Figure 30. As (III) sorption on Prestea LC as a function of pH and ionic strength. Lines are diffuse layer modeled calculations (see text for details). Solid suspension density = 5g/L, solution arsenic concentrations = 1.0mg/L, T=20°C. The 2σ error on arsenic analysis is 3%, based on the variance of measurements of 50 replicate samples.

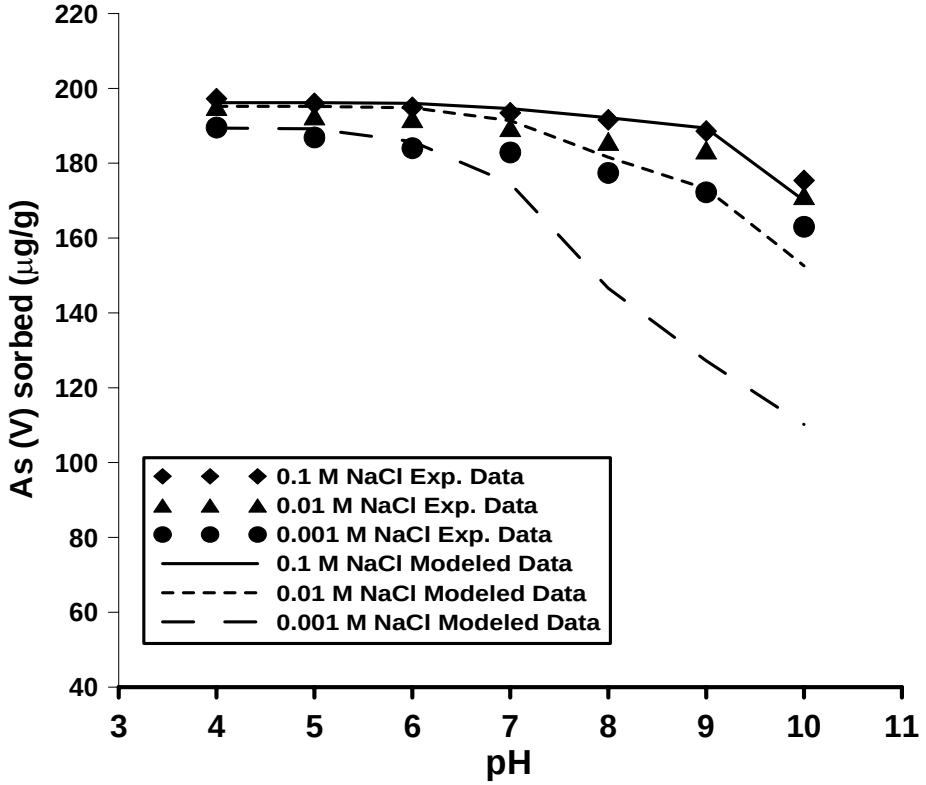

Figure 31. As (V) sorption on Prestea LC as a function of pH and ionic strength. Lines are diffuse layer modeled calculations (see text for details). Solid suspension density = 5g/L, solution arsenic concentrations = 1.0mg/L, T=20°C. The 2σ error on arsenic analysis is 3%, based on the variance of measurements of 50 replicate samples.

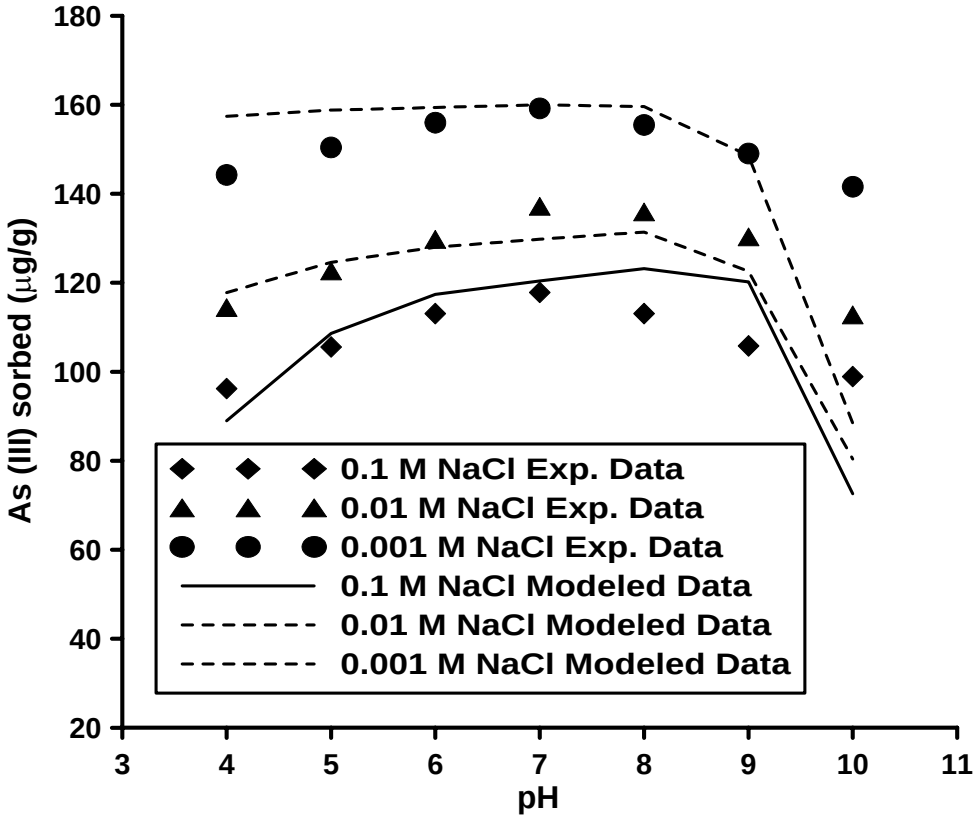

Figure 32. As (III) sorption on Awaso LC as a function of pH and ionic strength. Lines are diffuse layer modeled calculations (see text for details). Solid suspension density = 5g/L, solution arsenic concentrations = 1.0mg/L, T=20^{o}C. The 2σ error on arsenic analysis is 3%, based on the variance of measurements of 50 replicate samples.

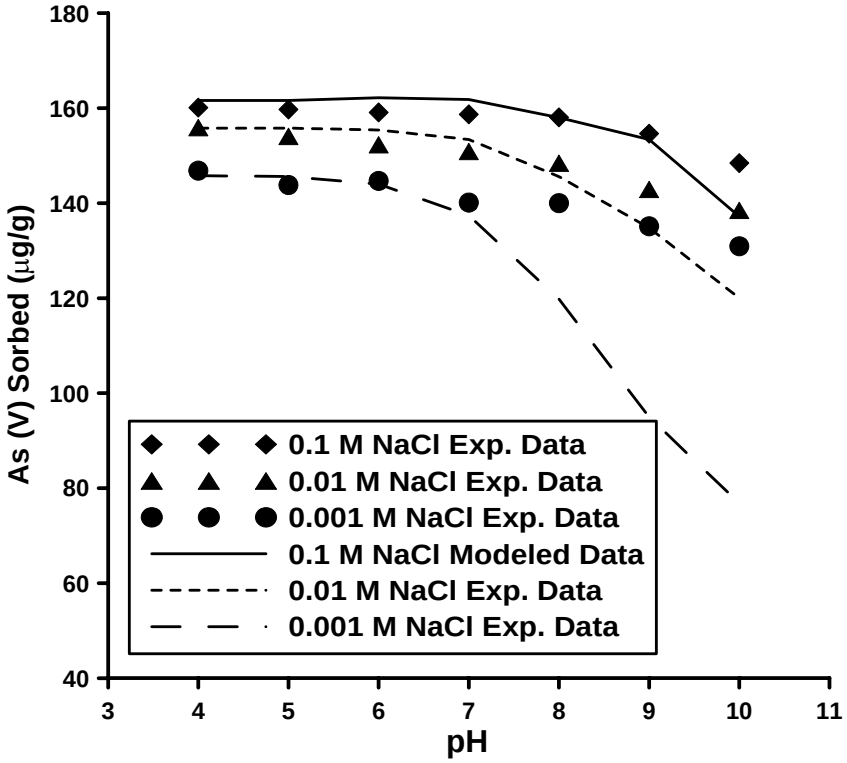

Figure 33. As (V) sorption on Awaso LC as a function of pH and ionic strength. Lines are diffuse-layer modeled calculations (see text for details). Solid suspension density = 5g/L, solution arsenic concentrations = 1.0mg/L, T=20^{o}C. The 2σ error on arsenic analysis is 3%, based on the variance of measurements of 50 replicate samples.

Figures 34 and 35 show triple-layer model fits to As (III) and As (V) sorption respectively on Prestea LC. Since the sorption data show some ionic strength dependence, the triple-layer model, which explicitly accounts for changes in sorption with changing solution ionic strength, was evaluated for its ability to describe the data. The triple-layer model describes As (III) experimental data better than the diffuse layer model (Fig. 34.) However, the triple-layer model fits to As (V) sorption data at 0.1M and 0.01M ionic strength are better than 0.001M ionic strength (Fig. 35).

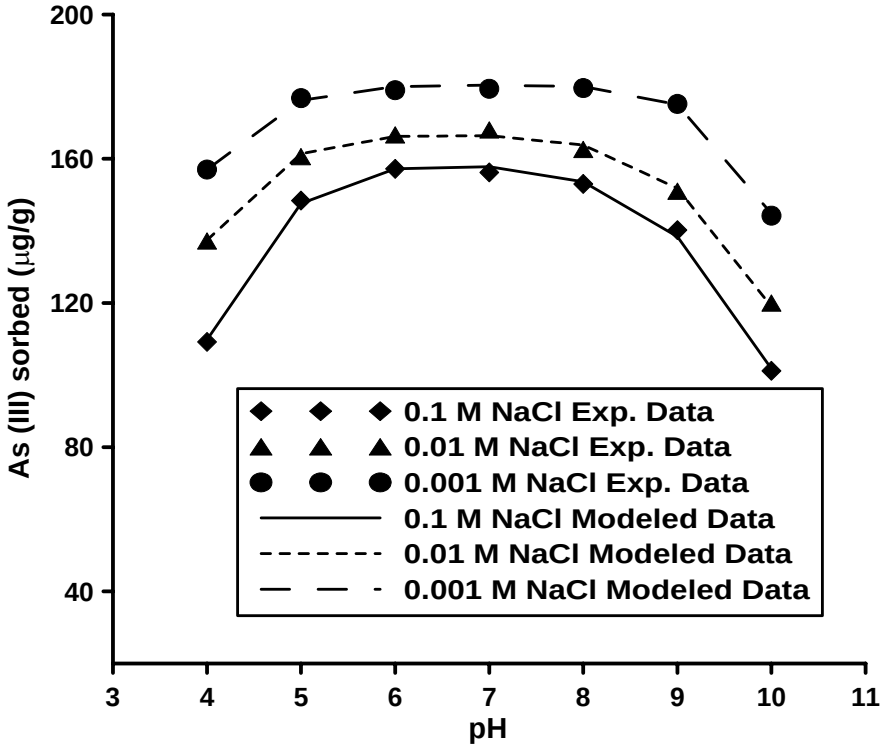

Figure 34. As (III) sorption on Prestea LC as a function of pH and ionic strength. Lines are triple-layer modeled calculations (see text for details). Solid suspension density = 5g/L, solution arsenic concentration = 1.0mg/L, T=20^{o}C. The 2σ error on arsenic analysis is 3%, based on the variance of measurements of 50 replicate samples.

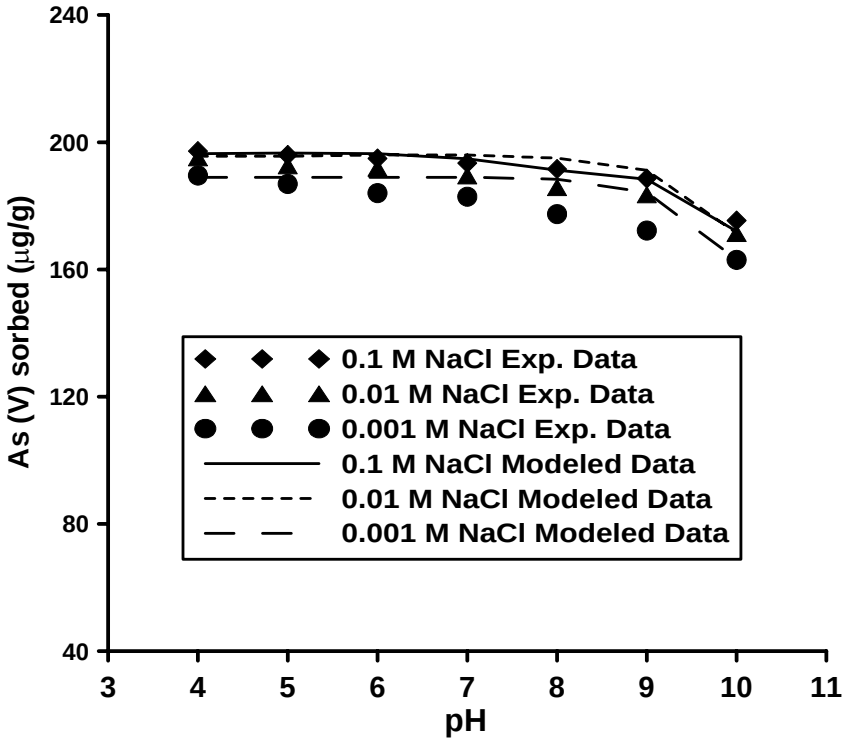

Figure 35. As (V) sorption on Prestea LC as a function of pH and ionic strength. Lines are triple-layer modeled calculations (see text for details). Solid suspension density = 5g/L, solution arsenic concentrations = 1.0mg/L, T=20^{o}C. The 2σ error on arsenic analysis is 3%, based on the variance of measurements of 50 replicate samples.

Figures 36 and 37 show triple-layer model fits to As (III) and As (V) sorption respectively on Awaso LC. Similarly to the Prestea LC, the triple-layer model shows a better fit to both As (III) and As (V) for Awaso than does the diffuse-layer model (Fig. 36 and 37). However the fits to As (V) experimental data for Awaso were not as good as the Prestea data, especially at 0.001M ionic strength (Fig. 35 and 37).

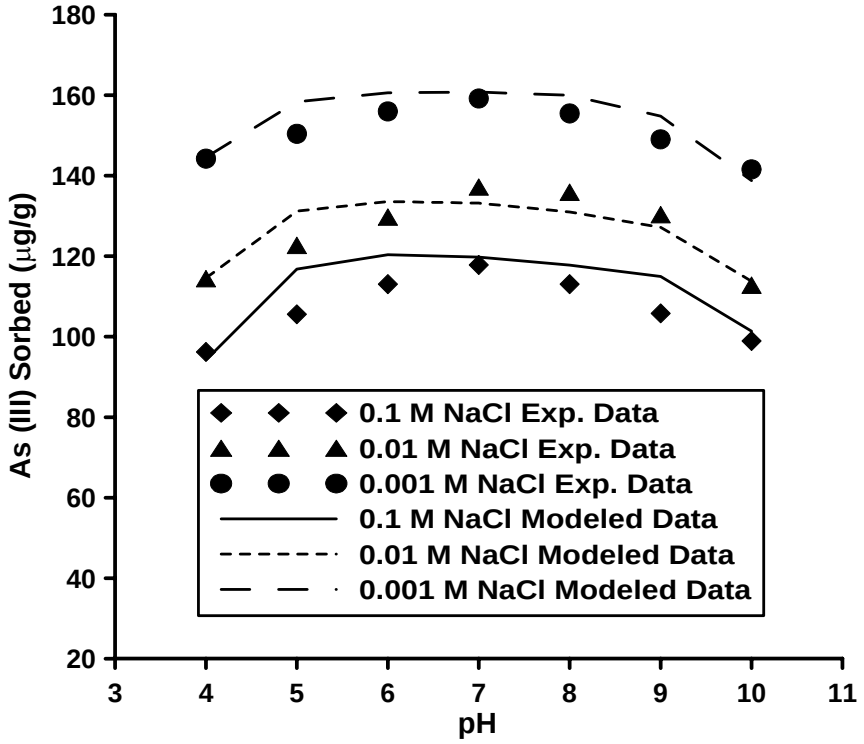

Figure 36. As (III) sorption on Awaso LC as a function of pH and ionic strength. Lines are triple-layer modeled calculations (see text for details). Solid suspension density = 5g/L, solution arsenic concentration = 1.0mg/L, T=20^{o}C. The 2σ error on arsenic analysis is 3%, based on the variance of measurements of 50 replicate samples.

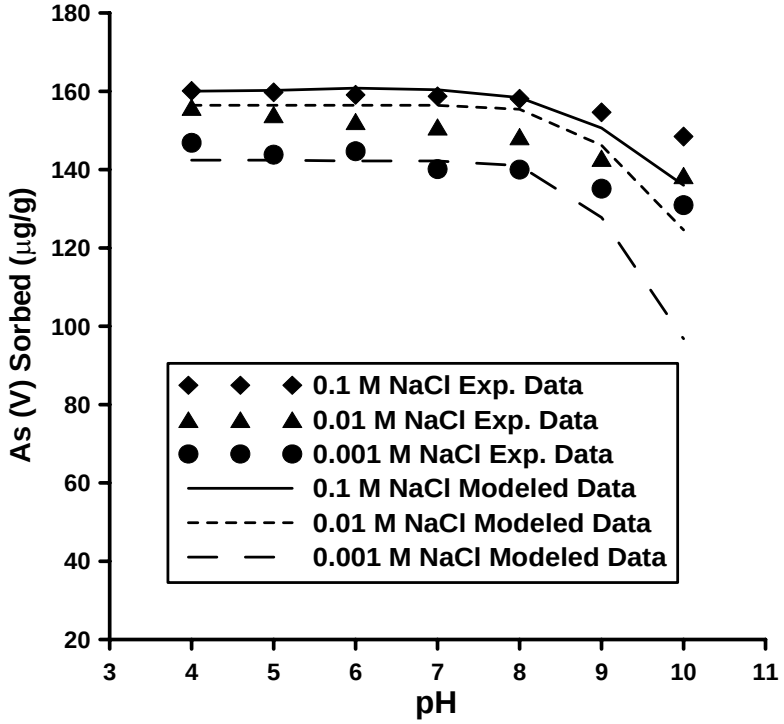

Figure 37. As (V) sorption on Awaso LC as a function of pH and ionic strength. Lines are triple-layer modeled calculations (see text for details). Solid suspension density = 5g/L, solution arsenic concentration = 1.0mg/L, T=20^{o}C. The 2σ error on arsenic analysis is 3%, based on the variance of measurements of 50 replicate samples.

CHAPTER 4

DISCUSSION

4.1 Sorption isotherm for Prestea and Awaso LC

The sorption isotherm data obtained from the Prestea and Awaso LC obeys the Langmuir isotherm with a high coefficient of determination for the model (Tables 5 and 6). The Langmuir isotherm, as a result, is used to study the sorption capacity of Prestea and Awaso LC. Linearization of the Langmuir equation allows calculation of the sorption capacity for both Prestea and Awaso LC.

The As (III) sorption capacity for Awaso LC is lower than As (V) at pH of 7.0 (Fig. 6). This is expected and agrees with ideas of sorption being related to electrostatic forces between surfaces and aqueous species [71, 86]. At pH 7.0 the surface of the Awaso LC is positively charged because the pHzpc is 8.3 and the predominant arsenic species in aqueous solution are $H_3AsO_3^0$ and $HAsO_4^{2-}$. The As (III) species has a neutral charge and the As (V) has a negative charge, thus $HAsO_4^{2-}$ should be attracted more strongly to the Awaso LC surface. This observed trend is consistent with other studies [15, 20, 87, 88] of As (III) and As (V) sorption onto aluminum and iron oxides (Awaso LC is predominantly aluminum and iron oxide). These studies also indicate that As (III) uptake from aqueous solution is much less than that for As (V).

Arsenic (III) sorption capacity for Prestea LC is, however, higher than that of As (V) at pH of 7.0 (Fig. 5). This is unusual, given the fact that the As (III) species ($H_3AsO_3^0$) has no charge in the pH range 4 to 8 and therefore is not expected to sorb better than As (V) ($HAsO_4^{2-}$), which exists as a charged aqueous species at pH 7.0. It

appears the sorbent mineralogy affects sorption. The mineralogical composition of Prestea LC is complex. Other oxides found in Prestea LC, such as manganese and titanium oxides, may oxidize As (III) to As (V) making it easier to remove, hence the observed increase in sorption. Maiti et al. [89] did speciation studies on lateritic soils where about 20% conversion of As (III) to As (V) was observed, with an initial As (III) concentration of 1000μg/l and at a 20g/l adsorbent dose. Their explanation for the conversion to the As (V) state is due to the presence of manganese oxide in the laterite. Manganese and titanium oxides are known as oxidants of As (III) to As (V) [90-92]. Other studies [89, 93-96] of arsenic uptake by natural lateritic soils similar to the Prestea LC show higher As (III) sorption than As (V) at pH 7.0. Arsenic sorption studies [15, 20] that used pure laboratory synthesized materials such as iron oxide or aluminum oxide observed the opposite, where As (V) sorption is higher than As (III) at pH 7.0. This behavior of LC gives it an advantage over other laboratory synthesized arsenic filtering media.

4.2 Effect of Temperature and thermodynamic parameters for Prestea LC

Table 5 shows higher sorption capacity (qm) for As (III) than As (V) at all temperatures. It appears arsenic sorption on Prestea LC is not simply controlled by electrostatic interaction between aqueous ions and mineral surfaces (Fig. 7 and 8). As (III) species ($HAsO_3^0$) does not dissociate in the pH range 4 to 8 and therefore is not expected to sorb better than As (V) ($H_2AsO_4^-$), which exists as a charged aqueous species for pH 7.0. Arsenic studies on metal oxides indicate that As (V) sorbs best in the pH range of 4-5 and that sorption decreases as pH increases [97-100]. Other

studies [89, 101, 102] on the temperature effects on arsenic uptake by natural materials show higher As (III) sorption than As (V). They attributed this observed behavior to an increase in repulsion due to the more negatively charged As (V) species and negatively charged surface sites of the metal oxides [101]. Another reason for this trend is the increase in competition with OH^- for sorption sites with increasing pH [103].

Altundogan et al. [83] observed the opposite trend where As (III) sorption on red mud decreases with increasing temperature, but As (V) sorption increases with increasing temperature. They concluded that this observed trend is due to the nature of As (III) sorption being physical, while that of As (V) is chemical. They, however, show no spectroscopic evidence to delineate the mechanism of arsenic sorption onto the red mud.

Several factors may account for the increase in sorption with increase in temperature: chemisorption or inner-sphere sorption mechanisms (discussed later in the chapter) may be taking place on the Prestea LC and possibly causing some tunneling of adsorbed ions into Prestea LC mineral phases [104]. Moreover, an increased diffusion rate of adsorbate molecules into the Prestea LC pores due to increased temperature may account for the observed behavior [102]. Changes in the adsorbent pore sizes and an increase in the number of sorption sites due to the breaking of some internal bonds near the edge of the particle are expected at higher temperatures [105-108]. An increase in temperature may also effect an increase in proportion and activity of arsenic ions in solution, the affinity of the ions for the surface, or the charge and therefore the potential of the surface [109].

The negative ΔG^o values (Table 5) for As (III) and As (V) sorption agree with the spontaneous nature of the arsenic sorption process. The decrease in $\Delta G°$ with increasing temperature implies stronger sorption at a higher temperature. The relationship between sorption and temperature agrees with the observed increase in sorption capacity q_m with temperature for both As (III) and As (V). The ΔH^o value is positive for both As (III) and As (V), indicating the endothermic nature of arsenic sorption. Altundogan et al. [83] and Zeng [101], however, observed an opposite effect of temperature on As (III) and As (V) sorption on mixed oxides, explaining why As (V) sorption is more affected by temperature. The positive ΔS^o values reflect the affinity of LC for As (V) and As (III) and suggest some structural changes in the arsenic species and the adsorbent [83, 84]; moreover, the positive value of ΔS^o show the increasing randomness at the solid/liquid interface during arsenic sorption [101].

4.3 ATR-FTIR Spectroscopy

A comparism of the peaks at $1088cm^{-1}$, $1027cm^{-1}$, and $1006cm^{-1}$ for the untreated Prestea LC with those for the arsenic-treated Prestea LC shows a lowering of the peaks to$1085cm^{-1}$, $1022cm^{-1}$, and $1003cm^{-1}$ when arsenic was adsorbed onto Prestea LC (Fig. 26 and 27). The shift in peaks from $1088cm^{-1}$ to $1085cm^{-1}$, from $1027cm^{-1}$ to $1022cm^{-1}$, and from $1006cm^{-1}$ to $1003cm^{-1}$ may be a consequence of arsenic sorption because arsenic was the only sorbed ion added to the treatment water [63, 110]. The arsenic treated LC shows peaks at $906cm^{-1}$ and $792/794cm^{-1}$ respectively for As (III) and As (V) that are not observed on the untreated LC spectra. The presence of these peaks on the treated LC spectra that are not present in the

untreated sample are an indication of chemical bonding between the arsenic species and the surface of the Prestea LC [63, 110]. The peak shift and the change in peak intensity may be an indication of an inner-sphere sorption mechanism as this is in agreement with previously published data [15, 62, 63].

Sun and Doner investigated As (III) and As (V) bonding structures on goethite by ATR-FTIR. They realized that the addition of either As (III) or As (V) caused a reduction in peak wavelength; they also showed a new peak appearing at 2686cm^{-1} as a result of splitting of the initial peak. They concluded such a reaction may be attributed to chemical bonding or an inner-sphere bonding mechanism.

Awaso LC spectra are similar; treatment with As (III) shifts the 1021cm^{-1} peak to 1018cm^{-1} and the 971cm^{-1} peak to 968cm^{-1}. Also the peak intensities are stronger for the As (III) treated sample than the untreated sample (Fig. 28). Again, the 794 cm^{-1}, 738 cm^{-1}, and 672 cm^{-1} peaks that are not present in the untreated Awaso LC are showing up on the As (III) treated samples (Fig. 28). These may be a split of the 909cm^{-1} peak from the untreated Awaso LC. Sun and Doner observed splitting of peaks from untreated goethite samples when treated with As (III) and concluded that such a reaction may be attributed to chemical bonding or an inner-sphere bonding mechanism. Goldberg et al. however, in the case of As (III) sorption to amorphous aluminum oxide, observed no discernible features on FTIR spectrum that could be attributed to As (III) surface complexation. They concluded that As (III) sorption on amorphous aluminum oxide is by an outer-sphere sorption mechanism.

Arsenic (V) treated Awaso LC shows the same wave numbers as the untreated Awaso LC, with the addition of a 935cm^{-1} peak (Fig. 29). The peak

intensities on As (V) treated samples are also stronger than the untreated samples and also show a split of the 909cm^{-1} peak to the 794cm^{-1} , 744cm^{-1}, and 672cm^{-1} peaks as in the case of As (III) (Fig. 29). These changes suggest specific ion sorption between As (V) and Awaso LC and are indications of inner-sphere formation complexes [62, 63].

The peak positions of the arsenic treated samples (sorbed samples for both Prestea and Awaso LC) (Figures 26, 27, 28, and 29) were significantly different from those of the dissolved arsenic species (Fig. 25), which can be attributed to sorption of the arsenic species. In general, the spectra of both As (III) and As (V) sorbed to the Prestea and Awaso LC are very different from those of arsenic aqueous solutions. This difference and the lack of pH dependence on the positions of the vibrational modes indicate that these modes are "protected" from changes in pH and indicate that these groups are involved in direct complexation to the surface [15, 62].

If the shift were caused by protonation, as would it be in the case of outer-sphere sorption, the bands would exhibit similar positions with regard to the corresponding dissolved arsenic species in that pH range [15, 71, 111]. The different peak intensities, band shifts, and splits may all indicate the formation of inner-sphere complexes.

Where as the ATR-FTIR spectra for dissolved arsenic species do change as pH is varied. A shift in band position with changing pH was not observed in As (V) and As (III) adsorbed spectra (Figures 26, 27, 28, and 29). The lack of change in band position at various pH values suggests that arsenic formed the same inner-sphere surface complexes on both Prestea and Awaso LC [71]. Other researcher studies on

single metal oxides [15, 63, 112] observe different peak intensities for As (III) and As (V) sorption on metal oxides, though that was not observed in this work. Prestea and Awaso LC consist of mixed oxides, therefore it is not surprising that different peak intensities were observed in the FTIR spectrum that were not observed in published data on single metal oxides. The ATR-FTIR data and the above discussions suggest an inner-sphere sorption mechanism for both As (III) and As (V) on Prestea and Awaso LC.

Although the XRD spectra of the Prestea and Awaso LC (Figs. 3 and 4) suggest the Awaso is more crystalline than the Prestea, they didn't show much difference in the ATR-FTIR data. In contrast published ATR- FTIR data by Goldberg et al. [15] on As (III) sorption onto amorphous aluminum oxide show sorption is by an outer-sphere sorption mechanism. This confirms the previous discussions on As (III) sorption data that suggest manganese and titanium oxide may be oxidizing As (III) to As (V), which could explain why this work observes a different sorption mechanism than is reported in the previously published data on single metal oxides.

4.4 Electrophoretic Mobility

The shift of Prestea LC pHzpc to a lower pH range with increasing As (V) and As (III) concentrations is evidence of inner-sphere surface complex (specific ion sorption) formation (Figs. 20 and 21). This is where $H_3AsO_3^0$ and $H_2AsO_4^-$ for As (III) and As (V) respective species form complexes directly with the coordination environment of the LC surfaces [113]. Shifts in pHzpc and reversals of EM with increasing ion concentration are both characteristics of inner-sphere sorption.

Arsenic (V) also forms an inner-sphere surface complex with Awaso LC indicated by shifts in pHzpc to lower pH values with increasing arsenic concentration (Fig. 24). Arsenic (III) however, does show a shift in pHzpc when Awaso LC is initially treated with 0.035mM As (III), but no shift is observed in pHzpc as As (III) concentrations increase (Fig 23). This behavior suggests either inner-sphere or outer-sphere surface complexation. Although shifts in pHzpc and reversal of EM with increasing ionic concentration are considered characteristics of specific ion sorption; lack of shift in PZC cannot be used to infer an outer-sphere adsorption mechanism since inner-sphere surface complex formation is not necessarily accompanied by a change in the mineral surface charge [15].

The results of the EM measurements indicate that both As (III) and As (V) form inner-sphere complexes on Prestea LC. Arsenic (III) forms either inner-sphere or outer-sphere sorption mechanisms on Awaso LC because the lack of shift in pHzpc does not necessarily indicate outer-sphere surface complexation. Arsenic (V) sorption on Awaso LC forms inner-sphere complexes due to shifts in pHzpc and reversals of EM with increasing ion concentration. Goldberg et al. [15] also report a similar results where there was no shift in pHzpc to increasingly lower pH values with increasing arsenic concentration when As (III) sorbed on amorphous aluminum oxide. They suggested either inner-sphere or outer-sphere surface complexation occurred between As (III) and amorphous aluminum oxide.

4.5 Effect of pH on Prestea and Awaso LC

The variation of As (V) sorption with pH onto Prestea and Awaso LC is similar to arsenic sorption reported on iron and aluminum oxy-hydroxides [114]. The sorption behavior of As (III) is less easily explained. Sorption of As (III) (Figs. 9 and 11) does show a little variation with pH near neutral pH, as is reported for As (III) sorption onto iron and aluminum hydroxides [15]

Arsenic (V) shows decreasing sorption as pH increases for both Prestea and Awaso LC (Figs. 10 and 12). This is compatible with increasing repulsion occurring between negatively-charged As (V) species and negatively-charged surface sites, thus increasing competition with OH^- for sorption sites.

The data suggest at least two mechanisms controlling sorption. One is electrostatic that increases As (V) sorption at pH below 6; the other is a chemical process. When pH - pH_{zpc} is less than zero, the surface of the LC is positive and sorption of the anion is facilitated by coulombic or electrostatic attraction and is at a maximum. When pH - pH_{zpc} is greater than zero, the surface of the LC is negative and specific As (V) sorption must compete with columbic repulsion. The fact that there is a reduction in sorption when pH is greater than pH_{zpc} is attributable to the specific binding or chemical sorption of As (V) to the surface of the LC [115].

Neutral species ($HAsO_3^0$) sorption at pH > pH_{zpc} may be a chemical reaction or a specific sorption. Goldberg et al. 2001used a combination of macroscopic and microscopic techniques to show that As (III) sorption on amorphous iron and aluminum oxides below pH 6 shows an outer-sphere sorption mechanism. However, at pH above 6, As (III) occurring as $HAsO_3^0$ shows chemical or inner-sphere sorption mechanisms. Similar sorption behavior is observed for As (III) sorption in the pH

range 7–7.6 onto activated alumina [116, 117] and onto iron-oxide coated sand [39]. Both iron and aluminum oxide present in the Prestea and Awaso laterite contribute to As (III) sorption. In general LV sorption of As (III) is greater than iron or aluminum oxides; it is not clear if the behavior observed is the result of several oxides acting together or is an inherent property of oxides with several constituents.

The characteristic of LC removing As (III) better than As (V) at a high pH is uncommon with commercially available media, which are mostly mixtures of iron and aluminum oxides. These media show a drastic reduction in As (III) sorption at solution pH > 9 [15, 85]. Goldberg and Johnson [15] show little change in As (III) and As (V) sorption onto iron and aluminum oxide over the pH range of 4 to 6, but sorption density of As (III) and As (V) shows a drastic reduction in pH > 8 solutions. The fact that the Prestea and Awaso LC show no drastic change in sorption at pH > 8 shows that they are superior over the laboratory synthesized materials.

4.6 Effect of ionic strength on Prestea and Awaso LC

Arsenic (III) and As (V) sorption onto Prestea and Awaso LC at solution ionic strength values of 0.001, 0.01, and 0.1 M NaCl is depicted in Figs. 9, 10, 11, and 12. Arsenic (III) sorption on both Prestea and Awaso LC exhibits decreasing sorption with increasing ionic strength (Figs. 9 and 11). This result indicates an outer-sphere sorption mechanism [70, 118]. Hayes et al. [70] postulates that anion sorption, which is markedly reduced by increasing ionic strength, is best modeled assuming that the anion forms an outer-sphere (ion-pair) surface complex. Outer spherically bonded surface complexes exhibit a marked effect on ionic strength, yielding distinctly

separated sorption edges. Outer-sphere complexes are expected to be more sensitive to changes in ionic strength since the electrolyte is expected to be in the same plane as the outer-sphere complexes [70].

Arsenic (V) sorption (Fig. 10 and 12) on Prestea and Awaso LC shows an increase in sorption with increasing solution ionic strength. These behavior is indicative of an inner-sphere sorption mechanism for As (V) on both types of LC [15]. Several studies of As (V) sorption onto Fe and Al oxides report strong sorption of As (V) onto mineral surfaces by forming inner sphere complexes [15, 66, 119]. Goldberg et al., [15] observed a decrease in As (V) sorption with increasing solution pH but no ionic strength dependence or increasing As (V) sorption with increasing solution ionic strength. They concluded this behavior is indicative of an inner-sphere sorption mechanism for As (V) onto amorphous Al and Fe oxides. The data on the effect of ionic strength suggest As (III) and As (V) sorption onto Prestea and Awaso LC forms outer-sphere and inner-sphere respectively on both media.

4.7 Competitive sorption on Prestea and Awaso LC

All the competitive sorption experiments were conducted in the presence of phosphate and sulfate, as this represents the case of greatest threat to arsenic remediation in most ground waters and sulfide mining waste waters from stock piles. The presence of phosphate reduces the amount (mg) of both As (V) and As (III) sorbed per gram of Prestea and Awaso LC (Figures 13, 14, 17, and 18). Experiments conducted in the presence of phosphate reduce the amount of As (III) sorbed more than that of As (V,) especially at neutral pH (Figures 13, 14, 17, and 18). Both As

(III) and phosphate sorb best on both LC at neutral pH, thus creating a competition for sorption sites; since As (III) is a neutral species, its attraction to the available sites is slower compared to phosphate. As (V) sorbs better than As (III) at lower pH (4-5), consequently there is less competition for sites at neutral pH. Roberts et al. [120] also observed a similar effect when the addition of phosphate also decreased As (III) sorption somewhat more steeply than As (V) when 3 mg/L phosphate was added to the As (III) solution.

A similar result was observed for sulfate (Figures 15, 16, 19, and 20), and the effect was greater on As (III) than on As (V). The fact that As (III) has a neutral oxidation state means that it will be less attracted to the positively charged surfaces of both LC compared to the negatively charged sulfate species. The presence of phosphate affected As (III) and As (V) sorption on Prestea LC (Figures 13 and 14) more than on Awaso LC (Figures 17 and 18). This observation suggests that phosphate has a slightly higher sorption affinity for Fe_2O_3 as compared to Al_2O_3 since Prestea LC is predominantly iron hydroxide and Awaso is predominantly aluminum hydroxide. Roberts et al., [120] observed a similar trend of phosphate having a strong affinity for HFO.

The effect on arsenic sorption due to the presence of sulfate differs on Prestea and Awaso LC (Figs. 15, 16, 19 and 20). Aqueous As (V) solution spiked with sulfate showed a higher affinity for Awaso LC than does an aqueous solution without spiked sulfate. This is unusual since the presence of sulfate is expected to reduce sorption not to increase it due to the competition for sorption sites. It appears the presence of sulfate alters the surface characteristics of the Awaso LC making it more conducive

to As (V) sorption. Another possible explanation for this behavior is that when sulfate-reducing bacteria are active, the sulfide produced reacts to precipitate As (V), or co-precipitate it with iron or aluminum, leaving little As (V) in solution [121]. The X-ray absorption near edge structures is needed to prove this hypothesis.

Zhang et al. [122] studied the effect of sulfate on As (V) removal from water and realized that the presence of sulfate is found to be favorable for As (V) sorption. However no explanation was given for that behavior.

The significant decrease in the arsenic removal (only As (III)) at high phosphate and sulfate concentrations can be attributed to the ion shielding of the effective charge of the LC and the consumption of the available binding sites of the LC. The cumulative effect is an increase in the electric repulsion, the effective charge of the LC, and the available binding sites of the LC surface [123]. As a result, greater amounts of arsenic ions passed through the LC pores without sorbing, yielding lower arsenic removal at high ion (phosphate and sulfate) concentrations. The high phosphate concentration tested in this study, however, is very unlikely to occur in drinking water and therefore may not cause problems.

4.8 Surface Complexation Models

The ATR- FTIR results indicate that both As (III) and As (V) form inner-sphere surface complexes on Prestea and Awaso LC. I therefore modeled the surface complexation of both types of laterite concretions applying the diffuse-layer model since this model assumes sorption is by inner-sphere complex. The triple-layer model was also used to test its suitability to model the sorption data since it inherently

assumes sorption is by inner- and outer-sphere. All the models are based on the generalized composite approach (GC) that assumes all mineral phases contribute to sorption and that the sorption sites are represented by one type of surface group. The computer program FITEQL [81] was used to determine surface acidity and arsenic binding constants. Surface complexation constants were optimized using MINTEQA2 [82].

The diffuse-layer model shows a poor fit to As (III) experimental data over the pH measured for both Prestea and Awaso LC (Figs. 30 and 32). The reason for the poor fit is As (III) experimental data show ionic strength dependence and, since the diffuse-layer model does not account for ionic strength dependence without fitting the arsenic binding constants, a poor fit is expected. Moreover the model assumes sorption is only by inner-sphere and since As (III) sorption data shows both inner-sphere and outer-sphere sorption mechanisms, the poor predictions of the model for As (III) are expected for both Prestea and Awaso LC.

The diffuse layer model is able to describe As (V) experimental data quite well between pH 4-7 for both Prestea and Awaso; however after pH 7 the model shows a poor description of the experimental data (Figs. 31 and 33). The possible explanation for this behavior is at higher pH there is a drastic increase in the solubility of silica [124] and silica and As (V) ions compete for sorption sites. Also the charge on the As (V) species ($H_2AsO_4^-$, $HAsO_4^{2-}$) becomes more negative as pH increases and there are more hydroxyl ions (OH^-) in solution. Therefore there is an increase in competition for sorption sites; hence the poor model predictions at higher pHs. Good fits were observed for both As (III) and As (V) experimental data using

the diffuse-layer model only when the arsenic binding constants were optimized at different measured ionic strengths (Figs. A 10-A 13). The reason for this behavior is that the model inherently assumes sorption is only by inner-sphere complex and that sorption is not affected by changes in ionic strength. The triple-layer model provided a better fit in its description of As (III) sorption onto both Prestea and Awaso LC without fitting the arsenic binding constants since the model inherently assumes sorption is by both inner- and outer-sphere (Figs. 34 and 36). The general approach was to determine the best fit to the sorption data at median ionic strength (eg. 0.01 M). Then using the best fit value, model computations were made for the other two ionic strength values (0.1 M and 0.001 M).

The triple-layer model that unequivocally accounts for ionic strength dependence is used to assess its ability to describe the data for As (III) and As (V) for both Prestea and Awaso LC since they show ionic strength dependence from the sorption experimental data (Figs. 34, 35, 36, and 37). The triple-layer model is capable of providing some ionic strength dependence in its description of As (III) and As (V) sorption data as the data indicates some ionic strength dependence. Also, As (III) sorption data indicate both inner-sphere and outer-sphere sorption mechanisms on both Prestea and Awaso LC and since the triple-layer model assumes both sorption mechanisms, good model fits were obtained using the triple-layer model (Figs. 34, 35, 36, and 37). The intrinsic surface complexation constants for the sorption of Na^+ and Cl^- from the background electrolyte were optimized to obtain ionic strength-dependent model fits.

The inner- and outer-sphere sorption mechanisms used in the triple-layer model for As (III) conforms to the pHzpc shifts, electrophoretic mobility measurements, and sorption data since they all predicted both an inner-sphere or out-sphere sorption mechanism for As (III) on both Prestea and Awaso LC.

The effect of changes in ionic strength on sorption of As (III) and As (V) on Prestea and Awaso was modeled using both the diffuse- and the triple-layer model. Arsenic (V) sorption, which is slightly affected by ionic strength, can be modeled with both the diffuse-layer (Figs. 31 and 32) and the triple-layer models (Figs 35 and 37), although the triple-layer model gave a better fit at higher pHs than the diffuse-layer model. However, As (III) sorption, which is markedly reduced by increasing ionic strength, is best modeled using the triple-layer model.

4.9 Sorption mechanisms

Mechanisms dictating the observed increase in sorption with temperature may include both an increase in pore size due to the breaking of some internal bonds near the edge of the particles at higher temperatures [106-108, 125], as well as an increase in the rate of diffusion of the adsorbate into the sorption sites [102]. Other possible mechanisms include an increase in the activity of arsenic ions in solution and the affinity of the ions for the surface or the charge and, therefore, the potential of the surface [109]. I speculate that the above reasons may account for the increase in sorption with a corresponding increase in temperature.

Macroscopic evidence shows that the sorption capacity is almost the same irrespective of the size of the LC used in the sorption experiments, indicating that

chemisorption may be taking place on the laterite concretion surfaces and possibly that there is ligand exchange between the adsorbed ions and the hydroxyl group on LC mineral phases. The ionic size of the hydroxyl group on the surface of the LC when in contact with water allows ligand exchange between the arsenic molecule and the hydroxyl group, forming specific adsorbed complexes (inner-sphere complexation).

Arsenic (III) sorption on both LCs exhibited decreasing sorption with increasing ionic strength (Figs. 9 and 11). This result is indicative of an outer-sphere sorption mechanism [70, 118]. Outer-sphere-bonded surface complexes exhibit a marked effect on ionic strength, yielding distinctly separated sorption edges. Outer-sphere complexes are expected to be more sensitive to changes in ionic strength since the electrolyte is expected to be in the same plane as the outer-sphere complexes [70].

Arsenic (V) sorption on both Prestea and Awaso LCs, as represented in Figures 10 and 12, decreases with increasing solution pH and exhibits either no ionic strength dependence or increasing sorption with increasing solution ionic strength. Both of these behaviors are indicative of an inner-sphere sorption mechanism [15].

The results of the EM measurements indicate that both As (III) and As (V) form inner-sphere complexes on Prestea LC. The shift of pHzpc to a lower pH range with increases in both As (V) and As (III) concentrations for Prestea LC is evidence of inner-sphere complex (specific ion sorption) formation, where $H_3AsO_3^0$ and $H_2AsO_4^-$ for As (III) and As (V) species respectively form complexes directly with the coordination environment of the LC surfaces [113]. Shifts in pHzpc and reversals of EM with increasing ion concentration are characteristics of inner-sphere sorption.

Arsenic (III) sorbs by both inner- and outer-sphere sorption mechanisms on Awaso LC because there is an initial shift in pHzpc when the media is treated with 0.035mM As (III). However, no shift in pHzpc is observed even with an increase in concentration of As (III) from 0.035mM to 3.5mM on Awaso LC. This behavior suggests either inner- or outer-sphere surface complexation since a lack of shift in pHzpc does not necessarily mean the formation of outer-sphere surface complexes [62, 126].

The ATR-FTIR analysis shows an increase in peak intensities and band shift to lower wavelengths for both As (III) and As (V) on Prestea and Awaso LCs. The presence of the peaks in the treated LC spectra that are not present in the untreated sample is an indication of chemical bonding between the arsenic species and the surface of the Prestea LC [63, 110]. The peak shift and the change in peak intensity may be an indication of an inner-sphere sorption mechanism [15, 62, 63]. The peak positions of the arsenic-treated samples (sorbed samples for both Prestea and Awaso LC) (Figs. 26, 27, 28, and 29), are significantly different from those of the dissolved arsenic species (Fig. 25), which can be attributed to sorption of the arsenic species. In general, the spectra of both As (III) and As (V) sorbed onto the Prestea and Awaso LCs are very different from those of arsenic aqueous solutions. This difference and the lack of pH dependence on the positions of the vibrational modes indicate that these modes are “protected” from changes in pH and indicate that these groups are involved in direct complexation to the surfaces [15, 62]. Another line of evidence for the mechanism of sorption that is converse to the ATR-FTIR spectra for dissolved arsenic species is that a shift in band position was not observed in As (V) and As (III)

adsorbed spectra with changing pH (Figures 26, 27, 28, and 29). The lack of change in band position at various pH values suggests that arsenic formed the same inner-sphere surface complexes on both Prestea and Awaso LCs [71].

The model predictions from the triple-layer surface complexation illustrate a good fit at all pHs measured for As (III) sorption onto both Prestea and Awaso LCs (Figs. 34 and 36). Since As (III) sorption is markedly reduced by increasing ionic strength, and the model accounts for ionic strength dependence. However, As (V) sorption for both Prestea and Awaso LC can be modeled with both the diffuse-layer (Figs 31 and 32) and the triple-layer model (Figs. 35 and 37), although the triple-layer model gives a better fit at higher pHs than the diffuse layer model (Figs. 31, 33, 35, and 37). The model results confirm the sorption data, which suggest As (III) sorption is by inner-sphere and outer-sphere, but As (V) is by inner-sphere for both concretions tested.

The sorption data, the pHzpc shifts, and the EM measurements indicate an inner-sphere sorption mechanism for As (V) on both Prestea and Awaso LC. The sorption data suggests that the As (III) sorption mechanism is outer-sphere for both Prestea and Awaso LC; however, the pHzpc shifts and the EM measurements for As (III) indicate an inner-sphere sorption mechanism on Prestea LC and both inner- and outer-sphere sorption mechanisms for Awaso LC.

The ATR-FTIR data suggest an inner-sphere sorption mechanism for both As (III) and As (V) on Prestea and Awaso LC. Apart from the sorption data indicating an outer-sphere sorption mechanism for As (III) on both Prestea and Awaso LC, the EM data and the ATR-FTIR data all indicate an inner-sphere sorption mechanism for both

As (III) and As (V) for the Prestea and Awaso concretions. The reason why there exist differences in As (III) sorption mechanisms for the three methods is unknown. I speculate that both sorption mechanisms (inner- and/or outer-sphere) might be at work and both mechanisms are eminent depending on the arsenic concentration in the aqueous solution. This also confirms that the two arsenic species not only behave differently but that their affinity for metal oxide surfaces can also be different. A summary of the sorption mechanisms is shown in Table A-36 in the appendix.

4.10 Comparing Prestea and Awaso LC

The sorption data from the Socorro pilot test site (Fig. A-2 and A-3) agrees with laboratory studies (Tables 5 and 6) showing that Prestea LC has higher sorption capacity than Awaso LC. There are several explanations for this difference. Studies on pure element oxides [15, 127, 128] indicate arsenic has a higher affinity for iron oxides than for aluminum oxides. Degree of crystalinity also affects arsenic sorption. Dixit and Hering [20] show that the transformation of amorphous iron oxides to more crystalline phases decreased the specific surface area and hence the site density of the oxide. This transformation decreased the sorption capacity of the oxide.

The X-ray powder diffraction pattern for Prestea laterite concretions differs from that of the Awaso laterite concretions. Prestea LC peaks are broader than Awaso peaks. Peak broadening is attributed to small grain size or poor crystalinity [20]. Awaso LC sharper XRD peaks suggest a higher degree of crystalinity. Hence, difference in degree of crystalinity may explain the differences in arsenic sorption. The height of iron oxide mineral peaks in comparison to aluminum oxide peaks differ

as expected because of the composition differences. However, both concretions exhibit the same mineral phases. The difference in sorption capacity between the two LC maybe related to the difference in crystalinity. The single-point BET N_2 sorption isotherms indicate surface areas of $32m^2/g$ and $18m^2/g$ for Prestea and Awaso, respectively. The higher specific surface area of the Prestea LC is compatible with it having a smaller grain size compared to the Awaso LC.

The degree of lateritization estimated from the silica-sesquioxide (S-S) ratio ($SiO_2/(Fe_2O_3 + Al_2O_3)$) indicates that both concretions can be described as laterites by definition, since they both have S-S ratios far less than 1.33. It is not clear if the higher silica in Prestea LC affects sorption. Study of several Prestea samples with differing concentrations of silica would have to be done to quantify the effects of silica on sorption. Since silica has a weak sorption capacity for metals, it is expected that silica simply dilutes the arsenic-sorbing aluminum and iron oxides and hydroxides. Thus, iron/aluminum ratio of a laterite and its maturity is more important than the silica content so far as sorption is concerned.

Prestea LC, and by inference other high Fe/Al concretions, is more practical to use for filtering especially in areas where the predominant arsenic species in aqueous solution is As (III). Analysis of sorption mechanisms (Table A-36) indicates that As (III) sorption on Awaso LC is controlled both by weak electrostatic forces and strong covalent bonding. However, As (III) sorption on Prestea LC is predominantly controlled by strong covalent bonding (specific ion adsorption). Thus, longer and better sorption of arsenic is expected by use of high Fe/Al LC. In the practical application of LC to rural Africa well water remediation it may not be possible to

determine As(III)/As(V) and local LC Fe/Al ratios. The good news from the studies on the two end member composition LC is that all LC are expected to sorb both forms of arsenic, but that Fe rich-LC will work somewhat better.

4.11 Low cost arsenic filter

The data above suggests that both Prestea and Awaso laterite concretions will work for low-tech applications because both arsenic species sorb over a broad pH range. No pretreatment is required for LC use, compared to high priced laboratory synthesized materials [102, 129]. Arsenic (V) sorption on LC showed almost no ionic strength dependence, indicating that it could be used to treat arsenic contaminated drinking water with high amounts of dissolved salts without affecting the sorption capacity. The sorption capacity of LC is at least 1.11 mg/g, which is a factor of one or two below engineered materials consisting of iron, aluminum, and titanium oxides [130] (see appendix Table A-3). This sorption capacity value of LC indicates that significant sorption sites are available for specific sorption of both arsenic species. The development of low-cost arsenic filters using LC is practical. The Prestea and Awaso LC can both treat approximately 5000 bed volumes of 42µL As (V) Socorro water to the maximum contamination limit of 10ppb (Figs. A-2 and A-3). The treatment process cost, including materials for construction and maintenance, is estimated to be US$0.003/100L contaminated water. It cost approximately $60.00 to make a village filter for a village the size of 200-300 people. Water quality assessment after treatment with both Prestea and Awaso LC indicates that none of the trace elements tested are released from the adsorbent (Fig. A-4 toA-7). A Toxicity

Characterization Leaching Procedure (TCLP) [131] test also reveals that the used adsorbent is not toxic (Table A-3 and A-4; Appendix 4.0).

The positive sorption temperature dependence will enhance sorption in tropical climates, and more especially in areas where groundwater sources are related to geothermal springs. The occurrence of high arsenic water is a problem in rural communities with low capital income; hence the low-cost filter will be cost effective and user friendly for them.

4.12 Ramifications

The positive temperature dependence on arsenic sorption shown by our experiments helps explain the widespread occurrence of elevated arsenic concentration in groundwater fluxing Tertiary volcanic rocks. Volcanic rocks are commonly oxidized, which is best observed in pink to red felsic volcanics that were white or gray when erupted [132, 133]. Geothermal waters active after intrusion and eruption events are typically charged with mg/L concentrations of arsenic [11, 132, 134]. Arsenic is likely sorbed onto volcanic rock iron oxide minerals. If at a later time, cooler groundwater fluxes through the same rocks, this arsenic will be leached because of the decreased sorption at lower temperatures. Our data does not cover temperatures >60°C, but suggests that the increase in sorption with temperature can be extrapolated to 80°C or possibly 100°C. Hot springs 10's of km's from geothermal centers indicate that larger volumes of rock in a geothermal system [132, 134] are subjected to 100°C fluids.

CHAPTER 5

APPLICATIONS AND RECOMMENDATIONS FOR FUTURE WORK

5.1. Extension of Prestea and Awaso laterite concretion results to other laterite concretions.

Prestea and Awaso laterite concretions represent the end members of most laterite concretions (Table A-37; Fig. A-14). Investigations of arsenic sorption onto these two end members show that they filter arsenic from arsenic-bearing drinking water. All other laterites whose mineralogical compositions fall within these two end members, should filter arsenic from drinking water. Laterites from India [89] and Sri Lanka [85] whose mineralogical composition (Table A-37) represents a mixture of the two end members show that the natural medium (laterite) is capable of remediating arsenic from drinking water. The results from this study and other studies [85, 89, 93-96] indicate that laterite concretions work in filtering arsenic from drinking water.

There are factors that increase or decrease arsenic sorption. For example minerals such as titanium and manganese oxides are known to oxidize As (III) if present to As (V) [89], which increases total arsenic sorption. Although there are traces of manganese and titanium oxides in the laterites tested, they worked equally well in sorbing both arsenic species. Soluble silica is known to inhibit arsenic sorption, since it competes for sorption sites with the arsenic species [122]. Table A-39 shows variable silica content in the laterites found in the world. Although the effect of silica could not be quantified in this work, the results from this work show

that its effect was minimal. It turns out that silica has a stronger effect on laboratory synthesized material than it does on the two laterite end members tested.

The crystalinity or amorphous nature of any laterite controls its specific surface area and hence its sorption capacity. Dixit and Hering [20] show that the transformation of amorphous iron oxides to more crystalline phases decreased the specific surface area and hence site density of the iron oxide. This transformation decreased the sorption capacity of the iron oxide. Although Prestea laterite is amorphous (Fig. 2) while Awaso is crystalline (Fig. 3), they both sorbed arsenic well.

To decide whether or not any laterite found elsewhere in the world could be used for arsenic remediation, the degree of lateritization should be estimated from the silica-sesquioxide (S-S) ratio ($SiO_2/(Fe_2O_3 + Al_2O_3)$). In this work silica sesquioxide ratios indicated that both concretions can be described as laterites by definition, since they both have S-S ratio less than 1.33. The implication to other lateritic material is that if the S-S ratio is less than 1.33, then the material should be able to remediate arsenic from arsenic-bearing drinking water.

A summary of the sorption mechanisms (Table A-36) indicates that As (III) sorption on laterites whose predominant mineral phase is aluminum oxide is controlled by both weak electrostatic forces and strong covalent bonding. Other researchers [15, 61] who looked at the mechanism of arsenic sorption on pure (single mineral phase) aluminum oxide also concluded that As (III) sorption is controlled by both weak electrostatic forces and strong covalent bonding. However, Prestea LC which is predominantly iron oxide shows that As (III) sorption is controlled by strong covalent bonding (specific ion sorption). Goldberg and Johnson [15], Suarez [62], and

Sun and Doner [63], who studied As (III) sorption mechanisms on pure iron oxide, show that strong covalent sorption (specific sorption) controls As (III) sorption. The cumulative impact of this research is a prescription for effective groundwater remediation requiring: (1) the oxidation of As (III) to As (V) where aluminum oxide is the predominant laterite mineral; (2) No pre-oxidation for sorption of As (III) where iron oxide is the predominant mineral.

In any arsenic remediation effort using laterite concretions, the general water chemistry will play a major role. Competing ions such as phosphate and sulfate if present in high quantities present a threat to arsenic remediation; this work argues that the greatest threat to arsenic remediation is phosphate. Again the effect will be higher on aluminum oxide-dominant laterite than it will be on iron oxide-dominant laterite. Sulfate, however, shows no diminishing effect on arsenic sorption on the two LC end members tested, rather its presence increased sorption. The type of inorganic arsenic species present (As (III) or As (V)) in the arsenic contaminated water will determine the effect of phosphate and sulfate competition for sorption sites. This research shows that in the presence of high phosphate and sulfate-bearing water, As (III) dominated water is affected more than As (V) dominated water. Other researchers show similar trends [89, 122]. These studies implicate the need for pre-oxidation of As (III) to As (V) in arsenic contaminated water for effective arsenic remediation in water containing high sulfate and phosphate content.

Another important parameter tested using these two LC end members is pH. The complex nature of the laterite concretions allows sorption over a wide pH range (4-9). Although As (V) showed better sorption than As (III) over the pH range tested,

both sorbed better than some laboratory synthesized materials [15]. Other researchers [89, 93-96] observed a similar superiority of laterite concretions over laboratory-synthesized oxides. The laboratory synthesized oxides sorb best at specific pHs and always require pH-controlled arsenic-contaminated water to filter arsenic effectively [135]. As a result, the use of naturally occurring laterites in place of laboratory-synthesized oxides removes the need for additional pH-controlling systems. Such pH-management systems often cost between $25,000 and $ 40,000 and require electrical power, making such arsenic-remediation systems inaccessible and unaffordable for rural communities in developing countries

Tests of Prestea laterite concretion show sorption increases with increasing temperature up to 60ºC. This implies sorption will be enhanced in tropical climates, and more especially in areas where groundwater sources are related to geothermal springs. This finding could be extended to other laterite concretions (Table A-37) since other workers observed a similar trend [89, 93-96].

In summary, the Al-oxide and Fe-oxide end members tested show that alternative laterite concretions can be used in arsenic remediation. Comparism with the commercially available media (Table A-3) show that ground laterite concretion works better for low-tech applications and that the treatment process cost is estimated to be only US$0.003/100L of contaminated water, hence the low-cost filter will be cost-effective and user friendly since no pretreatment is required for its use. Based on these findings, I speculate that laterite concretions found elsewhere in the world can be used in arsenic remediation.

5.2 Recommendations for future work

Experiments could be done to determine how laterite concretions can be improved by simple treatments. Prestea and Awaso LC can treat up to 5000 bed volumes of water contaminated with 42 ppb arsenic: this is comparable to some of the commercial material available (Table A-3) [135]. Much can be done to improve the sorption capacity of ground LC. Acid treatment and heat treatment of laterite concretions can improve the sorption capacity of LC [102, 136]. Acid treatment with HCl can remove salts that adversely affect the arsenic sorption [102, 136]. Sorption capacity of Prestea and Awaso LC can also be increased by the addition of ferric chloride or aluminum chloride as these could act as coatings on the silica found in both laterite concretions [102].

Prestea and Awaso LC tested using Socorro and Sedillo springs water indicate that trace element (chromium, copper, iron, lead, lithium, manganese, strontium, silica, uranium and zinc) concentrations were reduced by 50-80 % (Figs. A-4-9), illustrating the potential of arsenic sorbing media like Prestea and Awaso LC to remove other toxic trace elements. Laboratory, pilot, and full-scale studies can be carried out to determine which trace elements are sorbed by Prestea and Awaso LC.

Although the sorption data, EM measurements, and ATR-FTIR spectroscopy data aided in determining the mechanisms of arsenic sorption onto LC, Extended X-ray Absorption Fine Structure Studies (EXAFS) will further confirm the arsenic sorption mechanisms. X-ray Absorption Near Edge Structure (XANES) work is also needed to define the type and valence state of the arsenic species on the laterite

concretions after sorption (the detailed theory and application of ATR-FTIR, EXAFS and XANES are presented in appendix 2.0).

This study has shown that arsenic sorption onto natural materials can be described by surface complexation modeling. The next step is to incorporate these sorption models into reactive transport models to predict the fate and transport of contaminants in the subsurface. This has not been previously examined extensively due to problems associated with the detailed characterization of natural materials.

CHAPTER 6

6.0 Conclusions.

1. The As (III) and As (V) sorption isotherm data best fit the Langmuir isotherm model. The values of the "Gibbs free energy ($\Delta G°$)", "standard enthalpy ($\Delta H°$)", and "standard entropy changes ($\Delta S°$)" calculated establish favorable sorption of arsenic onto laterite concretion over a wide range of temperatures.
2. The sorption capacity for As (III) and As (V) increases with temperature, with As (III) showing a greater increase than As (V) at all temperatures. As (V) sorption shows little change with increasing solution pH, while As (III) sorption increases with increasing solution pH to a sorption maximum around pH 8 and decreases with any further increase in solution pH.
3. Ionic strength experiments show that an inner-sphere sorption mechanism is responsible for As (V) sorption on both Prestea and Awaso LC, while As (III) sorption is by an outer-sphere mechanism on both concretions.
4. Electrophoretic mobility measurement results indicate that both As (III) and As (V) form inner-sphere complexes on Prestea LC, while As (III) sorption on Awaso is by both inner- and outer-sphere and As (V) is by inner-sphere.
5. The ATR-FTIR data indicate an inner-sphere surface complex sorption mechanism for As (III) and As (V) for Prestea. However, As (III) sorption on Awaso shows both inner-sphere and outer-sphere sorption mechanisms, while As (V) shows an inner-sphere sorption mechanism.
6. Arsenic (III) sorption onto both Prestea and Awaso, which is markedly reduced by increasing ionic strength, is best modeled using the triple-layer model. While

As (V) sorption onto Prestea and Awaso can be modeled equally well using both either diffuse- or the triple-layer modeling.

7. No pretreatment is required for Prestea and Awaso LC and its cost is only a fraction of a penny to remove the arsenic from 100 liters of drinking water, therefore it is a much better choice for low-tech applications than commercially available arsenic filtering media. Laterite concretions are cost effective and user friendly as a drinking water filter.
8. The positive sorption-temperature dependence will enhance sorption in tropical climates, and more especially in areas where groundwater sources are related to geothermal springs.
9. The media has potential in remediating other toxic trace elements to very low concentrations.
10. A TCLP leaching test also reveals that the used adsorbent is not toxic and can be disposed of without the need for confinement.
11. Investigations of arsenic sorption onto the two laterite end members (Prestea and Awaso LC) show that they have excellent arsenic remediation potential and can effectively filter arsenic from arsenic-bearing drinking water. Parameters obtained can be used to optimize other LCs for similar applications and to design appropriate and effective arsenic filtering devices.
12. Investigations of arsenic sorption onto these two end members show that, all other laterites whose mineralogical compositions fall within these two end members should filter arsenic from drinking water.

References Cited

1. Frankenberger, W.T., ed. *Environmental chemistry of arsenic*. Books in soils, plants, and the environment. 2002, Marcel Dekker: New York. xiii, 391.
2. Pinon-Miramontes, M., R.G. Bautista-Margulis, and A. Perez-Hernandez, *Removal of arsenic and fluoride from drinking water with cake alum and a polymeric anionic flocculent.* Fluoride, 2003. **36**(2): p. 122-128.
3. USEPA, *Capital Costs of Arsenic Removal Technologies: U.S. EPA Arsenic Removal Technology Demonstration Program Round 1 (EPA, 2004b).* EPA, Editor. 2004.
4. Schellmann, W., *GEOCHEMICAL DIFFERENTIATION IN LATERITE AND BAUXITE FORMATION.* Catena, 1994. **21**(2-3): p. 131-143.
5. Bourman, R.P. and C.D. Ollier, *A critique of the Schellmann definition and classification of 'laterite'.* Catena, 2002. **47**(2): p. 117-131.
6. Mazumder, D.N.G., et al., *Bronchiectasis in persons with skin lesions resulting from arsenic in drinking water.* Epidemiology, 2005. **16**(6): p. 760-765.
7. Science, N.A.o. *Arsenic in Drinking Water*. 1999. Washington, D.C.: National Academy Press.
8. Hsieh, L.L., et al., *ARSENIC-RELATED BOWENS-DISEASE AND PARAQUAT-RELATED SKIN CANCEROUS LESIONS SHOW NO DETECTABLE RAS AND P53 GENE ALTERATIONS.* Cancer Letters, 1994. **86**(1): p. 59-65.
9. Miller, G.P., *Surface Complexation Modeling of Arsenic in Natural and Sediment Systems*, in *Earth and Environmantal Science*. 2001, New Mexico Tech: Socorro. p. 118.
10. WHO, *Guidelines for drinking water quality, 2nd ed.; Geneva, Switzerland, .* 1993.
11. Smedley, P.L. and D.G. Kinniburgh, *A review of the source, behaviour and distribution of arsenic in natural waters.* Applied Geochemistry, 2001. **17**(5): p. 517-568.
12. National Research Council (U.S.). Subcommittee on Arsenic in Drinking Water. and National Research Council (U.S.). Division on Earth and Life Studies., *Arsenic in drinking water : 2001 update*. 2001, Washington, D.C.: National Academy Press. xiv, 225.
13. Duker, A.A., A. Stein, and M. Hale, *A statistical model for spatial patterns of Buruli ulcer in the Amansie West district, Ghana.* International Journal of Applied Earth Observation and Geoinformation, 2006. **8**(2): p. 126-136.
14. WHO, *Arsenic, Geneva.* Environmental Health Criteria, 2001. **224**.
15. Goldberg, S. and C.T. Johnston, *Mechanisms of arsenic adsorption on amorphous oxides evaluated using macroscopic measurements, vibrational spectroscopy, and surface complexation modeling.* Journal of Colloid and Interface Science, 2001. **234**(1): p. 204-216.
16. Schreiber, M.E., J.A. Simo, and P.G. Freiberg, *Stratigraphic and geochemical controls on naturally occurring arsenic in groundwater, eastern Wisconsin, USA.* Hydrogeology Journal, 2000. **8**(2): p. 161-176.

17. Chen, H.W., et al., *Arsenic treatment considerations.* Journal American Water Works Association, 1999. **91**(3): p. 74-85.
18. Welch, A.H., et al., *Arsenic in ground water of the United States: Occurrence and geochemistry.* Ground Water, 2000. **38**(4): p. 589-604.
19. Masscheleyn, P.H., R.D. Delaune, and W.H. Patrick, *EFFECT OF REDOX POTENTIAL AND PH ON ARSENIC SPECIATION AND SOLUBILITY IN A CONTAMINATED SOIL.* Environmental Science & Technology, 1991. **25**(8): p. 1414-1419.
20. Dixit, S. and J.G. Hering, *Comparison of arsenic(V) and arsenic(III) sorption onto iron oxide minerals: Implications for arsenic mobility.* Environmental Science & Technology, 2003. **37**(18): p. 4182-4189.
21. Martell, A.E.e., al.,, *NIST critically selected stability constants of metals complexes*, U.d.o.C.N.I.o.S.a.T.S.r.d. program, Editor. 2001, NIST.
22. Cummings, D.E., et al., *Arsenic mobilization by the dissimilatory Fe(III)-reducing bacterium Shewanella alga BrY.* Environmental Science & Technology, 1999. **33**(5): p. 723-729.
23. Ahmann, D., et al., *Microbial mobilization of arsenic from sediments of the Aberjona Watershed.* Environmental Science & Technology, 1997. **31**(10): p. 2923-2930.
24. Cummings, D.E., et al., *Arsenic mobilization by the dissimilatory Fe(III)-reducing bacterium Shewanella alga BrY.* Environmental Science & Technology, ES & T, 1999. **33**(5): p. 723-729.
25. Macur, R.E., et al., *Microbial populations associated with the reduction and enhanced mobilization of arsenic in mine tailings.* Environmental Science and Technology, 2001. **35**(18): p. 3676-3682.
26. Masscheleyn, P.H., R.D. Delaune, and W.H. Patrick, *ARSENIC AND SELENIUM CHEMISTRY AS AFFECTED BY SEDIMENT REDOX POTENTIAL AND PH.* Journal of Environmental Quality, 1991. **20**(3): p. 522-527.
27. Nickson, R.T., et al., *Mechanism of arsenic release to groundwater, Bangladesh and West Bengal.* Applied Geochemistry, 2000. **15**(4): p. 403-413.
28. Nickson, R., et al., *Arsenic poisoning of Bangladesh groundwater.* Nature, 1998. **395**(6700): p. 338-338.
29. Violante, A., et al., *Coprecipitation of arsenate with metal oxides: Nature, mineralogy, and reactivity of aluminum precipitates.* Environmental Science & Technology, 2006. **40**(16): p. 4961-4967.
30. Tokunaga, S., S. Yokoyama, and S.A. Wasay, *Removal of arsenic(III) and arsenic(V) ions from aqueous solutions with lanthanum(III) salt and comparison with aluminum(III), calcium(II), and iron(III) salts.* Water Environment Research, 1999. **71**(3): p. 299-306.
31. Liu, R.P., et al., *Silicate hindering in situ formed ferric hydroxide precipitation: Inhibiting arsenic removal from water.* Environmental Engineering Science, 2007. **24**(5): p. 707-715.

32. Thirunavukkarasu, O.S., T. Viraraghavan, and K.S. Subramanian, *Arsenic removal from drinking water using granular ferric hydroxide.* Water Sa, 2003. **29**(2): p. 161-170.
33. Herbel, M. and S. Fendorf, *Transformation and transport of arsenic within ferric hydroxide coated sands upon dissimilatory reducing bacterial activity*, in *Advances in Arsenic Research*. 2005, AMER CHEMICAL SOC: 1155 SIXTEENTH ST NW, WASHINGTON, DC 20036 USA. p. 77-90.
34. Hering, J.G., et al., *Arsenic removal by ferric chloride.* Journal American Water Works Association, 1996. **88**(4): p. 155-167.
35. Wickramasinghe, S.R., et al., *Arsenic removal by coagulation and filtration: comparison of groundwaters from the United States and Bangladesh.* Desalination, 2004. **169**(3): p. 231-244.
36. Thirunavkukkarasu, O.S., T. Viraraghavan, and K.S. Subramanian, *Removal of arsenic in drinking water by iron oxide-coated sand and ferrihydrite - Batch studies.* Water Quality Research Journal of Canada, 2001. **36**(1): p. 55-70.
37. Vaishya, R.C. and S.K. Gupta, *Modeling arsenic(V) removal from water by sulfate modified iron-oxide coated sand (SMIOCS).* Separation Science and Technology, 2004. **39**(3): p. 645-666.
38. Thirunavukkarasu, O.S., T. Viraraghavan, and K.S. Subramanian, *Arsenic removal from drinking water using iron oxide-coated sand.* Water Air and Soil Pollution, 2003. **142**(1-4): p. 95-111.
39. Gupta, V.K., V.K. Saini, and N. Jain, *Adsorption of As(III) from aqueous solutions by iron oxide-coated sand.* Journal of Colloid and Interface Science, 2005. **288**(1): p. 55-60.
40. Ning, R.Y., *Arsenic removal by reverse osmosis.* Desalination, 2002. **143**(3): p. 237-241.
41. Pawlak, Z., S. Zak, and L. Zablocki, *Removal of hazardous metals from groundwater by reverse osmosis.* Polish Journal of Environmental Studies, 2006. **15**(4): p. 579-583.
42. Lin, T.F., et al., *Removal of arsenic from groundwater using point-of-use reverse osmosis and distilling devices.* Environmental Technology, 2002. **23**(7): p. 781-790.
43. George, C.M., et al., *Reverse osmosis filter use and high arsenic levels in private well water.* Archives of Environmental & Occupational Health, 2006. **61**(4): p. 171-175.
44. Frank, P., D.A. Clifford, and Water Engineering Research Laboratory., *Arsenic (III) oxidation and removal from drinking water*. 1986, Cincinnati, OH: U.S. Environmental Protection Agency Water Engineering Research Laboratory. 9.
45. Manna, B.R., et al., eds. *Removal of arsenic from groundwater using crystalline hydrous ferric oxide (CHFO)*. 2003, Canadian Association on Water Quality, Toronto, ON, Canada. 193-210.
46. Zaw, M. and M.T. Emett, *Arsenic removal from water using advanced oxidation processes.* Toxicology Letters, 2002. **133**(1): p. 113-118.

47. Gregor, J., *Arsenic removal during conventional aluminium-based drinking-water treatment.* Water Research, 2001. **35**(7): p. 1659-1664.
48. Bourman, R.P., *MODES OF FERRICRETE GENESIS - EVIDENCE FROM SOUTHEASTERN AUSTRALIA.* Zeitschrift fur Geomorphologie, 1993. **37**(1): p. 77-101.
49. Schellmann, W., *A new definition of laterite.* Natural Resources and Development
1983. **18** p. 7-21.
50. EYLES. V. A, B., F. A, Brindley, G. W, ed. *The composition and origin of Antrim Laterites and Bauxites*. 1952, Government of Northern Ireland: Leeds.
51. De Medina, J., *Laterites and their application to higth way construction, based on the text of a course at the Brazilian highway Research institute.* Brazilian highway Research institute
1972.
52. Persons, B.S., *Laterites, Genesis, Location, Use.* Plenum press, New York London, 1970.
53. Mountain, M.J. *The location of pedogenetic materials using aerial photographs, with some examples from south Africa.* in *Proceedings of 4th regional conference for Africa on soil mechanics and foundation engineering*. 1967. Cape Town South Africa.
54. Wright, J.B., ed. *Geology and mineral resources of West Africa / J.B. Wright, editor and principal author ; with contributions from D.A. Hastings, W.B. Jones, and H.R. Williams*. 1985, Allen & Unwin, : London [England] ; Boston :.
55. Kesse, G.O., *The Mineral and Rock Resources of Ghana*. 1985: A A Balkema, Rotterdam, The Netherlands. 610 pp.
56. Bhattacharyya, R., et al., eds. *Technique for arsenic removal from groundwater utilizing geological options; an innovative low cost remediation*. 2002, International Association of Hydrological Sciences, International. 391-396.
57. Jana, J., et al., eds. *A renovative low cost technique for removal of arsenic from groundwater; integrated field study*. 2000, A. A. Balkema, Rotterdam, Netherlands. 255-256.
58. Ndur, S.A. and D.I. Norman, *Sorption of arsenic onto laterite; a new technology for filtering rural water.* Geological Society of America, 2003 annual meeting Abstracts with Programs - Geological Society of America, 2003. **35**(6): p. 413.
59. Sahu, S.J., et al., *Use of low cost natural material for removal of arsenic in ground water.* Proceedings of the Eighty sixth annual session of the Indian Science Congress Association Proceedings of the Indian Science Congress, 1999. **86**(4): p. 211.
60. Davis, J.A. and D.B. Kent, *Surface Complexation Modeling in Aqueous Geochemistry.* . Reviews
in Mineralogy: Mineral-Water Interface Geochemistry,, ed. M.F. Hochella, Jr., White, A. F., Ribbe, P. H. (Eds). . Vol. 23. 1990: Mineralogical
Society of America, Washington D.C. pp. 177-248 (Chapter 5).

61. Arai, Y., E.J. Elzinga, and D.L. Sparks, *X-ray absorption spectroscopic investigation of arsenite and arsenate adsorption at the aluminum oxide-water interface.* Journal of Colloid and Interface Science, 2001. **235**(1): p. 80-88.
62. Suarez, D.L., S. Goldberg, and C.M. Su, *evaluation of oxyanion adsorption mechanisms on oxides using FTIR spectroscopy and electrophoritic mobility. In Mineral-water interfacial reactions-Kinetics and Mechanisms*. ACS Symposium series 219, ed. D.L. Sparks and G. T.J. 1998, Washinton D.C: American chemical society.
63. Sun, X.H. and H.E. Doner, *An investigation of arsenate and arsenite bonding structures on goethite by FTIR.* Soil Science, 1996. **161**(12): p. 865-872.
64. Manning, B.A., S.E. Fendorf, and S. Goldberg, *Surface structures and stability of arsenic(III) on goethite: Spectroscopic evidence for inner-sphere complexes.* Environmental Science & Technology, 1998. **32**(16): p. 2383-2388.
65. Ladeira, A.C.Q., et al., *Mechanism of anion retention from EXAFS and density functional calculations: Arsenic (V) adsorbed on gibbsite.* Geochimica et Cosmochimica Acta, 2001. **65**(8): p. 1211-1217.
66. O'Reilly, S.E., D.G. Strawn, and D.L. Sparks, *Residence time effects on arsenate adsorption/desorption mechanisms on goethite.* Soil Science Society of America Journal, 2001. **65**(1): p. 67-77.
67. Waychunas, G.A., et al., *EXAFS STUDY OF THE GEOMETRY OF ZN(II) SURFACE COMPLEXES SORBED ON FERRIHYDRITE.* Abstracts of Papers of the American Chemical Society, 1993. **205**: p. 83-GEOC.
68. Fendorf, S., et al., *Arsenate and chromate retention mechanisms on goethite .1. Surface structure.* Environmental Science & Technology, 1997. **31**(2): p. 315-320.
69. Arai, Y., D.L. Sparks, and J.A. Davis, *Arsenate adsorption mechanisms at the allophane - water interface.* Environmental Science & Technology, 2005. **39**(8): p. 2537-2544.
70. Hayes, K.F., C. Papelis, and J.O. Leckie, *MODELING IONIC-STRENGTH EFFECTS ON ANION ADSORPTION AT HYDROUS OXIDE SOLUTION INTERFACES.* Journal of Colloid and Interface Science, 1988. **125**(2): p. 717-726.
71. Pena, M., et al., *Adsorption mechanism of arsenic on nanocrystalline titanium dioxide.* Environmental Science & Technology, 2006. **40**(4): p. 1257-1262.
72. Hunter, R.J., *Zeta potential in colloid science*. 1981, N.Y: Academic press New York.
73. WAYCHUNAS, G.A., et al., *SURFACE-CHEMISTRY OF FERRIHYDRITE .1. EXAFS STUDIES OF THE GEOMETRY OF COPRECIPITATED AND ADSORBED ARSENATE.* Geochimica et Cosmochimica Acta, 1993. **57**(10): p. 2251-2269.
74. Waychunas, G.A., J.A. Davis, and C.C. Fuller, *GEOMETRY OF SORBED ARSENATE ON FERRIHYDRITE AND CRYSTALLINE FEOOH - REEVALUATION OF EXAFS RESULTS AND TOPOLOGICAL FACTORS IN PREDICTING SORBATE GEOMETRY, AND EVIDENCE FOR*

MONODENTATE COMPLEXES. Geochimica et Cosmochimica Acta, 1995. **59**(17): p. 3655-3661.
75. Waychunas, G.A., et al., *Wide angle X-ray scattering (WAXS) study of "two-line" ferrihydrite structure: Effect of arsenate sorption and counterion variation and comparison with EXAFS results.* Geochimica et Cosmochimica Acta, 1996. **60**(10): p. 1765-1781.
76. Sun, X.H. and H.E. Doner, *Adsorption and oxidation of arsenite on goethite.* Soil Science, 1998. **163**(4): p. 278-287.
77. Davis, J.A., et al., *Application of the surface complexation concept to complex mineral assemblages.* Environmental Science & Technology, 1998. **32**(19): p. 2820-2828.
78. Services, J.S.T., *Materials data, Jade version 3.1, XRD pattern processing and identification software*. 1998, J S Technical Services: Aubrey, TX.
79. Partey, F.P., et al., *Arsenic sorption onto laterite iron concretions from Prestea, Ghana.* . Geological Society of America Abstracts with Programs, 2005. **37**(7).
80. Ndur, *containment of Arsenic in sansu Tailings Dam, Obuasi Ghana.* PhD Dissertation, 2007.
81. Herbelin, A.L. and J.C. Westall, *FITEQL 4.0 - A Computer Program for Determination of Chemical Equilibrium Constants From Experimental Data.* Report 99-01,, 1999(Department of Chemistry, Oregon State University, Corvallis.).
82. Allison, J.D., D.S. Brown, and K.J. Novo-Gradac., *MINTEQA2/ PRODEFA2, A geochemical assessment model for environmental systems: Ver. 3.0 Users manual. Environ. Res. Lab.,*. 1991, USEPA: Athens, GE.
83. Altundogan, H.S., et al., *Arsenic removal from aqueous solutions by adsorption on red mud.* Waste Management, 2000. **20**(8): p. 761-767.
84. Gupta, V.K., *Equilibrium uptake, sorption dynamics, process development, and column operations for the removal of copper and nickel from aqueous solution and wastewater using activated slag, a low-cost adsorbent.* Industrial & Engineering Chemistry Research, 1998. **37**(1): p. 192-202.
85. Vithanage, M., et al., *Mechanistic modeling of arsenic retention on natural red earth in simulated environmental systems.* Journal of Colloid and Interface Science, 2006. **294**(2): p. 265-272.
86. Manning, B.A. and S. Goldberg, *Adsorption and stability of arsenic(III) at the clay mineral-water interface.* Environmental Science & Technology, 1997. **31**(7): p. 2005-2011.
87. Lin, T.F. and J.K. Wu, *Adsorption of arsenite and arsenate within activated alumina grains: Equilibrium and kinetics.* Water Research, 2001. **35**(8): p. 2049-2057.
88. Clifford, D.A., C.-C. Lin, and Risk Reduction Engineering Laboratory (U.S.), *Arsenic (III) and arsenic (V) removal from drinking water in San Ysidro, New Mexico project summary*. 1991, Cincinnati, OH: U.S. Environmental Protection Agency Risk Reduction Engineering Laboratory. 1 v.
89. Maiti, A., et al., *Adsorption of arsenite using natural laterite as adsorbent.* Separation and Purification Technology, 2007. **55**(3): p. 350-359.

90. Feng, X.H., et al., *Arsenite oxidation by three types of manganese oxides.* Journal of Environmental Sciences-China, 2006. **18**(2): p. 292-298.
91. Power, L.E., Y. Arai, and D.L. Sparks, *Zinc adsorption effects on arsenite oxidation kinetics at the birnessite-water interface.* Environmental Science & Technology, 2005. **39**(1): p. 181-187.
92. Pena, M.E., et al., *Adsorption of As(V) and As(III) by nanocrystalline titanium dioxide.* Water Research, 2005. **39**(11): p. 2327-2337.
93. Maji, S.K., A. Pal, and T. Pal, *Arsenic removal from aqueous solutions by adsorption on laterite soil.* Journal of Environmental Science and Health Part A-Toxic/Hazardous Substances & Environmental Engineering, 2007. **42**(4): p. 453-462.
94. Maji, S.K., et al., *Sorption kinetics of arsenic on laterite soil in aqueous medium.* Journal of Environmental Science and Health Part A-Toxic/Hazardous Substances & Environmental Engineering, 2007. **42**(7): p. 989-996.
95. Maji, S.K., et al., *Modeling and fixed bed column adsorption of As(V) on laterite soil.* Journal of Environmental Science and Health Part A-Toxic/Hazardous Substances & Environmental Engineering, 2007. **42**(11): p. 1585-1593.
96. Maji, S.K., et al., *Modeling and fixed bed column adsorption of As(III) on laterite soil.* Separation and Purification Technology, 2007. **56**(3): p. 284-290.
97. Raven, K.P., A. Jain, and R.H. Loeppert, *Arsenite and arsenate adsorption on ferrihydrite: Kinetics, equilibrium, and adsorption envelopes.* Environmental Science & Technology, 1998. **32**(3): p. 344-349.
98. Jain, A. and R.H. Loeppert, *Effect of competing anions on the adsorption of arsenate and arsenite by ferrihydrite.* Journal of Environmental Quality, 2000. **29**(5): p. 1422-1430.
99. Pierce, M.L. and C.B. Moore, *ADSORPTION OF ARSENITE AND ARSENATE ON AMORPHOUS IRON HYDROXIDE.* Water Research, 1982. **16**(7): p. 1247-1253.
100. Wilkie, J.A. and J.G. Hering, *Adsorption of arsenic onto hydrous ferric oxide: Effects of adsorbate/adsorbent ratios and co-occurring solutes.* Colloids and Surfaces A-Physicochemical and Engineering Aspects, 1996. **107**: p. 97-110.
101. Zeng, L., *Arsenic adsorption from aqueous solutions on an Fe(III)-Si binary oxide adsorbent.* Water Quality Research Journal of Canada, 2004. **39**(3): p. 267-275.
102. Genc-Fuhrman, H., J.C. Tjell, and D. McConchie, *Adsorption of arsenic from water using activated neutralized red mud.* Environmental Science & Technology, 2004. **38**(8): p. 2428-2434.
103. Manna, B.R., et al., *Removal of arsenic from groundwater using crystalline hydrous ferric oxide (CHFO).* Water Quality Research Journal of Canada, 2003. **38**(1): p. 193-210.
104. Axe, L. and P.R. Anderson, *Experimental and theoretical diffusivities of Cd and Sr in hydrous ferric oxide.* Journal of Colloid and Interface Science, 1997. **185**(2): p. 436-448.

105. Pandey, P.K., et al., *Arsenic contamination of the environment; a new perspective from central-east India.* Environment International, 2003. **28**(4): p. 235-245.
106. Bye, G.C., M. McEvoy, and M.A. Malati, *ADSORPTION OF COPPER(II) IONS FROM AQUEOUS-SOLUTION BY 5 SILICA SAMPLES.* Journal of Chemical Technology and Biotechnology, 1982. **32**(8): p. 781-789.
107. Yadava, K.P., B.S. Tyagi, and V.N. Singh, *REMOVAL OF ARSENIC(III) FROM AQUEOUS-SOLUTION BY CHINA-CLAY.* Environmental Technology Letters, 1988. **9**(11): p. 1233-1244.
108. Low, K.S., C.K. Lee, and S.G. Tan, *Sorption of trivalent chromium from tannery waste by moss.* Environmental Technology, 1997. **18**(4): p. 449-454.
109. Barrow, N.J., *A BRIEF DISCUSSION ON THE EFFECT OF TEMPERATURE ON THE REACTION OF INORGANIC-IONS WITH SOIL.* Journal of Soil Science, 1992. **43**(1): p. 37-45.
110. Lumsdon, D.G., et al., *NEW INFRARED BAND ASSIGNMENTS FOR THE ARSENATE ION ADSORBED ON SYNTHETIC GOETHITE (ALPHA-FEOOH).* Journal of Soil Science, 1984. **35**(3): p. 381-386.
111. Wijnja, H. and C.P. Schulthess, *Vibrational spectroscopy study of selenate and sulfate adsorption mechanisms on Fe and Al (hydr)oxide surfaces.* Journal of Colloid and Interface Science, 2000. **229**(1): p. 286-297.
112. Myneni, S.C.B., et al., *Vibrational spectroscopy of functional group chemistry and arsenate coordination in ettringite.* Geochimica et Cosmochimica Acta, 1998. **62**(21-22): p. 3499-3514.
113. Hunter, R.J., ed. *Colloid science*. A series of monographs., ed. R.J. Hunter. 1981, Academic Press: San Diego.
114. Aggett, J., C. Camp, and G. Ridall, eds. *Mobility of arsenic in the sediments of the Waikato hydro lakes*. 1981, University of Waikato, Hamilton, New Zealand. 301-311.
115. Anderson, M.A., J.F. Ferguson, and J. Gavis, *ARSENATE ADSORPTION ON AMORPHOUS ALUMINUM HYDROXIDE.* Journal of Colloid and Interface Science, 1976. **54**(3): p. 391-399.
116. Kuriakose, S., T.S. Singh, and K.K. Pant, *Adsorption of As(III) from aqueous solution onto iron oxide impregnated activated alumina.* Water Quality Research Journal of Canada, 2004. **39**(3): p. 258-266.
117. Singh, T.S. and K.K. Pant, *Equilibrium, kinetics and thermodynamic studies for adsorption of As(III) on activated alumina.* Separation and Purification Technology, 2004. **36**(2): p. 139-147.
118. He, L.M., et al., *Ionic strength effects on sulfate and phosphate adsorption on gamma-alumina and kaolinite: Triple-layer model.* Soil Science Society of America Journal, 1997. **61**(3): p. 784-793.
119. Fuller, C.C., J.A. DAVIS, and G.A. WAYCHUNAS, *SURFACE-CHEMISTRY OF FERRIHYDRITE .2. KINETICS OF ARSENATE ADSORPTION AND COPRECIPITATION.* Geochimica et Cosmochimica Acta, 1993. **57**(10): p. 2271-2282.

120. Roberts, L.C., et al., *Arsenic removal with iron(II) and iron(III) waters with high silicate and phosphate concentrations.* Environmental Science & Technology, 2004. **38**(1): p. 307-315.
121. Kirk, M.F., et al., *Bacterial sulfate reduction limits natural arsenic contamination in groundwater.* Geology, 2004. **32**(11): p. 953-956.
122. Zhang, W., et al., *Arsenic removal from contaminated water by natural iron ores.* Minerals Engineering, 2004. **17**(4): p. 517-524.
123. Ergican, E., H. Gecol, and A. Fuchs, *The effect of co-occurring inorganic solutes on the removal of arsenic (V) from water using cationic surfactant micelles and an ultrafiltration membrane.* Desalination, 2005. **181**(1-3): p. 9-26.
124. Drever, ed. *The Geochemistry of Natural Waters*. 2002, Prentice Hall: New Jersey. 199.
125. Panday, K.K., G. Prasad, and V.N. Singh, *COPPER(II) REMOVAL FROM AQUEOUS-SOLUTIONS BY FLY-ASH.* Water Research, 1985. **19**(7): p. 869-873.
126. Stumm, W., *chemistry of the solid-water interface*. 1992, New york: John Wiley and sons.
127. Jeong, Y., et al., *Evaluation of iron oxide and aluminum oxide as potential arsenic(V) adsorbents.* Chemical Engineering and Processing, 2007. **46**(10): p. 1030-1039.
128. Jeong, Y.R., et al., *Effect of competing solutes on arsenic(V) adsorption using iron and aluminum oxides.* Journal of Environmental Sciences-China, 2007. **19**(8): p. 910-919.
129. Genc-Fuhrman, H., H. Bregnhoj, and D. McConchie, *Arsenate removal from water using sand-red mud columns.* Water Research, 2005. **39**(13): p. 2944-2954.
130. Malynda Aragon, M.D.S., Randy Everett, Alicia Aragon, William Holub, Jr, and J.W.a.B. Dwyer, *Pilot Tests of Adsorptive Media Arsenic Treatment Technologies in the Arsenic Water*

Technology Partnership. 2006, Sandia National Labs: socorro.
131. U.S. Environmental Protection Agency (USEPA), *Federal Register,*

40 CFR, Part 261, USEPA, Washington DC, USEPA, Editor. 1996, USEPA.
132. Criaud, A. and C. Fouillac, *THE DISTRIBUTION OF ARSENIC(III) AND ARSENIC(V) IN GEOTHERMAL WATERS - EXAMPLES FROM THE MASSIF CENTRAL OF FRANCE, THE ISLAND OF DOMINICA IN THE LEEWARD ISLANDS OF THE CARIBBEAN, THE VALLES CALDERA OF NEW-MEXICO, UNITED-STATES, AND SOUTHWEST BULGARIA.* Chemical Geology, 1989. **76**(3-4): p. 259-269.
133. Webster-Brown, J.G. and V. Lane, *Modeling seasonal arsenic behavior in the Waikato River, New Zealand*, in *Advances in Arsenic Research*. 2005, AMER CHEMICAL SOC: 1155 SIXTEENTH ST NW, WASHINGTON, DC 20036 USA. p. 253-266.
134. Webster, J.G., Nordstrom, D.K.,, ed. *Geothermal arsenic. In: Arsenic in Ground Water, Geochemistry and Occurrence.* 2003, Kluwer Academic Publishers: Dordrecht,. pp. 101–125.

135. Aragon, M.M.D.S., Everett R, Aragon A, Holub W, Wright J and Dwyer B, *Pilot Tests of Adsorptive Media Arsenic Treatment Technologies in the Arsenic Water Technology Partnership*. 2006, Sandia National Laboratory: socorro. p. p1-14.
136. Altundogan, H.S., et al., *Arsenic adsorption from aqueous solutions by activated red mud.* Waste Management, 2002. **22**(3): p. 357-363.
137. Sparks, D.L., ed. *Environmental soil chemistry*. 2 ed. Vol. 2. 2003, Academic press. 352.
138. Brown, G.E., Parks, G.A., AND O'Day, P.A, ed. *sorption at the mineral-water interface: macroscopic and microscopic perspective*. mineral surfaces, ed. D.V.a.R.A.D. Pattricks. 1995, Chapman and Hall: London.
139. Hair, M.L., *Infra red spectroscopy in surface chemistry*. 1967, New York: Marcel Dekker.
140. Brown, E.G., *Spectroscopic studies of chemisorption reaction mechanisms at oxide-water interfaces. In reviews in Mineralogy*. Review in mineralogy, ed. M.F. Hochella, Jr., White, A. F., Ribbe, P. H. (Eds). Vol. 23. 1990, Washinton DC: Mineralogical society fo America. 335pp.
141. Beebe, T.P., J.E. Crowell, and J.T. Yates, *INFRARED SPECTROSCOPIC STUDY OF THE ROTATION OF CHEMISORBED METHOXY SPECIES ON AN ALUMINA SURFACE.* Journal of Chemical Physics, 1990. **92**(8): p. 5119-5126.
142. Echterhoff, R. and E. Knozinger, *FTIR SPECTROSCOPIC CHARACTERIZATION OF THE ADSORPTION AND DESORPTION OF AMMONIA ON MGO SURFACES.* Surface Science, 1990. **230**(1-3): p. 237-244.
143. Matsumoto, A. and K. Kaneko, *GRADUAL CHANGE IN THE CHEMISORBED NO SPECIES ON ALPHA-FEOOH.* Langmuir, 1990. **6**(6): p. 1202-1204.
144. Tejedortejedor, M.I. and M.A. Anderson, *INSITU ATTENUATED TOTAL REFLECTION FOURIER-TRANSFORM INFRARED STUDIES OF THE GOETHITE (ALPHA-FEOOH)-AQUEOUS SOLUTION INTERFACE.* Langmuir, 1986. **2**(2): p. 203-210.
145. Chang, S.C. and M.J. Weaver, *INSITU INFRARED-SPECTROSCOPY OF CO ADSORBED AT ORDERED PT(110)-AQUEOUS INTERFACES.* Surface Science, 1990. **230**(1-3): p. 222-236.
146. Hochella, M.F., Jr., and A.F. White, *Mineral-Water Interface Geochemistry: An Overview.* Reviews in Mineralogy: Mineral-Water Interface Geochemistry,. Vol. 23. 1990: Mineralogical Society of America, Washington D.C.,. pp. 1-15 (Chapter 1).
147. Davis, J.A., R.O. James, and J.O. Leckie, *SURFACE IONIZATION AND COMPLEXATION AT OXIDE-WATER INTERFACE .1. COMPUTATION OF ELECTRICAL DOUBLE-LAYER PROPERTIES IN SIMPLE ELECTROLYTES.* Journal of Colloid and Interface Science, 1978. **63**(3): p. 480-499.
148. Davis, J.A. and J.O. Leckie, *SURFACE IONIZATION AND COMPLEXATION AT OXIDE-WATER INTERFACE .2. SURFACE*

PROPERTIES OF AMORPHOUS IRON OXYHYDROXIDE AND ADSORPTION OF METAL-IONS. Journal of Colloid and Interface Science, 1978. **67**(1): p. 90-107.

149. Dzomback, D.A. and Morel, *Surface complexation modeling: Hydrous ferric Oxide*. 1990: John Wiley and Sons New york

150. Goldberg, S., *Ion Adsorbtion At the Soil Particle-Solution Interface: Modeling and Mechanisms*. Structure and Surface Reactions of Soil Particles,, ed. P.M. and Huang. 1998, New York: Wiley and Sons, New York.

151. Davis, J.A. and J.O. Leckie, *SURFACE IONIZATION AND COMPLEXATION AT OXIDE-WATER INTERFACE.* Abstracts of Papers of the American Chemical Society, 1978. **176**(SEP): p. 49-49.

152. Meng, X.G. and R.D. Letterman, *MODELING ION ADSORPTION ON ALUMINUM HYDROXIDE MODIFIED SILICA.* Environmental Science & Technology, 1993. **27**(9): p. 1924-1929.

153. Hiemstra, T. and W.H. Van Riemsdijk, *Surface structural ion adsorption modeling of competitive binding of oxyanions by metal (hydr)oxides.* Journal of Colloid and Interface Science, 1999. **210**(1): p. 182-193.

154. Hiemstra, T. and W.H. VanRiemsdijk, *A surface structural approach to ion adsorption: The charge distribution (CD) model.* Journal of Colloid and Interface Science, 1996. **179**(2): p. 488-508.

155. Sposito, G., *ON THE SURFACE COMPLEXATION MODEL OF THE OXIDE-AQUEOUS SOLUTION INTERFACE.* Journal of Colloid and Interface Science, 1983. **91**(2): p. 329-340.

156. Westall, J. and H. Hohl, *COMPARISON OF ELECTROSTATIC MODELS FOR THE OXIDE-SOLUTION INTERFACE.* Advances in Colloid and Interface Science, 1980. **12**(4): p. 265-294.

157. Pauling, L., *The principles determining the structure of complex ionic crystal.* J. Am. Chem. Soc, 1929. **51**: p. 1010-1026.

158. Genc-Fuhrman, H., J.C. Tjell, and D. McConchie, *Increasing the arsenate adsorption capacity of neutralized red mud (Bauxsol).* Journal of Colloid and Interface Science, 2004. **271**(2): p. 313-320.

Appendix.

1.0 Application of Prestea and Awaso LC at the Socorro Pilot project

The ultimate goal of this project is to use laterite concretions from both Prestea and Awaso to develop an effective and inexpensive means of water purification system for communities that cost less and is easy to maintain, and produced drinking water of high quality. A pilot scale study was conducted in collaboration with Sandia National Laboratories with both Prestea and Awaso LC, to assess its promise in a point-of-use treatment unit. The study was performed at the Socorro drinking water treatment site (Socorro springs).

Socorro springs is located off Evergreen Road in Socorro, NM. Socorro and Sedillo springs supply continuous water to the Springs Site. These sources are spring boxes located in the foothills west of the City of Socorro, approximately three-quarters of a mile to the southwest at an elevation approximately fifty feet above the Springs Site. Water from both springs is mixed slightly down gradient of the spring boxes, followed by a shut-off valve. Below the shut-off valve, an eight-inch, subsurface, carbon steel line delivers via gravity the approximately 540 gpm, average 35°C water to the chlorination building where the water is disinfected and oxidized using chlorine gas injection just prior to storage in the Springs Site Storage Tank [135]. A photograph of the design is shown in Figure A-1. Crushed laterite concretions sized to 1.18 mm were loaded into columns provided by Sandia National Labs at the Socorro pilot test site.

Grab water samples from were collected from the feed at this site for laboratory analyses and treated (effluent through laterite). Field parameters measured

are shown in Table A-1 and Table A-2. The equipment characterization, field test design, and field operational procedures are documented in a bulletin produced by the Sandia Arsenic Water Treatment Program [135]. The feed and effluent water were analyzed for arsenic in the New Mexico Bureau of Geology and Mineral Resources (NMBGMR) Chemistry Laboratory at New Mexico Tech in Socorro. Separate samples were collected for major and trace element analysis. The testing period was for one month starting April 4 and ending on April 30, 2007. The results of arsenic removed per bed volume for Prestea and Awaso LC are presented in Figures A-2 and A-3, respectively. Both the Prestea and the Awaso LC could treat approximately 5000 bed volumes of 42µg/L As (V) Socorro water to the maximum contamination limit of 10 ppb. Laboratory sorption experiment shows that Prestea LC can sorb As (V) better than Awaso LC (Table 5 and 6), however the pilot test shows they sorb As (V) (Socorro springs is As (V) dominated) about the same. Reasons for the observed pattern are unknown. Table A-3 shows the results from the pilot scale test in bed volumes of water that can be treated with the various media tested to 10 ppb MCL. The results are comparable to other laboratory synthesized materials tested at the site. Although most of the media (description of other media tested is shown in Table A-5) could treat 2-3 times more arsenic contaminated water to 10 ppb MCL than the LCs tested, they cost 100 times more than the cost of LC. In fact the LC did even better than one of the laboratory synthesized materials (La-DE). These results confirm that the sorption capacity experiments I conducted show that Prestea and Awaso laterite concretions have excellent arsenic remediation potential for drinking water.

2.0. SPECTROSCOPIC THEORY AND APPLICATIONS

Recent developments in spectroscopic studies offer the opportunity to increase understanding of oxy-anion surface speciation and binding. This understanding is essential to the proper use of mechanistic sorption models, such as the diffuse -layer and triple-layer models. Among current spectroscopic methods X-ray Absorption Spectroscopy (XAS) (extended x-ray absorption fine structure spectroscopy (EXAFS) and x-ray absorption near edge structure (XANES)) have received the most attention, however other methods such as Infra Red (IR) spectroscopy have been used extensively in recent years to understand oxy-anion surface speciation and binding mechanisms [15, 62, 63, 112].

Synchrotron-based XAS can be used to study most elements in solid, liquid or gaseous states at concentrations ranging from parts per millions to pure elements. The high intensity of synchrotron radiation allows the study of very small (μg) or dilute (milli-molar, mM) samples and experimental conditions of high or low temperature or pressure and controlled atmospheres, including the presence of fluids such as water. X-ray Absorption Spectroscopy is an element specific, bulk method giving information about the average local structure and composition environment about the absorbing atom. It can be used to study compositionally complex materials such as natural materials [60].

X-ray absorption experiments that result in spectrums consist of exposing a sample to an incident monochromatic beam of synchrotron x-rays scanned over a range of energies below and above the absorption edge (K, L, M) of the element of interest [137]. In the x-ray range of 0.5 to 100 keV, photoelectron production

dominates and causes x-ray attenuation by matter. When the energy of the incident x-ray beam (hv) is less than the binding energy (E_b) of a core electron on the element of interest, absorption is minimal. However, when hv = E_b, electron transitions to unoccupied bound energy levels arise, contributing to the main absorption edge and causing features below the main edge, referred to as the pre-edge portion of the spectrum. As hv increases beyond E_b, electrons can be ejected to unbound levels and stay in the vicinity of the absorber for a short time with excess kinetic energy. In the energy region extending from just above to about 50eV above E_b (the absorption edge), electrons are multiplied and scattered among neighboring atoms, which produces the XANES portion of the spectrum [138]. Fingerprint information such as oxidation states can be gleaned from this portion of the x-ray absorption spectrum. When hv is about 50 to 1000 eV above E_b and the absorption edge, electrons are ejected from the absorber, singly- or multiply-scattered from first- or second-neighbor atoms back to the absorber, and they leave the vicinity of the absorber creating the EXAFS portion of the spectrum. Analyses of the EXAFS spectrum provide information on bond distance, coordination number, and next nearest neighbor [138]

The application of IR spectroscopy to the study of soil chemical processes and reaction has made a significant contribution to the development of new investigation techniques. Infra Red spectroscopy now far exceeds classical chemical analysis and is applied successfully to study sorption processes of inorganic and organic soil components [139]. It is one of the oldest and most sensitive methods used to study hydroxide groups and water molecules on oxide surfaces [140]. Fourier Infra Red

Spectroscopy (FTIR) can provide information on vibrational states of molecules sorbed to surfaces which allow different molecules to be "fingerprinted". In addition, Fourier Transform Infra-Red spectroscopy provides improved signal-to-noise ratios relative to conventional dispersive Infra Red methods. The reason being all the radiation passes through the sample and the entire spectrum of wavelength is detected at once, resulting in a greatly reduced time for spectrum collection, thus allowing dynamic (time resolved) studies [140]. Although the application of FTIR spectroscopy to surfaces are mostly concerned with characterization of gas phase molecules [141-143], it is also used to characterize the solid-liquid interface [144] and sorbed molecules at the solid-liquid interface [145].

Fourier Transform Infra-Red spectroscopic studies reveal a clear understanding of arsenic sorption mechanisms on single mineral phases [15, 62, 63, 112]. Goldberg and Johnson [2001] show that the mechanisms of arsenic sorption to aluminum and iron oxide surfaces based on the FTIR spectroscopy, sorption, and electrophoretic mobility measurements are as follows: As (V) forms inner-sphere surface complexes on both amorphous Al and Fe oxide, while As (III) forms both inner- and outer-sphere surface complexes on amorphous Fe oxide and outer-sphere surface complexes on amorphous Al oxide.

In this study, FTIR spectroscopic was combined with surface complexation modeling to investigate the position of As-O stretching bands for both As (V) and As (III) and their variation with pH instead of extended x-ray absorption fine structure spectroscopy (EXAFS) for two reasons: (1) Although EXAFS is considered to provide definitive information on inner-sphere bonding and is suitable for

determining the mode of attachment to the surface (mono-dentate, bidentate, binuclear), it does not resolve questions of surface speciation since it is not sensitive to H atoms. In addition, examination of the same system by different researchers in some instances resulted in different conclusions [62]; (2) The use of extended x-ray absorption fine structure spectroscopy in this work required a synchrotron radiation source; since there are only two such facilities in United States of America, waiting time and the complexity surrounding the use of such a facility did not allow the use of EXAFS. Moreover FTIR is available on the New Mexico Tech campus, so that is what I used.

3.0. Surface complexation theory

Numerous chemical reactions control the composition of water in contact with soils, sediments, and rocks. Elements and compounds are leached from the rocks while changing conditions can cause the precipitation of new solids. Included in these reactions are ion exchange and surface complexation processes. In natural systems, hydrous metal oxides are the most common minerals participating in surface complexation reactions. In surface complexation, ions are drawn near and held at the mineral surface by electrostatic forces. When there is no water molecule present between the ion and the ligand on the mineral surface they form what is known as inner-sphere complexes. On the other, hand when a water molecule is positioned between the ion and the ligand an outer-sphere complex is formed [146].

Numerous mathematical approaches [147, 148] are used to describe sorption equilibrium behavior. Sorption isotherms are used to calculate metal water-solid

partitioning distribution coefficients. However, field studies revealed problems in the application of sorption isotherms to calculate partition coefficients (the K_d approach). The SC (surface complexation) approach is superior to the K_d approach in modeling oxy-anion sorption because it extends the ion association of aqueous solutions to include chemical surface species [60, 146, 149].

The concepts behind several models and an excellent review of the current state of SC modeling theory are presented by Goldberg [1998]. Several mathematical formulations of SC models are currently available. The four most commonly cited [150] are the:

- Schindler and Stumm Constant Capacitance Model (CC) [60];
- Diffuse Double Layer Model (DDLM) [149];
- Triple Layer Model (TLM) of Davis and Leckie [148, 151]; and,
- Hiemstra and vanRiemsdijk Charge Distribution-Multi-Site Complexation Model (CD-MUSIC) [73, 152-154].

Even though a number of variations exist in these modeling approaches the following four tenets are common to all SC models [77]:

(a) The mineral surface is composed of specific functional groups that react with dissolved solutes to form surface species (coordinative complexes or ion pairs) in a manner analogous to complexation reactions in a homogeneous solution.

(b) The equilibria of SC and surface acidity reactions can be described by mass action equations. If desired, correction factors to these equations may be applied to account for variable electrostatic energy, using electrical double-layer theory.

(c) The apparent binding constants determined for the mass action equations are empirical parameters related to thermodynamic constants by the rational activity coefficients of the surface species [155].

(d) The electrical charge at the surface is determined by the chemical reactions of the mineral functional groups, including acid-base reactions and the formation of ion pairs and coordinative complexes.

The models are distinguished by differences in their respective molecular hypotheses. Each model assumes a particular interfacial structure resulting in the consideration of various kinds of surface reactions and electrostatic correction factors to mass law equations [60].

These models are used to fit laboratory-derived pure mineral SC data with equal success [149, 150, 153, 156]. In application, each of the four models has its own limitations.

The first three models are ranked in order of complexity and the number of fitting parameters used. The greater the number of fitting parameters, the more likely the model will fit experimental data. However, with a greater number of fitting parameters, it is less likely that a unique solution will be realized. Better fits are not completely indicative of a better model. The chemical significance of the modeling approach to the problem under consideration should be considered, in addition to the fit produced by modeling. Hiemstra and VanRiemsdijk's CD-MUSIC model [153, 154] is a newer approach to SC modeling. In this approach, CD-MUSIC surface charge is not assigned to the bonding sites as a point charge but as a spatial distribution of charge in the interfacial region. Because the charge distribution can be

described from Pauling bond theory [157] and spectroscopic studies, the CD-MUSIC model does not require the fitting of experimental data to determine sorption parameters (Hiemstra and vanRiemsdijk, 1995). The CD-MUSIC model has mechanistic properties because the charge distribution is determined from spectroscopically determined bond lengths on the mineral surface and within the solute of interest and it has fit for macroscopic observations.

Surface complexation models use the law of mass-action, expressed as an equilibrium constant, to define protonation (K_{S+}), deprotonation (K_{S-}), and ion-specific sorption to a surface (K_{int}). To implement SC in geochemical codes, these K's must be known for each mineral phase and ion modeled. Central to the SC model approach is that protonation and disassociation reactions and ion-specific complexation constants are reversible and apply over a range of pH and ionic strength conditions [60]. The equilibrium constants K_{S-} and K_{S+} are determined for protonation-deprotonation reactions at the oxide surface. The protonation reaction with the surface, S, in the CCM (constant capacitance model), DLM (double layer model) and TLM (triple layer model) are described by the two step reversible process below,

$$SOH + H^+ \Leftrightarrow SOH_2^+ \quad (56) \qquad SOH \Leftrightarrow SO^- + H^+ \quad (57)$$

$$K_{S+} = \frac{\left[SOH_2^+\right]}{\left[SOH\right]\left[H^+\right]} \exp\frac{\left(F\psi_o\right)}{RT} \quad (58) \qquad K_{S-} = \frac{\left[SO^-\right]\left[H^+\right]}{\left[SOH\right]} \exp\frac{\left(-F\psi_o\right)}{RT} \quad (59)$$

Where F is the Faraday constant (9.65×10^{-4} coulomb/mole), Ψ_o is the surface potential in volts, R is the universal gas constant (J/K.mol), and T is the absolute temperature (K). This exponential electrostatic term appended to the standard form of

the equilibrium mass-action equation is used to account for the change in surface potential because of the sorption of the modeled ion.

The K_{S-} and K_{S+} constants allow the surface-sorbing properties to change with changing pH. Constants for specific sorbing ions that meet these constraints are referred to as "intrinsic constants" or K_{int}. In order to apply these models to SC, K_{int} for surface reactions must be known for each surface to be used, each sorbing ion, and each site defined on the surface. To some degree K_{S-}, K_{S+}, and K_{int} values determined for a single mineral may be used interchangeably among the CCM, DLM and TLM (single site, 2-pK) models. This requires refitting and corrections for model geometry. Refitting of experimental data to different SC models can be accomplished using FITEQL computer algorithm [81].

4.0 The toxicity characteristic leaching procedure (TCLP)

The TCLP, developed by the U.S. EPA [131], provides a means of determining the potential for solid materials to release chemical contaminants into a landfill environment. The TCLP is applied to both Prestea and Awaso LC after completion of the pilot test. Herein, the TCLP involved agitating the used LC (<1.18 mm) in acetic acid using a leachant/waste ratio of 20 at pH 2.88 ± 0.05. The extraction (at 23± 1°C) was achieved by tumbling the specimens (end-over-end) for 18 hours, after which the liquid phase was separated off using a 0.22μm filter and analyzed for heavy metals by the ICP-MS. The TCLP results given in Tables A-3 and A-4 show only a very small amount of the arsenic bound to either Prestea or Awaso is released by acetic acid leaching at pH 2.88 ± 0.05. This suggests that either the

adsorbed As (V) is bound very tightly by surface charges or it is incorporated as a structural component of low-solubility minerals (e.g., calcium iron As (V)s or calcium aluminum As (V)s) [158]. More importantly, in relation to the management of either Prestea or Awaso LC used to adsorb arsenic, U.S. EPA limits for the eight Resource Conservation and Recovery Act (RCRA) elements (Ag, As, Ba, Cd, Cr, Hg, Pb, and Se) are not exceeded, indicating that spent laterite concretion is not hazardous.

Figure A-1. Socorro Pilot Test Equipment.

Table A-1. Prestea Field Test. Values shown are average measured for the period tested

	Feed water	Effluent water
Conductivity	350	340
Temperature	32	31
pH	6.8	6.5
Free chlorine	0.37	0.44
Turbidity	0.78	0.39
Alkalinity	162	153

Table A-2. Awaso Field Test. Values shown are average measured for the period tested

	Feed water	Effluent water
Conductivity	350	342
Temperature	32	30
pH	6.8	6.7
Free chlorine	0.37	0.46
Turbidity	0.78	0.41
Alkalinity	162	140

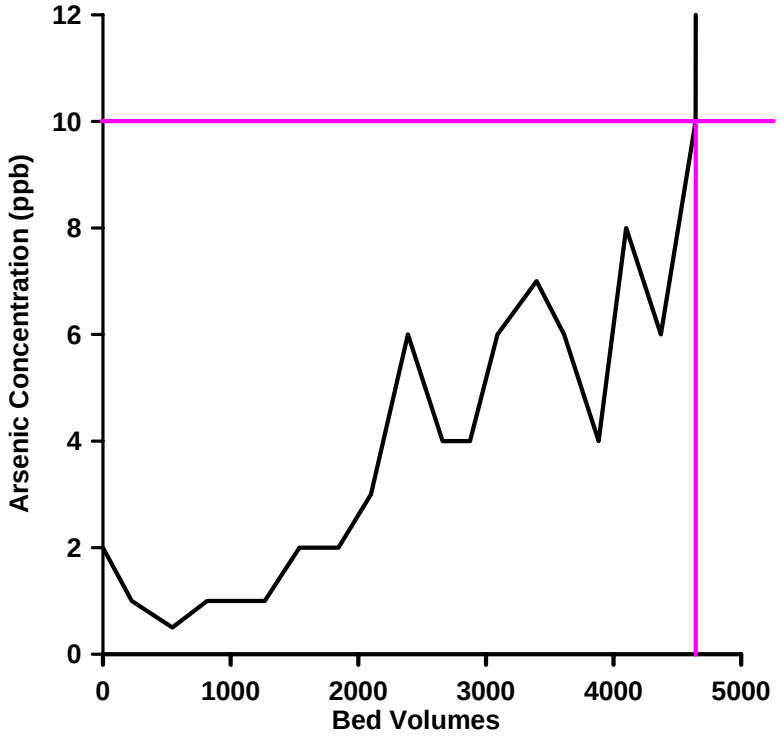

Figure A-2. Arsenic sorption on Prestea LIC from Socorro Pilot project, temperature 32^{o}C. Solid length in column = 38 inches. The pH is 8.2, The 2σ error on arsenic analysis is 3% based on the variance of measurements of 50 replicate samples. Influent arsenic = 42ppb, Kg of LC used = 7.3kg, size of LC = 1.18mm, Residence time = 0.3gpm.

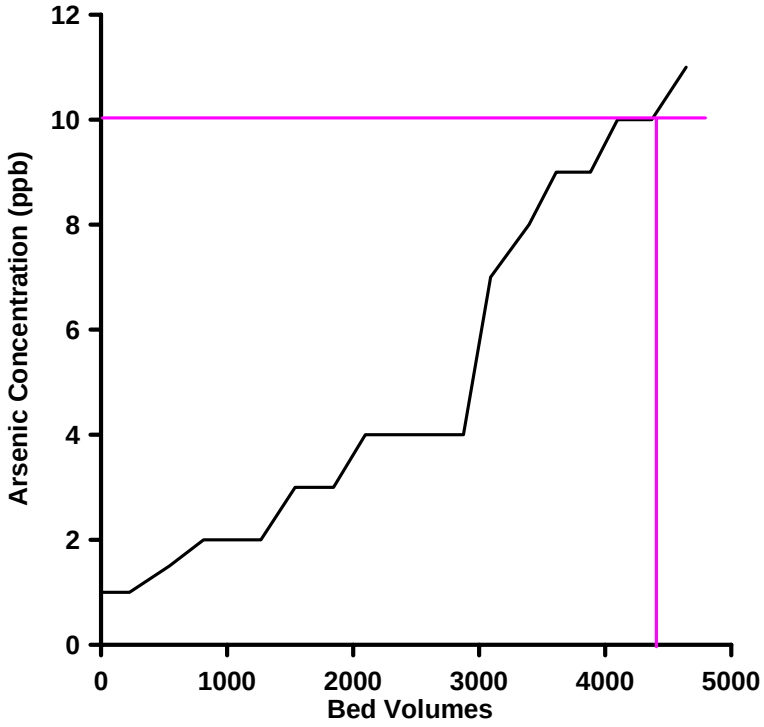

Figure A-3. Arsenic sorption on Awaso LIC from Socorro Pilot project, temperature 32^{o}C. Solid length in column = 38 inches. The pH is 8.2, The 2σ error on arsenic analysis is 3% based on the variance of measurements of 50 replicate samples. Influent arsenic = 42ppb, Kg of LC used = 7.3kg, size of LC = 1.18mm, Residence time = 0.3gpm.

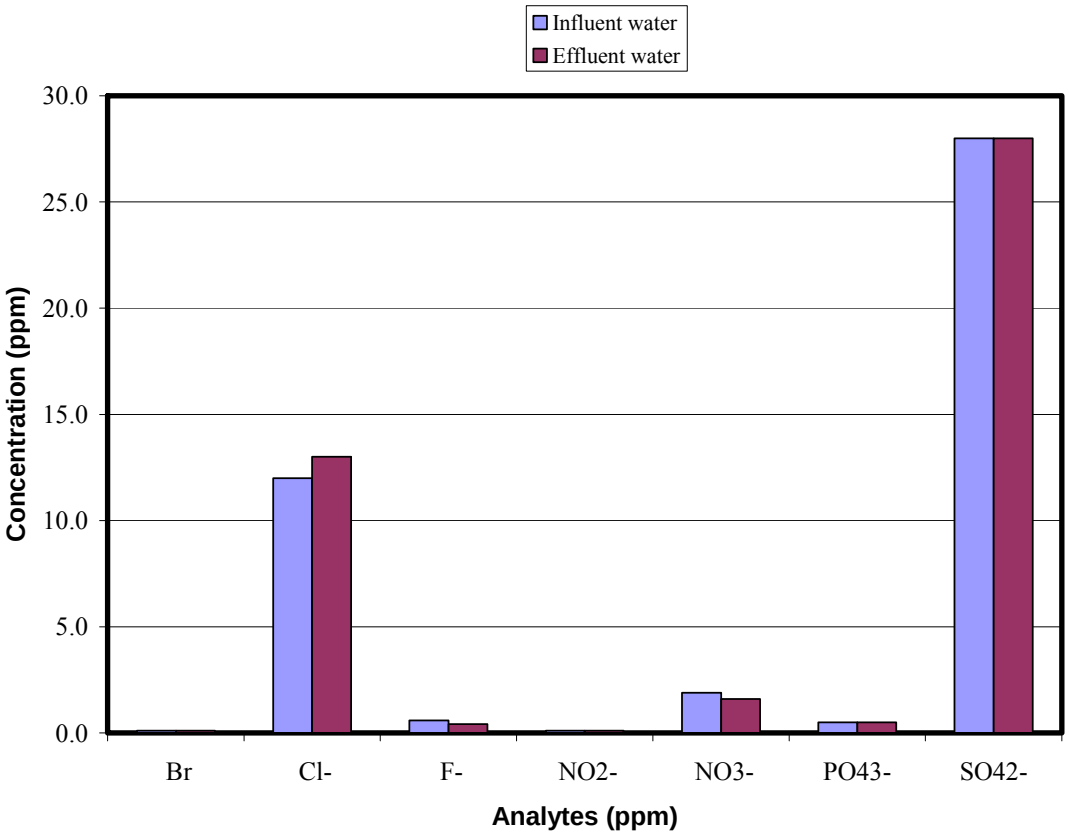

Figure A-4. Socorro water chemistry for major anions before going through Prestea LC and effluent water chemistry after filtering arsenic. Water temperature 32^{o}C. Solid length in column = 38 inches. The pH is 8.2, The 2σ error on arsenic analysis is 3% based on the variance of measurements of 50 replicate samples. Influent arsenic = 42ppb, Kg of LC used = 7.3kg, size of LC = 1.18mm, Residence time = 0.3gpm.

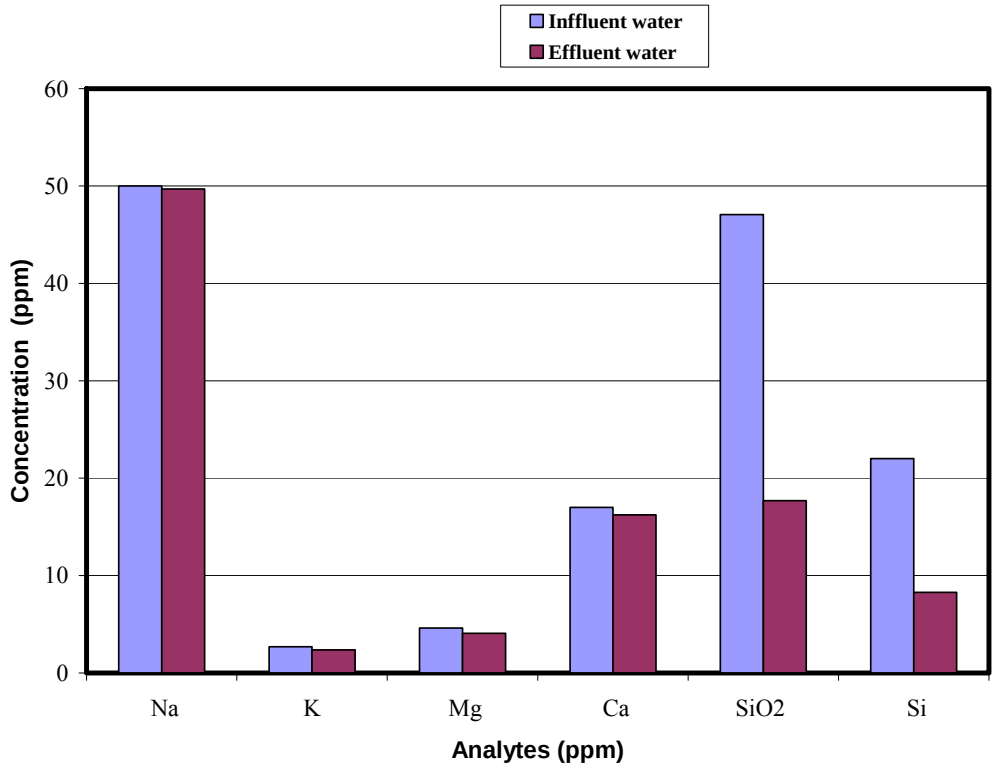

Fig A-5. Socorro water chemistry for Major cations before going through Prestea LC and effluent water chemistry after filtering arsenic. Water temperature = 32 ^{o}C. Solid length in column = 38 inches. The pH is 8.2, The 2σ error on arsenic analysis is 3% based on the variance of measurements of 50 replicate samples. Influent arsenic = 42 ppb, Kg of LC used = 7.3 kg, size of LC = 1.18 mm, Residence time = 0.3 gpm.

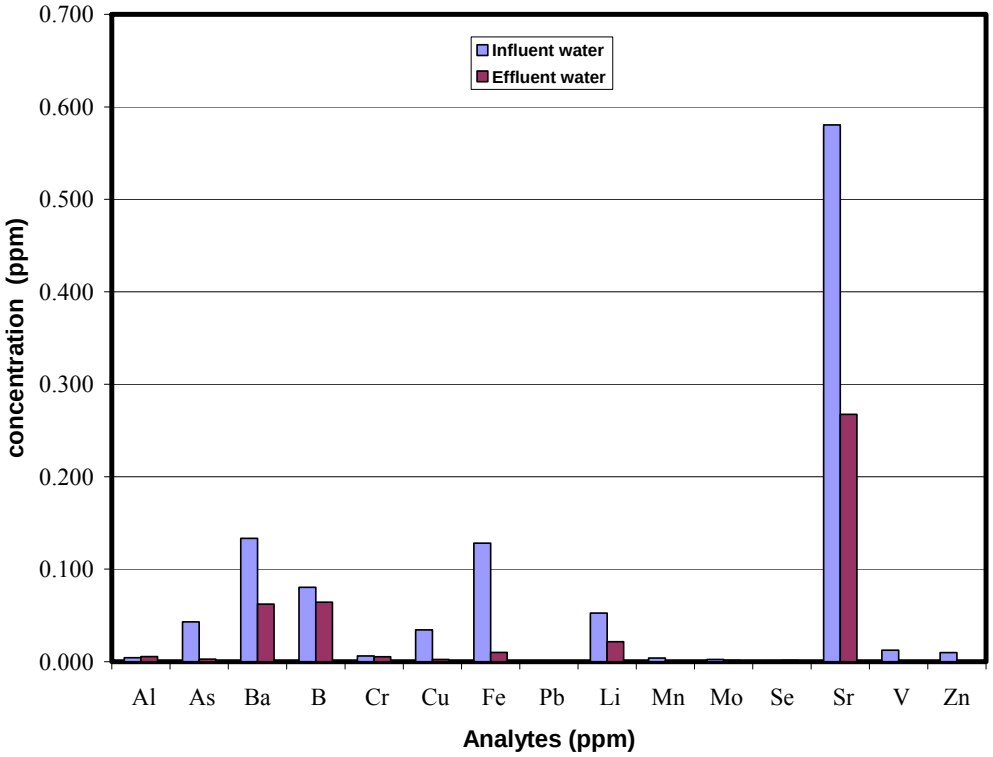

Figure A-6. Socorro water chemistry for trace elements before going through Prestea LC and effluent water chemistry after filtering arsenic through Prestea LC. Water temperature = 32 ^{o}C. Solid length in column = 38 inches. The pH is 8.2. The 2σ error on arsenic analysis is 3% based on the variance of measurements of 50 replicate samples. Influent arsenic = 42ppb, Kg of LC used = 7.3kg, size of LC = 1.18mm, Residence time = 0.3gpm

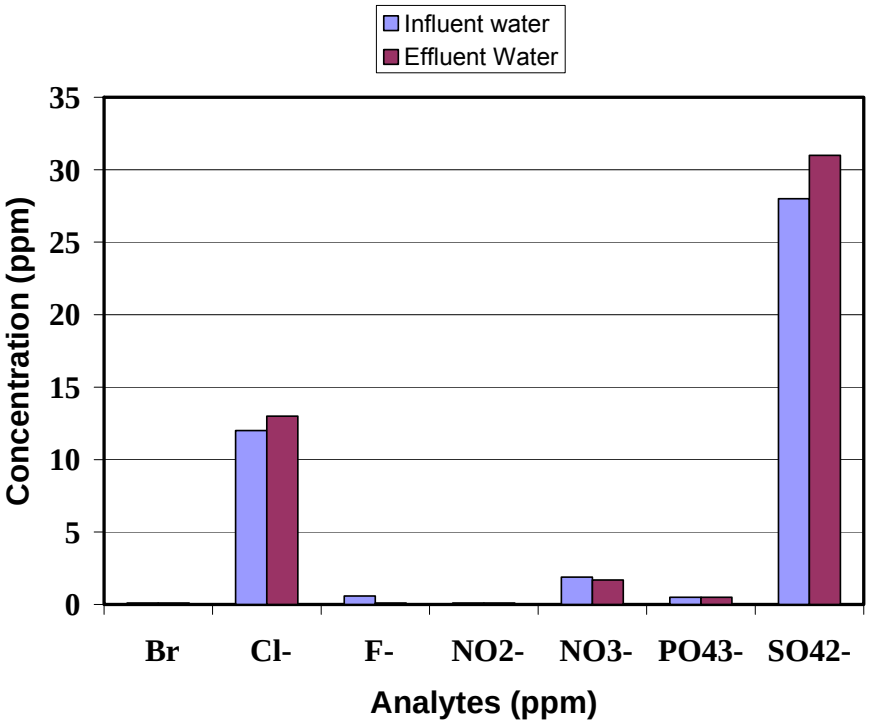

Figure A-7. Socorro water chemistry for major anions before going through Awaso LC and effluent water chemistry after filtering arsenic through Awaso LC. Water temperature = 32^{o}C. Solid length in column = 38 inches. The pH is 8.2. The 2σ error on arsenic analysis is 3% based on the variance of measurements of 50 replicate samples. Influent arsenic = 42ppb, Kg of LC used = 7.3kg, size of LC = 1.18mm, Residence time = 0.3gpm.

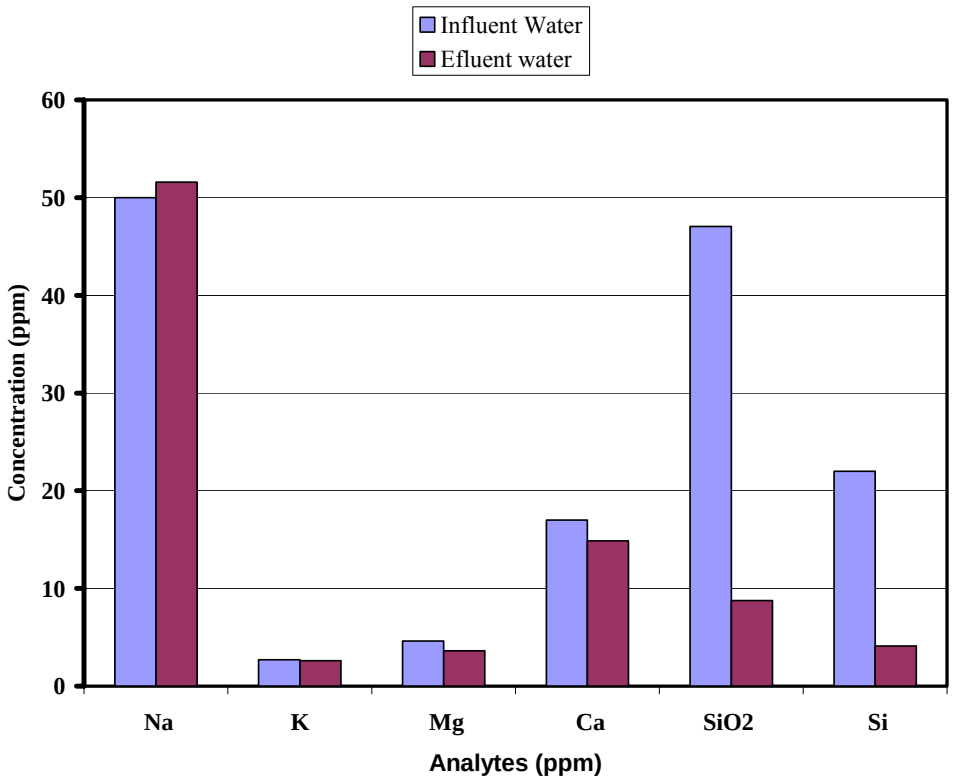

Figure A-8. Socorro water chemistry for major cations before going through Awaso LC and effluent water chemistry after filtering arsenic through Awaso LC. Water temperature = 32^{o}C. Solid length in column = 38 inches. The pH is 8.2, The 2σ error on arsenic analysis is 3% based on the variance of measurements of 50 replicate samples. Influent arsenic = 42ppb, Kg of LC used = 7.3kg, size of LC = 1.18mm, Residence time = 0.3gpm.

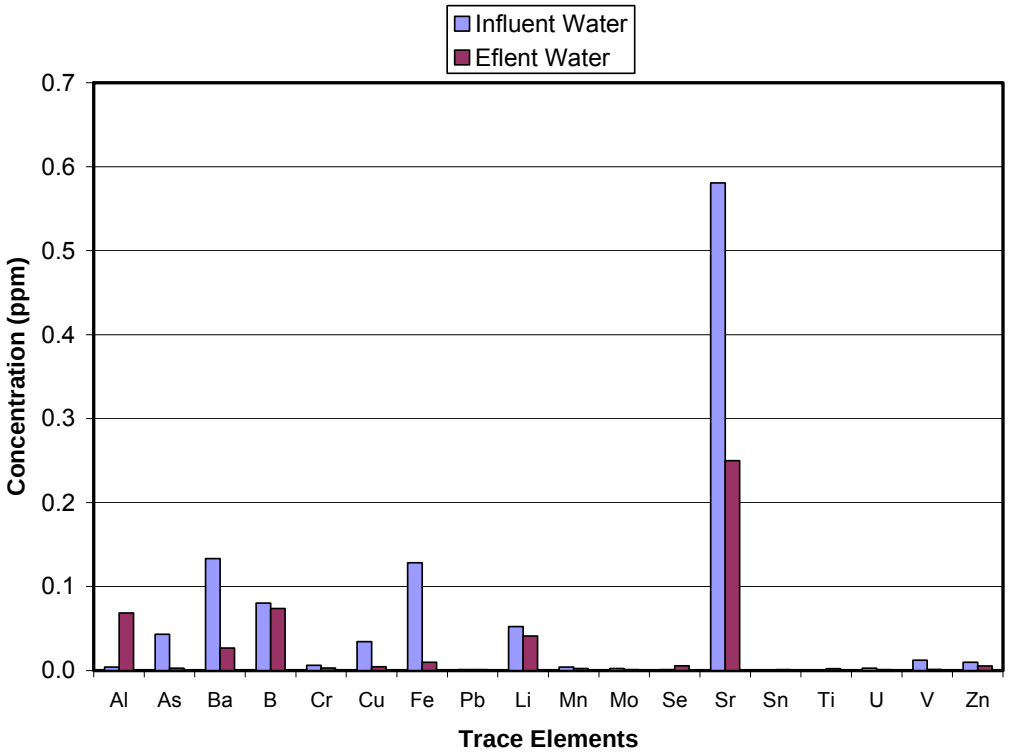

Fig A-9. Socorro water chemistry for trace elements before going through Awaso LC, and effluent water chemistry after filtering arsenic through Awaso LC. Water temperature = 32 ^{o}C. Solid length in column = 38 inches. The pH is 8.2. The 2σ error on arsenic analysis is 3% based on the variance of measurements of 50 replicate samples. Influent arsenic = 42ppb, Kg of LC used = 7.3kg, size of LC = 1.18mm, Residence time = 0.3gpm

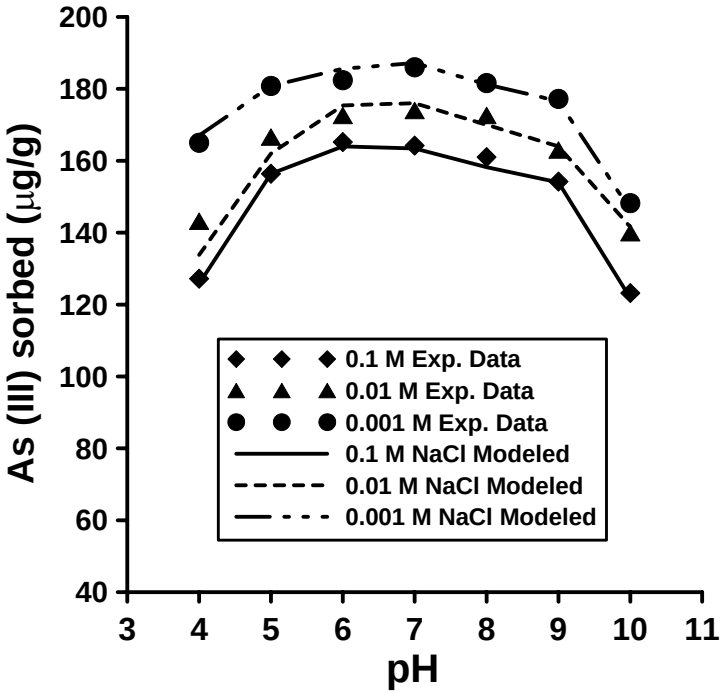

Figure A-10. As (III) sorption on Prestea LC as a function of pH and ionic strength. Lines are alternate diffuse-layer (see text for details) modeled calculations. Arsenic binding constants are optimized for individual ionic strengths. Solid suspension density = 5 g/L, solution arsenic concentration = 1.0mg/L, T=20^{o} C. The 2σ error on arsenic analysis is 3%, based on the variance of measurements of 50 replicate samples.

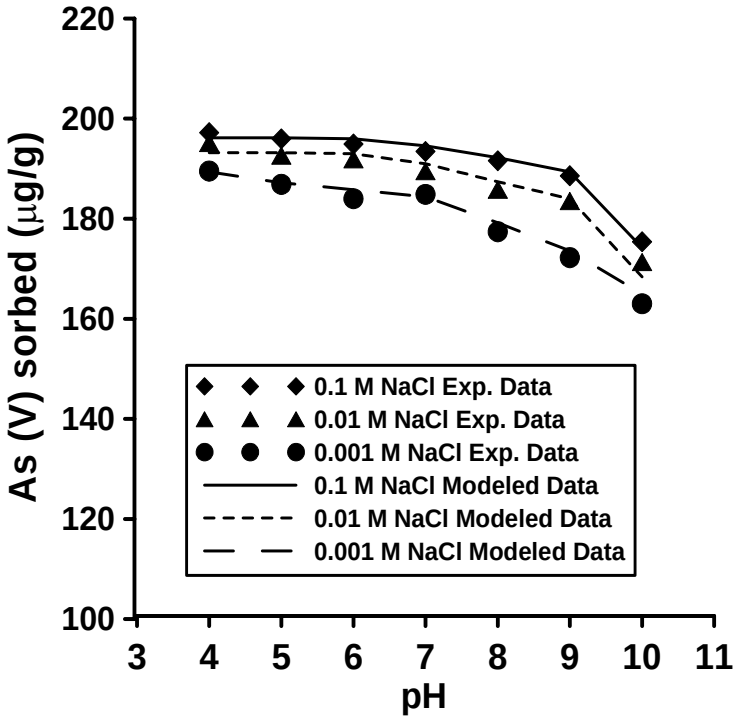

Figure A-11. As (V) sorption on Prestea LC as a function of pH and ionic strength. Lines are alternate diffuse-layer (see text for details) modeled calculations. Arsenic binding constants are optimized for individual ionic strengths. Solid suspension density = 5g/L, solution arsenic concentrations = 1.0mg/L, T=20^{o} C. The 2σ error on arsenic analysis is 3%, based on the variance of measurements of 50 replicate samples.

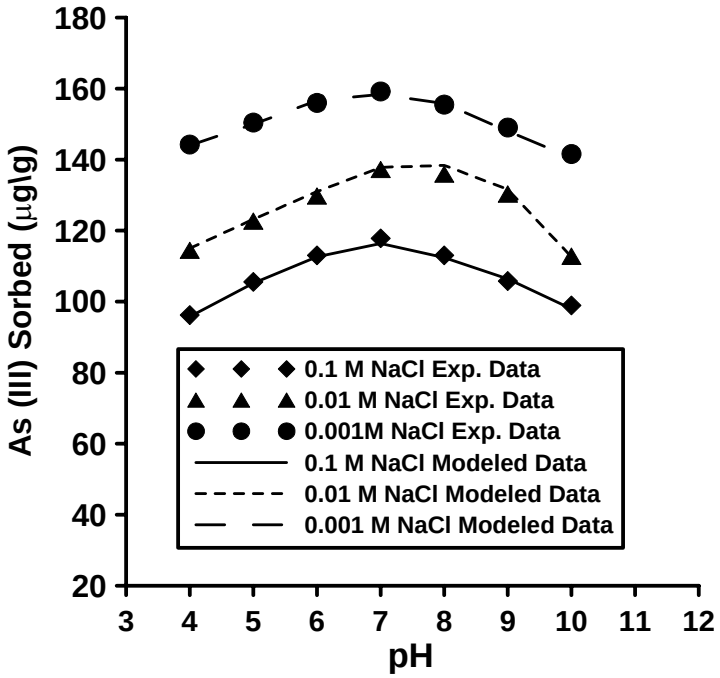

Figure A-12. As (III) sorption on Awaso LC as a function of pH and ionic strength. Lines are alternate diffuse-layer (see text for details) modeled calculations. Arsenic binding constants are optimized for individual ionic strengths. Solid suspension density = 5g/L, solution arsenic concentration = 1.0mg/L, T=20^{o}C. The 2σ error on arsenic analysis is 3%, based on the variance of measurements of 50 replicate samples.

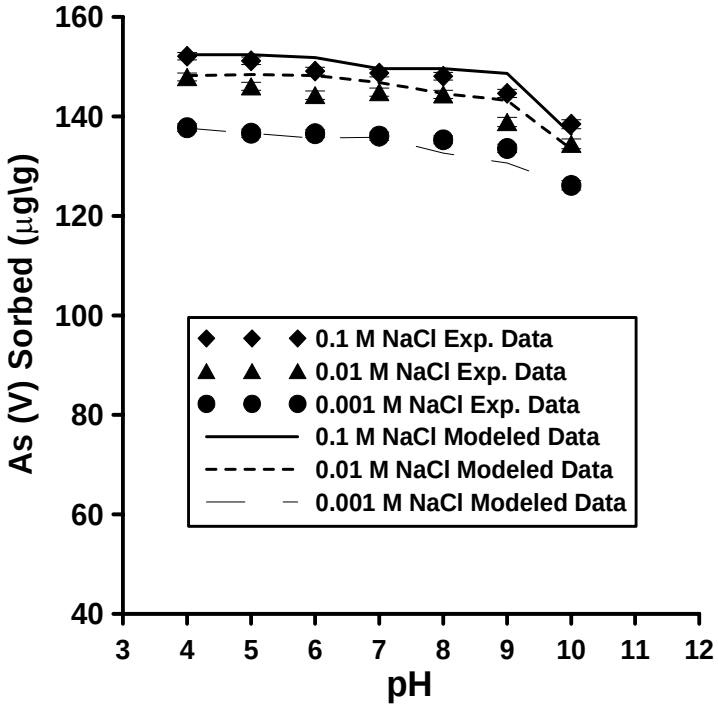

Figure A-13. As (V) sorption on Awaso LC as a function of pH and ionic strength. Lines are alternate diffuse-layer (see text for details) modeled calculations. Arsenic binding constants are optimized for individual ionic strengths. Solid suspension density = 5g/L, solution arsenic concentration = 1.0mg/L, T=20^{o}C. The 2σ error on arsenic analysis is 3%, based on the variance of measurements of 50 replicate samples.

Table A-3. The TCLP test results for the used Prestea LC and comparison with U.S. EPA Standards for classification as an inert solid

Parameter	Method	Results	Standards (mg l−1)
Antimony (mg l^{-1})	ICPMS	<0.001	1.0
Arsenic (mg l^{-1})	ICPMS	0.010	5.0
Barium (mg l^{-1})	ICPMS	<0.001	100.0
Beryllium (mg l^{-1})	ICPMS	0.003	0.1
Cadmium (mg l^{-1})	ICPMS	<0.001	1.0
Chromium (mg l^{-1})	ICPMS	<0.001	5.0
Copper (mg l^{-1})	ICPMS	0.688	-
Manganese (mg l^{-1})	ICPMS	0.037	-
Mercury (mg l^{-1})	ICPMS	<0.001	0.2
Nickel (mg l^{-1})	ICPMS	0.008	7.0
Lead (mg l^{-1})	ICPMS	0.026	5.0
Selenium (mg l^{-1})	ICPMS	<0.001	1.0
Silver (mg l^{-1})	ICPMS	<0.001	5.0
Zinc (mg l^{-1})	ICPMS	0.296	-

Table A-4. The TCLP test results for the used Awaso LC and comparison with U.S. EPA Standards for classification as an inert solid**.**

Parameter	Method	Results	Standards (mg l−1)
Antimony (mg l^{-1})	ICPMS	<0.001	1.0
Arsenic (mg l^{-1})	ICPMS	0.018	5.0
Barium (mg l^{-1})	ICPMS	<0.001	100.0
Beryllium (mg l^{-1})	ICPMS	0.003	0.1
Cadmium (mg l^{-1})	ICPMS	<0.001	1.0
Chromium (mg l^{-1})	ICPMS	<0.001	5.0
Copper (mg l^{-1})	ICPMS	0.688	-
Manganese (mg l^{-1})	ICPMS	0.037	-
Mercury (mg l^{-1})	ICPMS	<0.001	0.2
Nickel (mg l^{-1})	ICPMS	0.018	7.0
Lead (mg l^{-1})	ICPMS	0.048	5.0
Selenium (mg l^{-1})	ICPMS	<0.001	1.0
Silver (mg l^{-1})	ICPMS	<0.001	5.0
Zinc (mg l^{-1})	ICPMS	0.222	-

Table A-5. Summary of description of media tested and Pilot Demonstration Results

Media	Media Type	Socorro BV to 10 ppb breakthrough
IBS1	Iron based sorbent	9,000
IBS2	Iron based sorbent	26,000
ZrOx1	Zirconium Oxide	32,000
TiOx1	Titanium Oxide	13,000
Resin1	Iron-impregnated resin	27,000
La-DE	La-Coated DE	2,400
Prestea LC	Natural Laterite concretion	5,000
Awaso LC	Natural Laterite concretion	5,000

Table A-6. Arsenic (III) sorption onto Prestea laterite iron concretion as a function of equilibrium concentration at various temperatures. Solid suspension density = 15g/L. The pH is 7.0

Sample ID	Equil. conc.	adsorp Con.(mg/L)	adsorp Con.(mg/g)	1/S	1/C
As_3_25_0	0.00	0.00	0.00	0.0E+00	0.0E+00
As_3_25_200	21.04	178.96	17.90	5.6E-02	5.6E-03
As_3_25_400	39.57	360.43	36.04	2.8E-02	2.8E-03
As_3_25_600	57.92	542.08	54.21	1.8E-02	1.8E-03
As_3_25_800	83.50	716.50	71.65	1.4E-02	1.4E-03
As_3_25_1000	125.84	874.16	87.42	1.1E-02	1.1E-03
As_3_25_1500	251.12	1248.88	124.89	8.0E-03	8.0E-04
As_3_25_2000	571.96	1428.04	142.80	7.0E-03	7.0E-04
As_3_35_0	0.00	0.00	0.00	0.0E+00	0.0E+00
As_3_35_200	20.50	179.50	17.95	5.6E-02	5.6E-03
As_3_35_400	26.06	373.94	37.39	2.7E-02	2.7E-03
As_3_35_600	53.26	546.74	54.67	1.8E-02	1.8E-03
As_3_35_800	68.38	731.62	73.16	1.4E-02	1.4E-03
As_3_35_1000	85.55	914.45	91.45	1.1E-02	1.1E-03
As_3_35_1500	211.50	1288.50	128.85	7.8E-03	7.8E-04
As_3_35_2000	522.00	1478.00	147.80	6.8E-03	6.8E-04
As_3_45_0	0.00	0.00	0.00	0.0E+00	0.0E+00
As_3_45_200	19.77	180.23	18.02	5.5E-02	5.5E-03
As_3_45_400	28.54	371.46	37.15	2.7E-02	2.7E-03
As_3_45_600	50.56	549.44	54.94	1.8E-02	1.8E-03
As_3_45_800	62.06	737.94	73.79	1.4E-02	1.4E-03
As_3_45_1000	74.49	925.51	92.55	1.1E-02	1.1E-03
As_3_45_1500	197.12	1302.88	130.29	7.7E-03	7.7E-04
As_3_45_2000	472.60	1527.40	152.74	6.5E-03	6.5E-04
As_3_60_0	0.00	0.00	0.00	0.0E+00	0.0E+00
As_3_60_200	19.08	180.92	18.09	5.5E-02	5.5E-03
As_3_60_400	26.39	373.61	37.36	2.7E-02	2.7E-03
As_3_60_600	42.26	557.74	55.77	1.8E-02	1.8E-03
As_3_60_800	55.30	744.70	74.47	1.3E-02	1.3E-03
As_3_60_1000	69.50	930.50	93.05	1.1E-02	1.1E-03
As_3_60_1500	100.80	1399.20	139.92	7.1E-03	7.1E-04
As_3_60_2000	301.80	1698.20	169.82	5.9E-03	5.9E-04

Table A-7. (As (V)) sorption onto Prestea laterite iron concretion as a function of equilibrium concentration at various temperatures. Solid suspension density = 15g/L. The pH is 7.0.

Sample ID	Equil. conc.(mg/L	adsorp Con.(mg/L)	adsorp Con.(mg/g)	1/S	1/C
As_5_25_0	0.00	0.00	0.00	0.0E+00	0.0E+00
As_5_25_200	69.11	130.89	13.09	7.6E-02	7.6E-03
As_5_25_400	93.50	306.50	30.65	3.3E-02	3.3E-03
As_5_25_600	150.20	449.80	44.98	2.2E-02	2.2E-03
As_5_25_800	172.53	627.47	62.75	1.6E-02	1.6E-03
As_5_25_1000	307.24	692.76	69.28	1.4E-02	1.4E-03
As_5_25_1500	547.44	952.56	95.26	1.0E-02	1.0E-03
As_5_25_2000	965.60	1034.40	103.44	9.7E-03	9.7E-04
As_5_35_0	0.00	0.00	0.00	0.0E+00	0.0E+00
As_5_35_200	44.73	155.27	15.53	6.4E-02	6.4E-03
As_5_35_400	78.03	321.97	32.20	3.1E-02	3.1E-03
As_5_35_600	85.96	514.04	51.40	1.9E-02	1.9E-03
As_5_35_800	167.36	632.64	63.26	1.6E-02	1.6E-03
As_5_35_1000	263.76	736.24	73.62	1.4E-02	1.4E-03
As_5_35_1500	455.24	1044.76	104.48	9.6E-03	9.6E-04
As_5_35_2000	756.16	1243.84	124.38	8.0E-03	8.0E-04
As_5_45_0	0.00	0.00	0.00	0.0E+00	0.0E+00
As_5_45_200	27.77	172.23	17.22	5.8E-02	5.8E-03
As_5_45_400	58.54	341.46	34.15	2.9E-02	2.9E-03
As_5_45_600	80.56	519.44	51.94	1.9E-02	1.9E-03
As_5_45_800	151.01	648.99	64.90	1.5E-02	1.5E-03
As_5_45_1000	134.49	865.51	86.55	1.2E-02	1.2E-03
As_5_45_1500	197.12	1302.88	130.29	7.7E-03	7.7E-04
As_5_45_2000	549.50	1450.50	145.05	6.9E-03	6.9E-04
As_5_60_0	5.53	0	0.00	0.0E+00	0.0E+00
As_5_60_200	28.08	171.92	17.19	5.8E-02	5.8E-03
As_5_60_400	46.39	353.61	35.36	2.8E-02	2.8E-03
As_5_60_600	72.26	527.74	52.77	1.9E-02	1.9E-03
As_5_60_800	79.24	720.76	72.08	1.4E-02	1.4E-03
As_5_60_1000	90.76	909.24	90.92	1.1E-02	1.1E-03
As_5_60_1500	113.36	1386.64	138.66	7.2E-03	7.2E-04
As_5_60_2000	386.06	1613.94	161.39	6.2E-03	6.2E-04

Table A-8. Arsenic (III)) sorption onto Awaso laterite iron concretion as a function of equilibrium concentration at 25 C. Solid suspension density = 5 g/L. The pH is 7.0

Sample ID	Equil. Conc.(µg/L)	Amt Sorbed(µg/L)	Equil. Conc.(µg/g)	1/S	1/C
As (III)_0	0.0	0.0	0.0	0.0E+00	0.0E+00
As (III)_400	107.9	292.2	58.4	1.7E-02	9.3E-03
As (III)_800	138.9	661.1	132.2	7.6E-03	7.2E-03
As (III)_1200	383.5	816.5	163.3	6.1E-03	2.6E-03
As (III)_1600	652.0	948.0	189.6	5.3E-03	1.5E-03
As (III)_2000	968.6	1031.4	206.3	4.8E-03	1.0E-03
As (III)_2400	1252.1	1147.9	229.6	4.4E-03	8.0E-04
As (III)_2800	1552.2	1247.8	249.6	4.0E-03	6.4E-04

Table A-9. Arsenic (V) sorption onto Awaso laterite iron concretion as a function of equilibrium concentration at 25°C. Solid suspension density = 5g/L. The pH is 7.0

Sample ID	Equil. Conc.(µg/L)	Amt Sorbed(µg/L)	Equil. Conc.(µg/g)	1/S	1/C
As (V)_0	0.0	0.0	0.0	0.0E+00	0.0E+00
As (V)_400	4.5	4.5	395.5	7.9E+01	1.3E-02
As (V)_800	6.8	6.8	793.3	1.6E+02	6.3E-03
As (V)_1200	12.0	12.0	1188.1	2.4E+02	4.2E-03
As (V)_1600	41.9	41.9	1558.1	3.1E+02	3.2E-03
As (V)_2000	72.5	72.5	1927.5	3.9E+02	2.6E-03
As (V)_2400	79.1	395.4	2004.6	4.0E+02	2.5E-03
As (V)_2800	98.6	492.9	2307.2	4.6E+02	2.2E-03

Table A-10. Arsenic (III) sorption onto Prestea laterite iron concretion as a function of solution pH and ionic strength. Solid suspension density = 5g/L, T=20^{o} C.

As (III) R O + 0.1M pH	Equil. Conc.(µg/L)	Amount sorbed (µg/L)	Amount sorbed (µg/g)	% sorbed
4	364.0	636.0	127.2	63.6
5	218.0	782.0	156.4	78.2
6	174.0	826.0	165.2	82.6
7	179.0	821.0	164.2	82.1
8	195.0	805.0	161.0	80.5
9	229.0	771.0	154.2	77.1
10	384.0	616.0	123.2	61.6
As (III) R O + 0.01M pH	**Equil. Conc.(µg/L)**	**Amount sorbed (µg/L)**	**Amount sorbed (µg/g)**	**% sorbed**
4	284.0	716.0	143.2	82.5
5	167.0	833.0	166.6	90.4
6	137.0	863.0	172.6	91.2
7	130.0	870.0	174.0	93.0
8	137.0	863.0	172.6	90.8
9	185.0	815.0	163.0	88.6
10	300.0	700.0	140.0	74.1
As (III) R O + 0.001M pH	**Equil. Conc.(µg/L)**	**Amount sorbed (µg/L)**	**Amount sorbed (µg/g)**	**% sorbed**
4	175.0	825.0	165.0	71.6
5	96.0	904.0	180.8	83.3
6	88.0	912.0	182.4	86.3
7	70.0	930.0	186.0	87.0
8	92.0	908.0	181.6	86.3
9	114.0	886.0	177.2	81.5
10	259.0	741.0	148.2	70.0

Table A-11. As (V) sorption onto Prestea laterite iron concretion as a function of solution pH and ionic strength. Solid suspension density = 5g/L, T=20^{o}C.

As (V) R O + 0.1M pH	Equil. Conc.(µg/L)	Amount sorbed (µg/L)	Amount sorbed (µg/g)	% sorbed
4	13.90	986.10	197.22	98.6
5	20.00	980.00	196.00	98.0
6	25.30	974.70	194.94	97.5
7	32.70	967.30	193.46	96.7
8	42.00	958.00	191.60	95.8
9	57.00	943.00	188.60	94.3
10	123.00	877.00	175.40	87.7
As (V) R O + 0.01M pH	**Equil. Conc.(µg/L)**	**Amount sorbed (µg/L)**	**Amount sorbed (µg/g)**	**% sorbed**
4	24.20	975.80	195.16	97.6
5	36.80	963.20	192.64	96.3
6	40.50	959.50	191.90	96.0
7	52.50	947.50	189.50	94.8
8	70.80	929.20	185.84	92.9
9	82.30	917.70	183.54	91.8
10	143.30	856.70	171.34	85.7
As (V) R O + 0.001M pH	**Equil. Conc.(µg/L)**	**Amount sorbed (µg/L)**	**Amount sorbed (µg/g)**	**% sorbed**
4	52.30	947.70	189.54	94.8
5	65.60	934.40	186.88	93.4
6	79.90	920.10	184.02	92.0
7	75.60	924.40	184.88	92.4
8	112.90	887.10	177.42	88.7
9	138.80	861.20	172.24	86.1
10	184.90	815.10	163.02	81.5

Table A-12. As (III) sorption onto Awaso laterite iron concretion as a function of solution pH and ionic strength. Solid suspension density = 5g/L, T=20^{o}C.

As (III) R O + 0.1M pH	Equil. Conc.(µg/L)	Amount sorbed (µg/L)	Amount sorbed (µg/g)	% sorbed
4	518.9	481.1	96.2	57.2
5	472.1	527.9	105.6	61.3
6	434.6	565.4	113.1	64.9
7	410.8	589.2	117.8	68.6
8	434.6	565.4	113.1	68.0
9	470.9	529.1	105.8	65.2
10	505.3	494.7	98.9	56.4
As (III) R O + 0.01M pH	**Equil. Conc.(µg/L)**	**Amount sorbed (µg/L)**	**Amount sorbed (µg/g)**	**% sorbed**
4	427.8	572.2	114.4	72.1
5	386.5	613.5	122.7	75.2
6	351.2	648.8	129.8	78.0
7	314.0	686.0	137.2	79.6
8	320.4	679.6	135.9	77.7
9	348.4	651.6	130.3	74.5
10	436.0	564.0	112.8	70.8
As (III) R O + 0.001M pH	**Equil. Conc.(µg/L)**	**Amount sorbed (µg/L)**	**Amount sorbed (µg/g)**	**% sorbed**
4	278.8	721.2	144.2	48.1
5	247.9	752.1	150.4	52.8
6	220.1	779.9	156.0	56.5
7	204.0	796.0	159.2	58.9
8	222.6	777.4	155.5	56.5
9	254.8	745.2	149.0	52.9
10	292.1	707.9	141.6	49.5

Table A-13. As (V) sorption onto Awaso laterite iron concretion as a function of solution pH and ionic strength. Solid suspension density = 5g/L, T=20^{o}C.

As (V)R O + 0.1M NaCl				
pH	Equil. Conc.(µg/L)	Amount sorbed (µg/L)	Amount sorbed (µg/g)	% sorbed
4	239.5	760.5	152.1	76.1
5	244.1	755.9	151.2	75.6
6	254.5	745.5	149.1	74.6
7	256.5	743.5	148.7	74.4
8	259.6	740.4	148.1	74.0
9	276.9	723.1	144.6	72.3
10	307.8	692.2	138.4	69.2
As (V) R O + 0.01M				
pH	Equil. Conc.(µg/L)	Amount sorbed (µg/L)	Amount sorbed (µg/g)	% sorbed
4	260.4	739.6	147.9	74.0
5	269.8	730.2	146.0	73.0
6	278.6	721.4	144.3	72.1
7	275.6	724.4	144.9	72.4
8	277.9	722.1	144.4	72.2
9	305.6	694.4	138.9	69.4
10	327.6	672.4	134.5	67.2
As (V) R O + 0.001M				
pH	Equil. Conc.(µg/L)	Amount sorbed (µg/L)	Amount sorbed (µg/g)	% sorbed
4	311.4	688.6	137.7	68.9
5	316.9	683.1	136.6	68.3
6	317.4	682.6	136.5	68.3
7	319.8	680.2	136.0	68.0
8	323.5	676.5	135.3	67.6
9	332.3	667.7	133.5	66.8
10	369.4	630.6	126.1	63.1

Table A-14. Modeled As (III) sorption onto Prestea laterite iron concretion as a function of solution pH and ionic strength using the diffuse-layer model. Solid suspension density = 5 g/L, T = 25^{o} C.

As (III) R O + 0.1M	DLM	DLM	TLM	TLM
pH	Model % sorbed	Model Amt sorbed (µg/g)	Model % sorbed	Model Amt sorbed (µg/g)
4.0	62.9	125.8	63.0	126.0
5.0	78.2	156.4	78.9	157.8
6.0	82.0	164.0	82.7	165.4
7.0	81.7	163.4	82.9	165.8
8.0	79.1	158.2	80.8	161.6
9.0	77.0	154.0	75.7	151.4
10.0	60.9	121.8	61.6	123.2
As (III) R O + 0.01M				
pH	Model % sorbed	Model Amt sorbed (µg/g)	Model % sorbed	Model Amt sorbed (µg/g)
4.0	66.9	133.8	70.9	141.8
5.0	81.0	162.0	83.7	167.4
6.0	87.7	175.4	86.6	173.2
7.0	88.0	176.0	86.8	173.6
8.0	85.0	170.0	85.3	170.6
9.0	82.0	164.0	81.2	162.4
10.0	70.8	141.6	69.8	139.6
As (III) R O + 0.001M				
pH	Model % sorbed	Model Amt sorbed (µg/g)	Model % sorbed	Model Amt sorbed (µg/g)
4.0	83.5	167.0	82.0	164.0
5.0	90.4	180.8	90.3	180.6
6.0	92.8	185.6	91.9	183.8
7.0	93.6	187.2	92.0	184.0
8.0	90.6	181.2	91.3	182.6
9.0	88.3	176.6	87.5	175.0
10.0	73.2	146.4	74.9	149.8

Table A-15 Modeled As (V) sorption onto Prestea laterite iron concretion as a function of solution pH and ionic strength using the diffuse-layer model. Solid suspension density = 5g/L, T = 25°C.

As (V) R O + 0.1M	DLM	DLM
pH	**Model % sorbed**	**Model Amt sorbed (µg/g)**
4.0	98.1	196.2
5.0	98.1	196.2
6.0	98.0	196.0
7.0	97.3	194.6
8.0	96.1	192.2
9.0	94.7	189.4
10.0	87.1	174.2
As (V) R O + 0.01M		
pH	**Model % sorbed**	**Model Amt sorbed (µg/g)**
4.0	96.6	193.2
5.0	96.6	193.2
6.0	96.5	193.0
7.0	95.5	191.0
8.0	93.7	187.4
9.0	92.0	184.0
10.0	84.2	168.4
As (V) R O + 0.001M		
pH	**Model % sorbed**	**Model Amt sorbed (µg/g)**
4.0	94.7	189.4
5.0	93.6	187.2
6.0	92.9	185.8
7.0	92.2	184.4
8.0	89.6	179.2
9.0	86.8	173.6
10.0	82.5	165.0

Table A-16 Modeled As (III) sorption onto Awaso laterite iron concretion as a function of solution pH and ionic strength using the diffuse and triple-layer model. Solid suspension density = 5g/L, T = 25^{o}C.

As (III) R O + 0.1M	DLM	DLM	TLM	TLM
pH	Model % sorbed	Model Amt sorbed (µg/g)	Model % sorbed	Model Amt sorbed (µg/g)
4.0	57.5	115.0	57.0	114.0
5.0	61.6	123.2	61.8	123.6
6.0	65.5	131.0	65.8	131.6
7.0	68.9	137.8	68.9	137.8
8.0	69.2	138.4	69.3	138.6
9.0	65.8	131.6	65.2	130.4
10.0	56.3	112.6	56.5	113.0
As (III) R O + 0.01M				
pH	Model % sorbed	Model Amt sorbed (µg/g)	Model % sorbed	Model Amt sorbed (µg/g)
4.0	72.0	144.0	72.2	144.4
5.0	75.0	150.0	75.2	150.4
6.0	78.3	156.6	78.5	157.0
7.0	79.2	158.4	79.0	158.0
8.0	77.9	155.8	77.5	155.0
9.0	74.0	148.0	74.0	148.0
10.0	70.3	140.6	70.6	141.2
As (III) R O + 0.001M				
pH	Model % sorbed	Model Amt sorbed (µg/g)	Model % sorbed	Model Amt sorbed (µg/g)
4.0	47.9	95.8	48.0	96.0
5.0	52.6	105.2	52.4	104.8
6.0	56.3	112.6	56.0	112.0
7.0	58.2	116.4	58.0	116.0
8.0	56.2	112.4	56.6	113.2
9.0	53.2	106.4	53.3	106.6
10.0	49.0	98.0	49.3	98.6

Table A-17. Modeled As (V) sorption onto Awaso laterite iron concretion as a function of solution pH and ionic strength using the diffuse-layer model. Solid suspension density = 5g/L, T = 25°C.

As (V)R O + 0.1M	DLM	DLM
pH	**Model % sorbed**	**Model Amt sorbed (µg/g)**
4.0	76.2	152.4
5.0	76.2	152.4
6.0	75.9	151.8
7.0	74.8	149.6
8.0	74.8	149.6
9.0	74.3	148.6
10.0	68.2	136.4
As (V)R O + 0.01M		
pH	**Model % sorbed**	**Model Amt sorbed (µg/g)**
4.0	74.1	148.2
5.0	74.2	148.4
6.0	74.1	148.2
7.0	73.4	146.8
8.0	72.3	144.6
9.0	71.6	143.2
10.0	66.7	133.4
As (V)R O + 0.001M		
pH	**Model % sorbed**	**Model Amt sorbed (µg/g)**
4.0	68.8	137.6
5.0	68.3	136.6
6.0	67.8	135.6
7.0	67.9	135.8
8.0	66.3	132.6
9.0	65.3	130.6
10.0	63.0	126.0

Table A-18. Competitive sorption of As (III) and phosphate on Prestea LC. As (III) = 1.0mg/L, phosphate = 10mg/L. Suspension concentration, 15g/L.

As(III) + (10 mg/L PO4) pH	Equil. Conc.(µg/L)	Amount sorbed (µg/L)	Amount sorbed (µg/g)	% sorbed
4	201.0	799.0	53.3	79.9
5	165.1	834.9	55.7	83.5
6	169.8	830.2	55.3	83.0
7	155.7	844.3	56.3	84.4
8	146.5	853.5	56.9	85.4
9	137.6	862.4	57.5	86.2
10	168.7	831.3	55.4	83.1
As (III) pH	**Equil. Conc.(µg/L)**	**Amount sorbed (µg/L)**	**Amount sorbed (µg/g)**	**% sorbed**
4	110.3	889.7	59.3	89.0
5	41.1	958.9	63.9	95.9
6	18.4	981.6	65.4	98.2
7	14.4	985.6	65.7	98.6
8	25.4	974.6	65.0	97.5
9	56.6	943.4	62.9	94.3
10	124.3	875.7	58.4	87.6

Table A-19. Competitive sorption of As (III) and sulfate on Prestea LC. As (III) = 1.0mg/L, sulfate = 50mg/L. Suspension concentration, 15g/L.

As(III) + (50 mg/L SO4) pH	Equil. Conc.(µg/L)	Amount sorbed (µg/L)	Amount sorbed (µg/g)	% sorbed
4	332.1	667.9	44.5	66.8
5	309.4	690.6	46.0	69.1
6	284.8	715.2	47.7	71.5
7	277.8	722.2	48.1	72.2
8	293.7	706.3	47.1	70.6
9	304.6	695.4	46.4	69.5
10	378.5	621.5	41.4	62.2
As (III) pH	**Equil. Conc.(µg/L)**	**Amount sorbed (µg/L)**	**Amount sorbed (µg/g)**	**% sorbed**
4	110.3	889.7	59.3	89.0
5	41.1	958.9	63.9	95.9
6	18.4	981.6	65.4	98.2
7	14.4	985.6	65.7	98.6
8	25.4	974.6	65.0	97.5
9	56.6	943.4	62.9	94.3
10	124.3	875.7	58.4	87.6

Table A-20. Competitive sorption of As (V) and phosphate on Prestea LC. As (V) = 1.0mg/L, phosphate = 10mg/L. Suspension concentration, 15g/L.

As(V) + (10 mg/L PO4) pH	Equil. Conc.(µg/L)	Amount sorbed (µg/L)	Amount sorbed (µg/g)	% sorbed
4	132.1	867.9	57.9	86.8
5	75.4	924.6	61.6	92.5
6	62.3	937.7	62.5	93.8
7	59.5	940.5	62.7	94.1
8	83.5	916.5	61.1	91.7
9	93.5	906.5	60.4	90.7
10	157.4	842.6	56.2	84.3
As (V) pH	**Equil. Conc.(µg/L)**	**Amount sorbed (µg/L)**	**Amount sorbed (µg/g)**	**% sorbed**
4	12.9	987.1	65.8	98.7
5	15.2	984.8	65.7	98.5
6	14.4	985.6	65.7	98.6
7	14.0	986.0	65.7	98.6
8	14.8	985.2	65.7	98.5
9	17.7	982.3	65.5	98.2
10	23.2	976.8	65.1	97.7

Table A-21. Competitive sorption of As (V) and sulfate on Prestea LC. As (V) = 1.0mg/L, sulfate = 50mg/L. Suspension concentration, 15g/L.

As(V) + (500 mg/L SO4) pH	Equil. Conc.(µg/L)	Amount sorbed (µg/L)	Amount sorbed (µg/g)	% sorbed
4	9.4	990.6	66.0	99.1
5	9.1	990.9	66.1	99.1
6	5.5	994.5	66.3	99.5
7	10.5	989.5	66.0	99.0
8	5.9	994.1	66.3	99.4
9	6.6	993.4	66.2	99.3
10	7.3	992.7	66.2	99.3
As (V) pH	**Equil. Conc.(µg/L)**	**Amount sorbed (µg/L)**	**Amount sorbed (µg/g)**	**% sorbed**
4	12.9	987.1	65.8	98.7
5	15.2	984.8	65.7	98.5
6	14.4	985.6	65.7	98.6
7	14.0	986.0	65.7	98.6
8	14.8	985.2	65.7	98.5
9	17.7	982.3	65.5	98.2
10	23.2	976.8	65.1	97.7

Table A-22. Competitive sorption of As (III) and phosphate on Awaso LC. As (III) = 1.0mg/L, phosphate = 10mg/L. Suspension concentration, 15g/L

As(III) + (10 mg/L PO4) pH	Equil. Conc.(µg/L)	Amount sorbed (µg/L)	Amount sorbed (µg/g)	% sorbed
4	312.4	687.6	45.8	68.8
5	332.0	668.0	44.5	66.8
6	336.4	663.6	44.2	66.4
7	340.2	659.8	44.0	66.0
8	342.7	657.3	43.8	65.7
9	343.7	656.3	43.8	65.6
10	348.2	651.8	43.5	65.2
As (III) pH	**Equil. Conc.(µg/L)**	**Amount sorbed (µg/L)**	**Amount sorbed (µg/g)**	**% sorbed**
4	305.2	694.8	46.3	69.5
5	304.5	695.5	46.4	69.6
6	318.9	681.1	45.4	68.1
7	324.5	675.5	45.0	67.6
8	336.8	663.2	44.2	66.3
9	334.6	665.4	44.4	66.5
10	340.1	659.9	44.0	66.0

.

Table A-23. Competitive sorption of As (III) and sulfate on Awaso LC. As (III) = 1.0mg/L, sulfate = 50mg/L. Suspension concentration, 15g/L.

As(III) + (50 mg/L SO4) pH	Equil. Conc.(µg/L)	Amount sorbed (µg/L)	Amount sorbed (µg/g)	% sorbed
4.0	476.5	523.5	34.9	52.4
5.0	448.7	551.3	36.8	55.1
6.0	445.3	554.7	37.0	55.5
7.0	437.7	562.3	37.5	56.2
8.0	495.0	505.0	33.7	50.5
9.0	509.4	490.6	32.7	49.1
10.0	511.9	488.1	32.5	48.8
As (III) pH	**Equil. Conc.(µg/L)**	**Amount sorbed (µg/L)**	**Amount sorbed (µg/g)**	**% sorbed**
4.0	305.2	694.8	46.3	69.5
5.0	304.5	695.5	46.4	69.6
6.0	318.9	681.1	45.4	68.1
7.0	324.5	675.5	45.0	67.6
8.0	336.8	663.2	44.2	66.3
9.0	334.6	665.4	44.4	66.5
10.0	340.1	659.9	44.0	66.0

Table A-24. Competitive sorption of As (V) and phosphate on Awaso LC. As (V) = 1.0mg/L, phosphate = 10mg/L. Suspension concentration, 15g/L.

As(V) + (10 mg/L PO4) pH	Equil. Conc.(µg/L)	Amount sorbed (µg/L)	Amount sorbed (µg/g)	% Sorbed
4	63.6	936.4	62.4	63.2
5	56.5	943.5	62.9	64.6
6	33.1	966.9	64.5	64.8
7	70.4	929.6	62.0	65.0
8	82.6	917.4	61.2	64.5
9	87.6	912.4	60.8	63.0
10	167.6	832.4	55.5	62.5
As (V) pH	**Equil. Conc.(µg/L)**	**Amount sorbed (µg/L)**	**Amount sorbed (µg/g)**	**% Sorbed**
4	51.9	948.1	63.2	94.8
5	30.7	969.3	64.6	96.9
6	28.3	971.7	64.8	97.2
7	25.2	974.8	65.0	97.5
8	32.9	967.1	64.5	96.7
9	55.1	944.9	63.0	94.5
10	62.8	937.2	62.5	93.7

Table A 25. Competitive sorption of As (V) and sulfate on Awaso LC. As (V) = 1.0mg/L, sulfate = 50mg/L. Suspension concentration, 15g/L.

As(V) + (500 mg/L SO4) pH	Equil. Conc.(µg/L)	Amount sorbed (µg/L)	Amount sorbed (µg/g)	% Sorbed
4.0	20.0	998.0	66.5	63.2
5.0	20.1	997.9	66.5	64.6
6.0	20.7	997.3	66.5	64.8
7.0	20.9	997.1	66.5	65.0
8.0	30.0	997.0	66.5	64.5
9.0	30.3	996.7	66.4	63.0
10.0	40.8	995.2	66.3	62.5
As (V) pH	**Equil. Conc.(µg/L)**	**Amount sorbed (µg/L)**	**Amount sorbed (µg/g)**	**% Sorbed**
4.0	51.9	948.1	63.2	94.8
5.0	30.7	969.3	64.6	96.9
6.0	28.3	971.7	64.8	97.2
7.0	25.2	974.8	65.0	97.5
8.0	32.9	967.1	64.5	96.7
9.0	55.1	944.9	63.0	94.5
10.0	62.8	937.2	62.5	93.7

Table A-26. Electrophoretic mobility of Prestea laterite iron concretion as a function of pH in 0.01M NaCl solution. No Arsenic added.

	pH 3	pH 4	pH 5	pH 6	pH 7	pH 8	pH 9	pH 9	pH 10	pH 10
Measured pH	3.06	4.05	5.03	6.04	7.04	8.07	9.07	9.60	10.06	10.50
EM1	3.05	3.29	2.75	2.20	1.26	0.28	-1.16	-2.26	-3.30	-4.59
EM2	3.07	3.30	2.78	2.18	1.26	0.26	-1.14	-2.24	-3.33	-4.62
EM3	3.06	3.31	2.73	2.22	1.26	0.24	-1.12	-2.28	-3.33	-4.60
Average EM	3.06	3.30	2.75	2.20	1.26	0.26	-1.14	-2.26	-3.32	-4.60

Table A-27. Electrophoretic mobility of Prestea laterite iron concretion as a function of pH in 0.01M NaCl solution. 0.035mM As (III) concentration added.

	pH 3	pH3	pH 3	pH 4	pH 5	pH 6	pH 7	pH 8	pH 9	pH 9	pH 10
Measured pH	3.02	3.15	3.50	4.00	5.00	6.00	7.05	8.06	9.02	9.60	10.00
EM1	2.79	2.70	1.70	1.36	0.98	-1.21	-1.52	-2.10	-2.35	-2.90	-3.32
EM2	2.78	2.68	1.68	1.32	0.96	-1.23	-1.56	-2.14	-2.39	-2.96	-3.01
EM3	2.80	2.72	1.72	1.40	0.94	-1.25	-1.43	-2.10	-2.42	-2.86	-2.89
Average EM	2.79	2.70	1.70	1.36	0.96	-1.23	-1.50	-2.11	-2.39	-2.91	-3.07

Table A-28. Electrophoretic mobility of Prestea laterite iron concretion as a function of pH in 0.01M NaCl solution. 3.5mM As (III) concentration added.

	pH 3	pH3	pH 3	pH 4	pH 5	pH 6	pH 7	pH 8	pH 9	pH 9	pH 10
Measured pH	3.04	3.13	3.45	4.02	5.03	6.04	7.05	8.05	9.05	9.46	10.02
EM1	1.03	0.72	0.59	0.40	-0.74	-1.21	-2.41	-2.88	-3.02	-3.40	-3.75
EM2	1.02	0.75	0.53	0.45	-0.77	-1.13	-2.44	-2.79	-3.05	-3.55	-3.70
EM3	1.05	0.70	0.60	0.44	-0.66	-1.05	-2.39	-2.90	-3.06	-3.20	-3.66
Average EM	1.03	0.72	0.57	0.43	-0.72	-1.13	-2.41	-2.86	-3.04	-3.38	-3.70

Table A-29. Electrophoretic mobility of Prestea laterite iron concretion as a function of pH in 0.01M NaCl solution. 0.035mM As (V) concentration added.

	pH 3	pH3	pH 4	pH 5	pH 6	pH 7	pH 8	pH 9	pH 9	pH 10	pH 10
Measured pH	3.02	3.50	4.00	5.00	6.00	7.05	8.06	9.02	9.60	10.00	10.50
EM1	2.60	1.33	0.90	0.50	0.60	-0.99	-1.70	-2.03	-2.35	-2.36	-3.59
EM2	2.65	1.40	0.96	0.55	0.62	-0.96	-1.78	-2.05	-2.25	-2.38	-3.60
EM3	2.55	1.30	0.85	0.45	0.58	-0.95	-1.60	-2.00	-2.29	-2.20	-3.80
Average EM	2.60	1.34	0.90	0.50	0.60	-0.97	-1.69	-2.03	-2.30	-2.31	-3.66

Table A-30. Electrophoretic mobility of Prestea laterite iron concretion as a function of pH in 0.01M NaCl solution. 3.5mM As (V) concentration added.

	pH 3	pH3	pH 4	pH 5	pH 6	pH 7	pH 8	pH 9	pH 9	pH 10
Measured pH	3.05	3.56	4.01	5.02	6.02	7.06	8.06	9.02	9.71	10.00
EM1	1.59	1.39	-0.96	-1.95	-1.98	-2.73	-3.96	-3.97	-4.51	-4.96
EM2	1.61	1.34	-0.97	-1.93	-1.99	-2.70	-3.90	-3.99	-4.55	-4.99
EM3	1.59	1.38	-0.99	-1.94	-1.96	-2.76	-3.95	-3.95	-4.50	-4.86
Average EM	1.60	1.37	-0.97	-1.94	-1.98	-2.73	-3.94	-3.97	-4.52	-4.94

Table A-31. Electrophoretic mobility of Awaso laterite iron concretion as a function of pH in 0.01M NaCl solution. No Arsenic added.

	pH 3	pH 4	pH 5	pH 6	pH 7	pH 8	pH 9	pH 9	pH 9	pH 10	pH 10
Measured pH	3.08	3.9	5.16	6.05	7.00	8.14	9.04	9.4	9.85	10.08	10.58
EM1	2.67	1.98	1.23	0.96	0.60	0.10	-0.43	-1.08	-2.51	-3.34	-3.89
EM2	2.69	1.90	1.15	0.98	0.69	0.09	-0.45	-1.10	-2.49	-3.34	-3.99
EM3	2.59	1.98	1.23	0.85	0.55	0.12	-0.47	-1.22	-2.55	-3.44	-3.76
Average EM	2.65	1.95	1.20	0.93	0.61	0.10	-0.45	-1.13	-2.52	-3.37	-3.88

Table A-32. Electrophoretic mobility of Awaso laterite iron concretion as a function of pH in 0.01M NaCl solution. 0.035mM As (III) concentration added.

	pH 3	pH 4	pH 5	pH 6	pH 7	pH 8	pH 9	pH 9	pH 9	pH 10	pH 10
Measured pH	2.91	3.98	4.98	5.2	5.70	6.01	6.55	7.06	7.99	8.85	10.59
EM1	3.21	2.16	1.86	1.65	1.05	0.76	-0.11	-0.61	-1.8	-2.96	-3.29
EM2	3.32	2.18	1.90	1.70	1.10	0.77	-0.13	-0.61	-1.82	-2.94	-3.28
EM3	3.20	2.14	1.86	1.65	1.00	0.79	-0.11	-0.62	-1.78	-2.94	-3.29
Average EM	3.24	2.16	1.87	1.67	1.05	0.77	-0.12	-0.61	-1.80	-2.95	-3.29

Table A-33. Electrophoretic mobility of Awaso laterite iron concretion as a function of pH in 0.01M NaCl solution. 3.5mM As (III) concentration added

	pH 3	pH 4	pH 5	pH 6	pH 7	pH 8	pH 9	pH 9	pH 9	pH 10	pH 10
Measured pH	3.00	3.91	5.91	6.86	7.42	7.94	8.70	8.90	9.00	10.00	10.55
EM1	2.43	1.34	0.50	-0.51	-0.71	-1.20	-1.93	-2.57	-3.41	-3.76	-3.76
EM2	2.45	1.34	0.50	-0.51	-0.70	-1.22	-1.96	-2.58	-3.45	-3.74	-3.77
EM3	2.46	1.35	0.53	-0.52	-0.72	-1.25	-1.98	-2.55	-3.40	-3.70	-3.78
Average EM	2.45	1.34	0.51	-0.51	-0.71	-1.22	-1.96	-2.57	-3.42	-3.73	-3.77

Table A-34. Electrophoretic mobility of Awaso laterite iron concretion as a function of pH in 0.01M NaCl solution. 0.035mM As (V) concentration added.

	pH 3	pH 4	pH 5	pH 6	pH 7	pH 8	pH 9	pH 9	pH 9	pH 10	pH 10
Measured pH	2.97	3.98	4.99	5.51	6.02	7.02	7.85	8.51	9.00	9.52	10.14
EM1	2.05	1.99	1.59	0.33	0.09	-0.72	-0.96	-1.59	-2.06	-2.17	-3.43
EM2	2.07	1.98	1.60	0.33	0.09	-0.75	-0.96	-1.58	-2.08	-2.19	-3.77
EM3	2.09	1.99	1.62	0.33	0.10	-0.70	-0.99	-1.60	-2.10	-2.22	-3.00
Average EM	2.07	1.99	1.60	0.33	0.09	-0.72	-0.97	-1.59	-2.08	-2.19	-3.40

Table A-35. Electrophoretic mobility of Awaso laterite iron concretion as a function of pH in 0.01M NaCl solution. 3.5mM As (V) concentration added.

	pH 3	pH 4	pH 5	pH 6	pH 7	pH 8	pH 9	pH 9	pH 9	pH 10	pH 10
Measured pH	2.02	2.99	4.18	4.60	5.00	5.54	7.10	8.07	9.10	10.18	10.52
EM1	3.20	2.30	1.45	1.02	0.88	-0.46	-1.49	-2.98	-3.09	-3.64	-4.69
EM2	3.22	2.32	1.45	1.04	0.86	-0.44	-1.50	-2.99	-3.12	-3.64	-4.66
EM3	3.18	2.28	1.45	1.06	0.88	-0.48	-1.48	-2.99	-3.21	-3.66	-4.70
Average EM	3.20	2.30	1.45	1.04	0.87	-0.46	-1.49	-2.99	-3.14	-3.65	-4.68

Table A-36. Summary of the various methods indicating mechanism(s) of arsenic sorption.

Method	Prestea As (III)	Prestea As (V)	Awaso As (III)	Awaso As (V)
ATR-FTIR	Inner-Sphere	Inner-Sphere	Inner-Sphere	Inner-Sphere
EM	Inner-Sphere	Inner-Sphere	Inner or outer-Sphere	Inner-Sphere
Sorption Data	Outer-Sphere	Inner-Sphere	Outer-Sphere	Inner-Sphere

Table A-37. Chemical composition of laterite concretions found elsewhere in the world.

Constituents	This work Ghana (Prestea) W(%)	This work Ghana (Awaso) W(%)	[87] India W(%)	[83] Sri lanka W(%)	[4] Ivory coast W(%)
SiO_2	13.51	4.80	39.25	54.15	2
TiO_2	1.022	3.450	0.5	5.54	-
Al2O3	14.87	78.95	14.78	20.73	56
Fe_2O_3	70.05	8.19	45.64	12.39	21
Mn_2O_3	0.027	0.003	1.52	0.23	-
MgO	0.00	0.00	Trace	0.3	-
CaO	0.07	0.04	Trace	0.28	-
Na_2O	0.03	0.06	Trace	Trace	-
K_2O	0.03	0.06	1.04	1.17	-
P_2O_5	0.396	4.453	0.01	0.13	-
LOI*	8.96	11.36	-	-	-

Table A-37. Continuation of Table A-37.

Constituents	[4] south Africa W(%)	[50] Northern Ireland W(%)	[4] Australia W(%)	[4] Kenya W(%)	[4] Thialand W(%)
SiO_2	26	34.98	3	11	47
TiO_2	-	2.68	-	-	-
Al2O3	19	26.96	51.2	15	10
Fe_2O_3	35	16.41	12.8	25	30
Mn_2O_3	-	0.38	-	-	-
MgO	-	0.94	-	-	-
CaO	-	0.4	-	-	-
Na_2O	-	0.08	-	-	-
K_2O	-	0.17	-	-	-
P_2O_5	-	0.06	-	-	-
LOI*	-	-	-	-	-

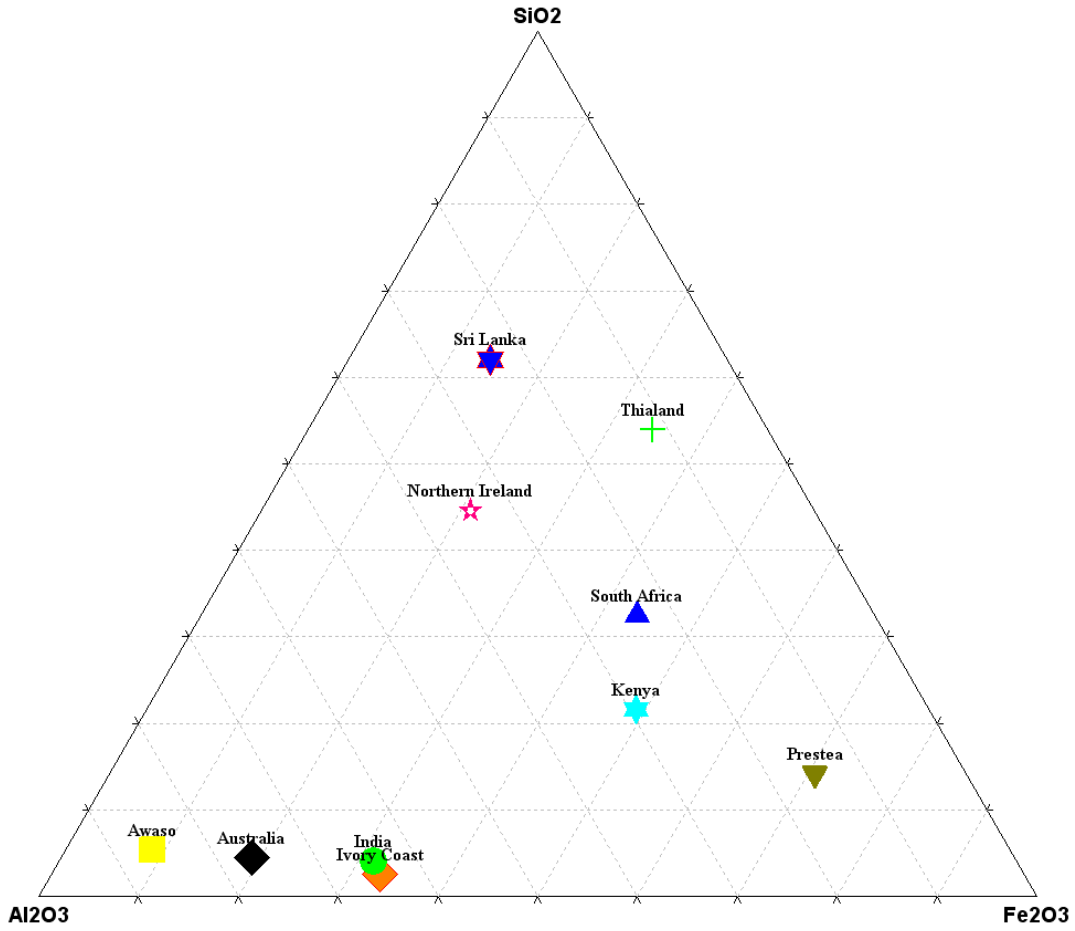

Figure A-14. Triangular diagram showing various lateritic soils found around the world. Prestea and Awaso laterite concretions represent the end members of most laterite concretions.